Locust thoracic dorsal unpaired median (DUM) neurons: Differential activation and peripheral distribution of octopamine and tyramine

Dissertation
zur Erlangung des akademischen Grades des
Doktors der Naturwissenschaften (Dr.rer.nat.)

eingereicht im Fachbereich Biologie, Chemie und Pharmazie
der Freien Universität Berlin

vorgelegt von

Bettina Stocker
aus München

Januar, 2011

Die Arbeit wurde von Oktober 2006 bis Januar 2011 unter der Leitung von Prof. Dr. Hans-Joachim Pflüger im Institut für Neurobiologie angefertigt.

1. Gutachter: Prof. Dr. Hans-Joachim Pflüger

2. Gutachterin: Prof. Dr. Dorothea Eisenhardt

Datum der Disputation: 29.03.2011

Contents

1 Introduction

"Nothing in neurobiology makes any sense except in the light of neuromodulation." By adapting and transferring the well-known quotation linking biology and evolution by T. Dobzhansky (1973) to the field of neuroscience, a conference speaker emphasised the phenomenon's crucial role for the complexity and adaptive power of animal behaviour. In its ability to bias rigid excitatory or inhibitory connections established between sensory, central and effector units of the nervous system, neuromodulation surpasses the borders of "hardwiring" by modifying cellular and synaptic properties, thereby drawing on a rich repertoire of substances and affecting various system levels.

Among the variety of substances mediating neuromodulatory effects including e.g. the highly complex family of neuropeptides, the small group of biogenic amines represents a multipotent set of neuroactive molecules derived from amino acids, which can act as neurotransmitters, -modulators or -hormones, often with overlapping function. In contrast to fast and direct chemical neurotransmission, neuromodulation via biogenic amines works indirectly, comparably slow, causes longlasting effects and, especially in the case of neurohormones, is not restricted to local release within minute compartments. At the cellular level, these features result from activation of metabotropic G-protein coupled receptors (GPCRs), which trigger, depending on the respective G-protein activated (Gudermann et al., 1996), intracellular signaling cascades involving second messengers like cyclic adenosine 3',5'-monophosphate (cAMP), calcium and inositol 1,4,5 trisphosphate (IP_3) and subcellularly localised enzymes such as protein kinases and phospholipases. These cellular responses can alter ion channel and receptor activites or can result in activation of transcription factors such as CREB and CREM inducing subsequent protein synthesis (De Cesare et al., 1999; Blenau and Baumann, 2001).

In vertebrates, loci of neuromodulation by noradrenaline are e.g. the neuromuscular junction, where this biogenic amine enhances the neurotransmission and thus end-plate potential amplitudes (Orbeli, 1923) or heart muscle cells, where it leads to an increased heart beat rate (Trautwein and Hescheler, 1990). In the hippocampus, the excitability of pyramidal cells is enhanced by noradrenaline (Madison and Nicoll, 1986). The significance of catecholamines such as serotonin and dopamine in human neurological disorders as e.g. Parkinson's disease and schizophrenia is undisputed (Kobayashi, 2001; Taylor et al., 2005). However, much fundamental insight into neuronal function and behaviour under influence of modulation could only be gained based on the study of less complex invertebrate model systems like molluscs, annelida and arthropods, which on this level share many mechanisms with higher phyla, but at the same time offer the researcher the invaluable advantage of identi-

fying individual neurons and networks consisting of only few constituents. Therefore principles of neuromodulation have been thoroughly studied in invertebrate species. The stomatogastric nervous system in decapod crustaceans is an excellent example of how neuromodulatory neurons can evoke and modulate multiple rhythmic behaviours (Flamm and Harris-Warrick, 1986a,b) either by intrinsic or extrinsic modulation (Katz, 1998; Pflüger and Büschges, 2006). Recently, the term meta-modulation has gained some interest, i.e. the modulatory process itself is under the control of neuromodulators. Biogenic amines can also serve as such meta-modulators, e.g. in the inhibition of swimming behaviour of the leech by serotonin and octopamine (Mesce, 2002).

In the 1950s, the biogenic amine octopamine was discovered in the salivary glands of the octopus (Erspamer and Boretti, 1951). Since then, this structural analogue of the vertebrate noradrenaline has been detected in many further species and is now accepted as one of the major modulators within the invertebrate nervous system, being effective on essentially all system levels (Roeder, 1999). In the peripheral nervous system, it enhances flight and leg muscle performance (Evans and O'Shea, 1977; Whim and Evans, 1988), negatively regulates visceral muscle contractions (Orchard and Lange, 1986; Lange and Orchard, 1986) and is a potent modulator of sensory organs of all modalities (Ramirez and Orchard, 1990; Farooqui, 2007). As a neurohormone released into the circulation, haemolymph octopamine acts on the insect fat body, by either mediating the release of adipokinetic peptide hormones (AKH I+II) from neurosecretory cells in the corpus cardiacum or exerting adipokinetic effects itself. Both pathways result in the liberation of lipids, which represent the main fuel during long-term flight in locusts (Wegener et al., 1986). In flight muscles, it stimulates oxidative metabolism by enhancing levels of fructose 2,6-bisphosphate, an activator of the important regulatory enzyme phosphofructokinase in glycolysis (Candy, 1978; Blau and Wegener, 1994). Octopamine also strengthens the cellular defense system by promoting the formation of new haemocytes (Roeder, 1999). Apart from peripheral effects, the generation of motor behaviours originating in the central nervous system is remarkably influenced by octopamine. In the locust, centrally applied octopamine can elicit rhythmic behaviours such as flight, running, swimming or riding, depending on the site of injection, and influences spiking properties of interneurons (Sombati and Hoyle, 1984; Stevenson and Kutsch, 1986; Ramirez and Pearson, 1991). Negative regulation of motor rhythms was observed e.g. in the lobster swimming behaviour (Roeder, 1999) and in the *Lymnaea* buccal motor output (Kyriakides and Mccrohan, 1989). Motivation in general seems to be correlated with octopamine level; the biogenic amine was shown to promote aggression in crickets (Stevenson et al., 2005; Rillich et al., 2010), flies (Zhou et al.,

2008; Potter and Luo, 2008) and honey bees (Robinson et al., 1999). Also desensitisation of visual interneurons can be mediated by octopamine (Stern, 1999, 2009). As a modulator of even more complex behaviours, octopamine in honey bees and flies has been proved to play a major role in appetitive learning (Hammer, 1993; Hammer and Menzel, 1998; Schwaerzel et al., 2003). Taken together, many of these effects imply that octopamine acts, similar to noradrenaline in vertebrates, as a substance mediating stress, arousal ("flight or fight response", see Orchard et al., 1993; Adamo et al., 1995) and enhanced attention, priming the organism to adapt to and cope with specific behavioural demands.

During the recent years, the focus of interest has been extended from octopamine to tyramine, its precursor in biosynthesis, since several studies from different invertebrate species suggested that tyramine may act as an individual neuroactive substance with possibly antagonistic function to octopamine (see Downer et al. (1993); Roeder (2005); Lange (2009); Fox et al. (2006); Fussnecker et al. (2006)). It was shown that mutant *Drosophila* larvae lacking the enzyme tyramine-ß-hydroxylase (Tßh), which mediates the conversion from tyramine into octopamine, displayed deficits in locomotion (Saraswati et al., 2004) and mutant adult flies were limited in their flight performance (Brembs et al., 2007). From these studies it was concluded that balanced levels of both monoamines may be decisive for normal behaviour (Saraswati et al., 2004). Similarly, *C. elegans* Tßh mutants had a distinct behavioural phenotype, which implied a specific role of tyramine in the inhibition of egg laying, reversal behaviour and head oscillations in response to touch (Alkema et al., 2005). Pirri et al. (2009) further stressed this role in the coordination of motor programs and surprisingly found that tyramine may act as a conventional transmitter in *C. elegans* via activation of a chloride-channel. Further evidence for its relevance for locomotion provided Vierk et al. (2009) by showing that depressor motor activity during "fictive flight" in the isolated *Manduca* nervous system was reduced when tyramine receptors were blocked. Cole et al. (2005) and Alkema et al. (2005) identified cells in *Drosophila* and *C. elegans* which expressed tyrosine decarboxylase, the enzyme catalysing the conversion from tyrosine into tyramine, but lacked Tßh, indicating the existence of true tyraminergic neurons. Experiments on peripheral tissue revealed that tyramine antagonises the effect of octopamine at the neuromuscular junction of *Drosophila* (Nagaya et al., 2002) and acts both antagonistically and synergistically on locust oviducts and the spermatheca (Donini and Lange, 2004; da Silva and Lange, 2008). Immunocytochemistry verified that these tissues received partially exclusive tyraminergic innervation. An individual role in *Drosophila* olfaction was proposed by Kutsukake et al. (2000). Recently, Kononenko et al. (2009) described purely tyraminergic cells in the locust brain, suboesophageal ganglion (SOG) and abdominal

fused ganglia.

The pharmacological characterisation and cloning of distinct tyramine receptors (TARs) provided especially potent arguments for an individual role of tyramine. Most of them belong to a family of tyramine/octopamine receptors, which preferentially bind tyramine in several species such as *Drosophila* (Saudou et al., 1990), locusts (Vanden Broeck et al., 1995), the honey bee (Blenau et al., 2000), the cockroach (Rotte et al., 2009), *C. elegans* (Rex and Komuniecki, 2002) and the silk moth (Ohta et al., 2003). These GPCRs have in common that they act via attenuation of adenylyl cyclase and are most efficiently blocked by yohimbine, which sets them apart from characterised octopamine receptors (Evans, 1981; Han et al., 1998; Gerhardt et al., 1997; Robb et al., 1994; Evans and Maqueira, 2005) and stress their similarity to vertebrate α_2-adrenergic receptors. Even specific re-uptake systems have been proposed for tyramine (Hiripi et al., 1994). The diversity of the responses and of receptor pharmacology plus the discovery of novel receptor families (Cazzamali et al., 2005; Pirri et al., 2009) indicate, however, that still many aspects of tyramine function and regulation in invertebrates remain to be identified.

Although in vertebrates octopamine and tyramine only appear as trace amines in nanomolar concentrations, their role has been recently reconsidered and awaits further investigation (Borowsky et al., 2001; Zucchi et al., 2006). However, the fact that the octopaminergic/tyraminergic system in invertebrates shares many physiological and pharmacological features with the noradrenergic/adrenergic system in vertebrates implies functional substitution of these systems (Roeder, 2005).

Similarly to vertebrates, where only a limited number of noradrenergic *Locus coereleus* neurons (approx. 20,000) supplies all major parts of the brain, the number of octopaminergic neurons in the insect nervous system is restricted to only 40-100 neurons. Their distribution is well documented in locusts (Stevenson et al., 1992; Kononenko et al., 2009), cockroaches (Eckert et al., 1992), honey bees (Kreissl et al., 1994), flies (Monastirioti, 1999) and tobacco sphinx moths (Dacks et al., 2005). Among these neuromodulatory neurons, the unique population of efferent dorsal/ventral unpaired median (DUM/VUM) neurons is the most conspicuous and probably best characterised group (Hoyle, 1975, 1978; Watson, 1984; Bräunig and Pflüger, 2001). In locusts, DUM neurons are present in all segmental ganglia of the ventral nerve cord except in the brain, possess somata in medial position on the dorsal surface of each ganglion and project bilaterally to the periphery, thereby exiting the ganglia via distinct nerves according to their affiliation to morphological subgroups (Watson, 1984; Campbell et al., 1995; Duch et al., 1999). Due to their large somata (30-90 μm in diameter) and their location on the dorsal surface, they are easily penetrated with intracellular microelectrodes and identifiable by their large

and characteristic soma spikes (see Grolleau and Lapied, 2000. They have been shown to innervate sets of peripheral muscles (Bräunig, 1997), glands (Bräunig, 1990) and sensory organs like stretch- and strand-receptors (Ramirez and Orchard, 1990; Bräunig and Eder, 1998) and the heart (Ferber and Pflüger, 1990) in abdominal ganglia. In addition, neurohaemal release sites on the surface of peripheral nerves have been described by Bräunig and Evans (1994). Octopamine released from DUM neurons (Evans and O'Shea, 1977; Morton and Evans, 1984; Stevenson and Spörhase-Eichmann, 1995) modulates neuronally evoked skeletal muscle contractions by increasing twitch tension, contraction and relaxation rate and by suppressing myogenic rhythms and reducing a muscle property termed catch-like tension (Evans and O'Shea, 1978; Evans and Siegler, 1982; Whim and Evans, 1988; Stevenson and Meuser, 1997). So far, it is unclear, whether octopamine released from DUM neurons may also play a role in central processing, since output synapses within the ganglia have been encountered rarely (Watson, 1984).

It is striking that efferent DUM neurons are most numerous in the (ptero)thoracic ganglia (19 cells), which house the neuronal machinery for the principal motor behaviours like flight, walking and jumping (Burrows, 1996) and in addition receive projections from many sensory organs possibly providing feedback (Altman et al., 1978; Pflüger et al., 1981; Ramirez and Orchard, 1990): Although it is presumed that the generation of rhythmic motor behaviour such as walking is the result of the interplay of central and peripheral mechanisms both in vertebrates and invertebrates, (Delcomyn, 1980; Grillner, 1985; Bässler, 1993; Pearson, 1993), one can elicit patterned motor output in isolated ganglia of insects by the application of the muscarinic agonist pilocarpine and thus localise the putative central pattern generator consisting of interneurons within the respective segment (Büschges et al., 1995; Ryckebusch and Laurent, 1993). In order to be most effective, peripheral modulation by octopaminergic DUM neurons would thus be expected to be coordinated with the respective motor behaviour, which could either be achieved by central coupling or sensory feedback. Several studies dealing with these issues showed that both mechanisms play a role in DUM neuron recruitment. Previously it was assumed that all locust DUM neurons are concomitantly active during arousal and were found to fire action potentials preceding the onset of specific movements (Hoyle, 1978; Ramirez and Orchard, 1990). This may be true for crawling *Manduca* larvae and walking stick insects, whose VUM/DUM neurons were collectively active (Johnston et al., 1999; Mentel et al., 2008). However, further experiments revealed that thoracic DUM neurons in the locust are differentially coupled to motor behaviours such as kicking (Burrows and Pflüger, 1995), walking (Baudoux et al., 1998) and flight (Duch and Pflüger, 1999) as well as to sensory stimulation (Field et al., 2008; Duch and Pflüger, 1999; Baudoux and Burrows,

1998). In principle, the locust pterothoracic DUM neurons were found to fall into two subpopulations: "Wing group" neurons, which are known or assumed to innervate flight muscles (DUM 1, DUM 3 and DUM 3,4 neurons), are inhibited during flight and other motor behaviours (Burrows and Pflüger, 1995; Duch and Pflüger, 1999), whereas "leg group" neurons (DUM 3,4,5 and DUM 5 neurons), which predominantly innervate muscles of the legs, show often rhythmic activation during motor behaviour and are highly responsive to all kinds of sensory stimulation (Field et al., 2008; Baudoux and Burrows, 1998).

Although the immediate presynaptic neurons are still unknown, it was shown in quiescent animals that DUM neurons belonging to the same subpopulations have many synaptic inputs in common, indicating that they are driven by the same presynaptic neurons; these latter are assumed to be either excitatory or inhibitory local or intersegmental interneurons, some of which may descend from the suboesophageal ganglion (Baudoux and Burrows, 1998; Duch et al., 1999; Johnston et al., 1999). The role of the suboesophageal ganglion in the processing of sensory information, provided to DUM neurons, has been stressed especially, since it was found that most reflex recruitment of DUM neurons depended on whether the connection to the suboesophageal ganglion was intact (Duch et al., 1999; Field et al., 2008). It was thus assumed that DUM neuron activation by sensory input may, different from cycle to cycle motor output during patterned locomotion, rely on a more general evaluation of the "sensory state" of the animal (Field et al., 2008).

In summary, these findings confirmed principle ideas of the "orchestration hypothesis" proposed by Sombati and Hoyle (1984), who suggested that for a specific motor behaviour to occur, the activation of subsets of DUM neurons and local octopamine release may be essential (see also Hoyle, 1985). However, we still lack knowledge of individual DUM neuron integration into central networks and thus of explicit control and activation of the octopaminergic system. Since only few DUM neurons have been individually characterised so far (Evans and O'Shea, 1978; Hoyle et al., 1980; Whim and Evans, 1988) and many of the peripheral targets of the larger groups of DUM 3 and DUM 3,4 neurons remain to be identified, it is possible that DUM neurons may, beyond common activation within the proposed subpopulations, possess a more individual input and output profile than previously assumed, with the consequence of a more adjusted modulation of peripheral targets matching the respective behavioural situation.

Finally, with respect to the significance of tyramine, the question arises, whether DUM neurons, which obviously contain tyramine (Kononenko et al., 2009) may also contribute to central or peripheral release of this neuroactive chemical.

To tackle some of these questions, the current study combines multiple approaches

to highlight (i) aspects of locust pterothoracic DUM neuron activation and (ii) neuromodulator localisation and function in the peripheral nervous system. In the first part, intracellularly recorded DUM neurons were analysed in their response pattern to stimulation of two flight specific pathways: Afferents from the tegula, a knob shaped sense organ at the wingbase, and the tritocerebral giant interneuron, which receives input from wind-sensitive hairs on the forehead, have both been shown to be relevant for the adjustment, resetting and initiation of the flight motor (Kien and Altman, 1979; Pearson and Wolf, 1988; Möhl and Bacon, 1983; Bicker and Pearson, 1983). Stimulation of either of these fibers was performed to investigate DUM neuron recruitment with respect to this motor task.

The second part analyses differential DUM neuron recruitment at the anatomical level and brings up the question, if the well-documented differences between "wing group" and "leg group" neurons with respect to their synaptic input, is reflected on the anatomical level by differential targeting of putative presynaptic inhibitory input synapses. Recently available neuron reconstruction tools facilitated this approach (Schmitt et al., 2004; Evers et al., 2005). These were used to spatially relate co-localised antibody staining, indicating putative GABAergic input sites, to selected branches of the surface of DUM 3,4 and DUM 3,4,5 neurons.

In the last section, the focus shifts to the peripheral nervous system as the principal output site of DUM neuron activity. The small pleuroaxillary flight steering muscle, which has been intensely studied regarding both neuroanatomy and function (Pflüger et al., 1986; Elson and Pflüger, 1986; Stevenson and Meuser, 1997; Meuser and Pflüger, 1998; Biserova and Pflüger, 2004) is known to be innervated by an identified DUM 3,4,5 neuron and served to address the following objectives: First, to elucidate the distribution of octopamine and tyramine with the help of reliable antibodies. Second, to examine the neuromodulator distribution in single varicosities in dependence of precedingly induced activity, namely tethered flight and arousal. Since in the locust central nervous system the ratio between octopamine and tyramine in DUM neurons was biassed to higher octopamine levels in DUM neuron somata, if the animal had been previously exposed to stress (Kononenko et al., 2009), similar dynamics on the level of single boutons are possible. Third, tyramine effects on muscle performance were determined in relation to octopamine and in presence of an octopamine receptor blocker to approach the question of possible tyramine release from DUM neuron terminals.

Drawing on physiological and anatomical data, this study provides further evidence of specific pathways for DUM neuron activation which are suited to match behavioural requirements during flight, and argues that on locust muscle tyramine may be restricted to its role as octopamine precursor.

2 Materials and Methods

2.1 Animals

Individuals of both sexes of *Schistocerca gregaria* (Forskål) were taken from our crowded colony at the institute of neurobiology (FU Berlin). Animals were kept at a constant 12 hour light/dark cycle at a temperature of 28°C. Prior to experiments, if not stated otherwise, the locusts were anaesthetized by chilling at 4°C for at least 30 minutes.

2.2 Antero-/retrograde nerve staining

The method is representatively described for the antero- and retrograde staining of N4D2/4. Locusts were mounted laterally in plasticine to bare the thoracic pleura. The motor nerves N4D4, innervating the pleuroaxillary flight steering muscle (M 85/ M 114) of the meso- or metathorax, or N4D2, innervating the (bifunctional) elevator muscle 120 (metathorax), were exposed by cutting a small window into the cuticle of the posterior pleuron of the second or third thoracic segment and removing the dorsoventral depressor muscle 129. The intact nerve was carefully cut and either its distal (for anterograde staining) or proximal (for retrograde staining) end enclosed by a vaseline pool subsequently filled with distilled water. After 10 minutes the water was exchanged for a neurobiotin (Neurobiotin tracer, Vector Laboratories) solution (10% in distilled water). The pool and the wound itself were sealed with vaseline and animals were placed in a moist chamber from 10 to 24 hours at 4°C to enable dye diffusion. Prior to fixation, muscles were excised together with their attachment sites at the pleural ridge and the axillary sclerite and transferred to a Sylgard dish filled with isotonic locust saline (Ringer's solution: 150 mM NaCl, 5 mM KCl, 5 mM $CaCl_2$, 2 mM $MgCl_2$, 10 mM HEPES, pH 7.4). In case of retrograde staining, the thoracic ganglia were isolated and freed from connective tissue, fat and trachea. For subsequent tissue fixation and further processing see 2.6.
The nomenclature of nerves and muscles is used according to Campbell (1961) and Snodgrass (1929).

2.3 Steady flight performance and stress exposure

Since central amounts of octopamine (OA) and tyramine (TA) change dynamically according to the locust's behavioural state (Kononenko et al., 2009), we were interested in whether peripheral OA and TA levels reflect respective pre-treatment as well. Animals of both sexes were either kept perfectly calm (N=6), constituting the control group, agitated and exposed to different disturbant stimuli (such as noise and visual

cues) for 15 to 20 minutes inside a plastic box (stressed group, N=4) or kept flying for 30 min to 1 hour (flight group, N=5). Steady flight was enabled by gluing (Pattex) a light metal clip to the locust's pronotum and linking it to a stand via a thin flexible plastic tube. Lack of tarsal contact to the ground and frontal exposure to a warm and perturbed air stream elicited flight in otherwise untethered animals. After the respective time interval the muscles were quickly dissected and fixed immediately as described in 2.6.

2.4 Intracellular recordings and sensory stimulation

Recording and staining of DUM neurons

Anaesthetized locusts of either sex were mounted with the dorsal side up in plasticine. Wings, legs and abdomen were either fixed with plasticine or removed. For thorax preparations animals were decapitated. A dorsal medial incision opened the thorax longitudinally right between the dorsolongitudinal flight muscles M85/M112. After removal of gut and sclerites, the meso- and metathoracic ganglia were exposed and supported by a wax-coated platform of stainless steel. Depending on the experiment, the ganglia were deafferentated. For experiments on isolated ganglia, the latter were dissected and transferred to a Sylgard dish filled with locust saline. Crystals of protease (P-5147, Sigma) applied directly onto ganglia for 1 to 2 minutes permeabilized the perineurum to facilitate the subsequent penetration with glass microelectrodes (Borosilicate, thick-walled, 1 mm diameter). Electrodes had a resistance of 20 to 50 MΩ and tips were filled with a 2 M potassium chloride solution containing 10% neurobiotin (see 2.2) and optionally crystals of dextran tetramethylrhodamine (MW 3000, anionic, lysine fixable, Molecular Probes). DUM neurons were identified due to their position in ganglia and their large overshooting soma spikes of characteristic size, duration and afterhyperpolarization. Signals were visualized with an oscilloscope (Gould 1425, Essex, U.K.), digitalised via an A/D converter (Power 1401Plus, CED) and recorded with Spike2 6.11 (CED). After successful recordings, DUM neurons were iontophoretically dye-filled by application of depolarising voltage pulses of 200 ms duration at 3 Hz, delivered by a stimulator (SD9, Grass Technologies, W.Warwick, RI U.S.A.), or constant current, respectively, resulting in a current injection of 2-8 nA for 20 to 40 minutes. Ganglia were subsequently isolated and fixed as described in 2.6.

Sensory nerve stimulation and extracellular recordings

To mimic excitation of the tegula, a knob shaped sense organ at the wing base, or the tritocerebral giant (TCG) interneuron, either nerve N1C1(a) or the tritocerebral

commissure (TCC) were stimulated. The stimulation sites are schematically illustrated in figure 4.1. To render the TCC accessible, the head capsule was opened

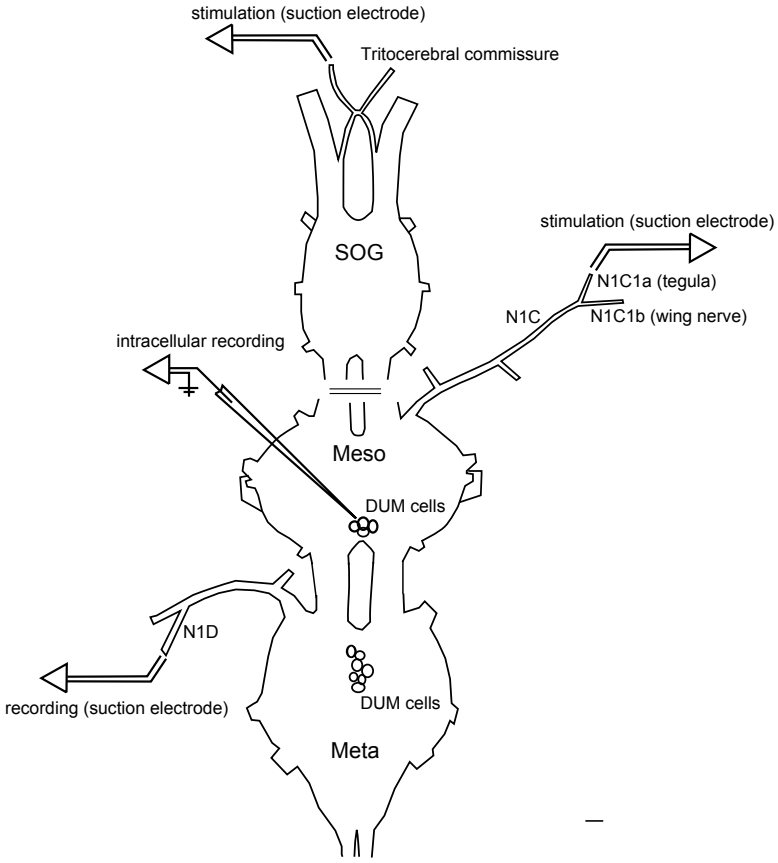

Figure 4.1: Stimulation scheme. Recording and stimulation site(s) at the suboesophageal, meso- and metathoracic ganglion (SOG, meso, meta). Either the suction electrode was positioned at the tritocerebral commissure (circumoesophageal connectives cut) for TCG stimulation, or placed at N1C1(a) to stimulate tegula afferents. DUM neurons from either the meso- or metathoracic cluster were recorded intracellularly. Motor activity in the metathoracic nerve 1D was monitored via a suction electrode. The lengths of the nerves (N1) are not sketched in scale. Scale bar 100 μm

dorsally with the help of a razor blade. The tentorium, mandibular muscles and the brain were abscised. Dissection of the tegula nerve required partial removal of the dorsoventral flight power muscles and of the dorsolongitudinal indirect flight muscles M85/M112. The nerves were carefully cut and taken up by a suction electrode. Either single stimuli of 0.1 ms duration at frequencies ranging from 1 to 10 Hz or stimulus trains of 100-500 ms duration at 100-200 Hz (single stimulus duration 0.1 ms) were applied by a stimulator via a stimulus isolation unit (S 48 and SIU5, Grass Technologies). The voltage pulses conveyed ranged from 2.5 to 8 Volt. Although excitation of wing nerve afferents could not be fully excluded, the stimulation of N1C1 to address tegula fibers has been performed in similar paradigms (Pearson and Wolf, 1988; Duch and Pflüger, 1999) and takes advantage of the fact that tegula afferents possess the largest diameter axons within N1C1 with up to 10 μm, whereas wing nerve

afferents, conveying information from wing surface sense organs like campaniform sensillae, are considerably smaller in diameter with less than 1 μm (Altman et al., 1978; Kutsch et al., 1980). Thus application of moderate voltages in the range of the excitation threshold for large fibers provides a means to selectively stimulate tegula afferents (Pearson and Wolf, 1988). The same holds true for stimulation of the tritocerebral commissure (TCC), where the large diameter axon of TCG measures 10-20 μm in diameter (Bacon and Tyrer, 1978) and is thought to be more readily excited than the axon of the second descending interneuron running through TCC, the tritocerebral "dwarf" (TCD), whose diameter amounts to only 4-5 μm (Tyrer et al., 1988).
The neurons were exposed to stimulation sequences of 1, 2, 5 and 10 Hz of at least 10 seconds with an intersequence interval of at least 30 seconds. For evaluation of their tendency to habituate, their responses to the first 10 stimuli of each sequence were calculated and determined as response rate.
In some cases an extracellular recording of metathoracic N1D via a suction electrode served to simultaneously monitor activity of flight depressor motor neurons during an experiment (see Neville (1963); Bentley (1970). The signals were preamplificated 1000fold (P55 A.C., Grass Technologies) and recorded as described above (see 2.4).

2.5 Muscle mechanograms and application of neurochemicals

Isolated flight steering muscles M85 or M114 (for preparation protocol see 2.2) with an intact motor nerve were pinned down as under natural conditions at their cuticular attachment sites in a Sylgard dish filled with isotonic locust saline. The axillary sclerite was linked to the sensitive element of a force transducer (SG 4-25, 41030, Swema) via a small metal hook coupled to a wire. The muscles were thereby held in approximately the same position. Stimulation of the motor nerve was achieved via a suction electrode transmitting voltage pulses of 1.8 V and 2 ms duration from a stimulus isolation unit connected to a stimulator (SIU5 and S 48, Grass Technologies). It is assumed that during motor nerve stimulation only the large motor neurons are excited, whereas the DUM 3,4,5 neuron innervating this muscle remains silent due to its smaller axon diameter and does not influence the measurements by additional octopamine release (Stevenson and Meuser, 1997). Signals encoding muscle force were amplified (DC1-S, Nr.116, Svemor), digitalized (Power 1401plus, CED) and recorded with the software Spike2 6.11 (CED). Before an experiment was run, muscles were continuously stimulated for about 5 min at a frequency of 0.5 Hz. Prior and during application of different substances dissolved in saline, namely D,L-octopamine-hydrochloride (Sigma), tyramine-hydrochloride (Sigma) and epinastine-hydrochloride (Sigma) in concentrations ranging from 0.1 mM to 0.1 μmM muscles were perfused

by saline at constant temperature (20-22°C) by means of a peristaltic pump. In cases where different substances were applied in succession, a wash-out of at least 10 minutes, until the response had diminished, preceded any new application. Relative changes of twitch tension, relaxation rate and contraction rate were extracted using Spike2 and subsequently evaluated with MATLAB R2007b (The MathWorks).

2.6 Immunocytochemistry

Octopamine and tyramine immunocytochemistry on muscles

Isolated muscles (for preparation protocol see 2.2) were fixed in 1% glutaraldehyde and 2% paraformaldehyde in 0,1M PBS (phosphate buffered saline, pH 7,4) for about 3 hours. After rinsing in PBS for 2 hours and dehydration by means of an ascending ethanol series (50%, 70%, 90%, 100%, 10 minutes each) the preparations were cleared in xylol (Merck) and subsequently rehydrated (100%, 90%, 70%, 50%, PBS). To reduce unspecific staining, 1% sodium borohydride (Merck) in PBS was applied for 10 minutes followed by incubation in 1% Triton X-100 (TX, Sigma) in PBS for better penetration of subsequently applied antibodies (2h). For another 1-2 hours the preparations were preincubated in 10% natural goat serum (NGS, ISN Biomedicals) in 1% TX in PBS to block unspecific binding sites. Primary antibodies used were a synapsin I (SynORF, 3C11) and a NC82 antibody (both anti-mouse, kindly provided by Prof. Erich Buchner, Würzburg) applied at a dilution of 1:7 (SynI) and 1:100 (NC82), a monoclonal octopamine antibody (anti-mouse, Bioscience, Jena, see Dacks et al. (2005)), 1:1000, and a polyclonal antibody to tyramine (anti-rabbit, Chemicon, see Kononenko et al., 2009), 1:500. To prevent samples from fungal infection, 0,02% sodium acid was added to the 1% TX 1% NGS antiserum solution. Binding of antibodies occurred at 4°C on a shaker for at least 3 days, followed by incubation in 1% TX in PBS for approximately 2 hours. Secondary antibodies, Cy2- or Cy3-conjugated goat anti-mouse (Dianova), for synapsin I, NC82 and octopamine, Cy3-conjugated streptavidin (Dianova) for amplification of neurobiotin, and Cy5-conjugated goat anti-rabbit (Dianova) for tyramine (all diluted at 1:200) were added in reasonable composition and kept overnight at room temperature. After repeated washing in PBS for 2 hours the preparations were dehydrated (50%, 70%. 90%, 100%) and finally mounted in methylsalicylate (Merck).

Synapsin- and GAD-immunocytochemistry on vibratome sections

Thoracic ganglia were fixed in 4% paraformaldehyde in 0,1M PBS for 12 to 16 hours (overnight). PBS incubation, de- and rehydration was performed as for muscle whole-mounts except of substitution of xylol by methylsalicylate. Ganglia with only nerve

roots left were rinsed in PBS for about 15 minutes and prior to embedding in viscous 5% Agarose solution (dissolved in Aqua dist. at 60 °C) carefully dried on filter paper. Hardening of the embedding medium occured at 8°C for at least 1 hour. Horizontal sectioning of trimmed blocks with a vibratome (VT 1000S, Leica, Wetzlar, Germany) yielded slices of 35 to 50 μm. Agarose slices were stored in PBS and, as described for muscles, subsequently treated with 1% sodium-borohydride (Merck) in PBS for 10 minutes, followed by 0,5% TX/PBS treatment for 2 hours and incubation in 2% BSA (Bovine serum albumine, Sigma), dissolved in 0,5% TX/PBS, for 1-2 hours. The primary antibodies, a synapsin I antibody (see 2.6) and commercially available antibodies to glutamic acid decarboxylase 65/67 (AB1151, Millipore) and to GABA (A2052, Sigma) were applied in a concentration of 1:400 in a 0,5% BSA/0,5% TX/0,02% sodium acid/PBS solution. The sections were gently stirred at 4°C for 5 days, followed by 2 hours of washing in 0,5% TX in PBS and secondary antibody application (see 2.6 for 8 to 48 hours at room temperature or 4°C, respectively. After at least 2 hours of rinsing in PBS, sections were successively transferred to glycerin/PBS mixtures with increasing share of glycerin (1:3, 1:1 and 4:1 gylcerin:PBS, 15 minutes each) and finally mounted in 4:1 glycerin/PBS onto glass slides (Roth).

2.7 Confocal microscopy and quantitative evaluation of data

Image acquisition

Immunofluorescent labels were visualized and scanned with a confocal scanning microscope (TCS SP2, Leica, Germany). For the scanning of neuropil or muscle stainings served either a HC PL 10x/0.5, a HC PL 20x/0.7 imm, a HC PL 40x/1.4 imm or a HC PL 63x/1.52 imm objective at a maximal zoom factor of 3. Signals from fluorophores were detected in serial stacks of appropriate slice numbers with a step size of 0.3 (Synapsin I- and GAD-immunolabels within the neuropil), 0.5 or 1 μm, respectively, and at an image resolution of 1024 x 1024 pixels. For sample stack generation of stained muscle tissue three different regions per muscle (proximal, medial, distal) were chosen and stacks of constant dimension and magnification were scanned (x,y 0.15 μm, step size 1 μm), at, as far as possible, constant laser intensity. Excitation of fluorescent dyes was enabled by usage of three different laser lines: an Ar/Kr-Laser at 488 nm and two He/Ne-Lasers at 543 nm and 633 nm. Images were scanned in a sequential mode to confine cross-excitation of different dyes. For analysis image stacks were processed with the software package Amira 4.1.1 (TGS, Mercury Computer Systems, Merignac, France).

Threshold-dependent labelling and evaluation of immunofluorescent staining

All images obtained from confocal microscopy were preprocessed to correct for slight gradients (module "correct z-drop" in Amira) and reduce background (median filter, rolling ball algorithm in ImageJ, open source software). Subsequently, the threshold for accepting voxels as immunopositive staining was determined for each image stack labeled with anti-SynI and anti-GAD separately. This was accomplished in the "Labelfield" mode in Amira. During the process the grey value histogram of each stack was examined in parallel, where profound slope changes indicated the transition from background to specific staining. The definite value was matched with an automatically assessed threshold value reflecting the 10 % brightest voxels. Since the label distribution within the neuropil was quite uniform, this represented a means to correct for intensity differences between image stacks. Threshold determination of neuromodulatory varicosities on muscular tissue was performed similarly. To assess bouton volumes one chain of varicosities per image stack was selected and labeled accordingly. This was performed two times by choosing a lower and a higher threshold value comparable for all samples dependent on the grey value histogram (see above), which went equally into the evaluation. Samples were processed in a random mode to exclude personal bias. Volume data were then obtained from the Amira table "Tissue Statistics". Additionally, from each segmented stack the mean grey value data of the so determined background and specific staining were extracted and used for a comparison of signal-to-noise, i.e. intensity ratios. Diagrams were designed and statistics (nonparametric tests) performed with MATLAB R2007b (The Mathworks).

Neuron reconstruction and distance map analysis

The geometric 3-dimensional reconstruction of selected dendrites was performed semi-automatically with a plugin tool implemented in Amira (Schmitt et al., 2004). Briefly, it is based on the model of generalized cylinders, which for reasons of simplicity are circular in cross-section, build segments and constitute the so called skeleton. An active contour model (snake algorithm) is used to fit the shape of the curve, thereby also adjusting midline and diameter. This is achieved by minimizing an energy functional. Energy is lowest, if bright voxels are assigned to the skeleton and a certain smoothness is preserved along the curvature and radii changes of the axes. Advantageously, coarse and thin structures are likewise comprised since only relative intensity differences are considered.

It was taken advantage of an Amira script ("autoskeleton") for the automatic generation of an initial skeleton version based on a threshold-dependent labeling of the stained neuron ("Labelfield" mode). Fitting to the data by application of the named

algorithm followed subsequently. Descriptive skeleton parameters like radius, segment length and branching orders are easily obtained ("SkeletonStats"). However, due to the idealized skeleton shape, a precise and reliable localization of immunolabels relative to the neuron (to extract putative synaptic contacts) is confined. This analysis was enabled by the generation of a surface (Amira module "ComputeSurface"), relying both on the original data and the information provided by the skeleton, using the geodesic active contours method (Schmitt et al., 2004). The staining intensities (grey values) of anti-synapsin and anti-GAD immunolabels were then assessed within a distance of 300 nm to the neuron surface, a value which accounts for the width of synaptic cleft (Rollenhagen and Lübke, 2006), presynaptic membrane and reserve vesicle pool, with the help of the module "TextureCorrelate". In consideration of a correlation factor, the assessed staining intensities of co-localised voxels were then mapped onto the surface. Since each triangle, the individual element of the surface, can be assigned to a respective skeleton element (module "SurfToSkel"), statistical data concerning the intensity values of all surface triangles were available. The data were exported to MATLAB for further analysis.

3 Results

3.1 Responses of DUM neuron subtypes to N1C1(a) and TCC stimulation

General remarks to DUM neuron responses

The following experiments were performed to elucidate two specific flight- relevant pathways in their role for providing input to DUM neuron subtypes. Stimulating pulses were selectively delivered to either N1C1(a), through which run tegula afferents, or to the tritocerebral commissure (TCC) in order to excite the tritocerebral giant interneuron (TCG). In both cases the stimulus voltage applied was assumed to excite only the fibers of larger diameter (see Methods 2.4). In cases where a DUM neuron responded with a postsynaptic potential (PSP) to N1C1(a) stimulation, slight increases of voltage delivered to the nerve sometimes resulted in a larger amplitude, probably indicating the recruitment of additional fibers. The response latencies observed and noted (table 1.2) are, if not otherwise stated, the time intervals measured from stimulation onset to DUM neuron reaction. The delay of conduction via the respective fibers was not independently determined in this study, but estimated from existing literature (Kien and Altman, 1979; Burrows and Fraser Rowell, 1973; Boyan and Ball, 1989) with respect to the preparation used (see Methods, 2.4).

To correlate DUM neuron activity to motor behaviour, in some cases a flight related acitivity was monitored in metathoracic nerve 1D, which contains axons of depressor motor neurons with somata in the meso- and metathoracic ganglion (fig. 1.1C), see also Neville (1963)). Only in some cases could rhythmic activity be evoked by either stimulation (fig. 1.1B, upper trace), but sporadic activity of motor units was often observed and sometimes appeared even correlated to DUM neuron activity. A phenomenon common to all neurons investigated was the attenuation or even the cessation of the responses during repeated stimulation. This property was determined as habituation, since the initial responsiveness returned after an interval without stimulation. The habituation was assumed to be a property of the interneurons conveying the signal from sensory afferents to DUM neurons - it was unlikely to result from synaptic depression at the afferents' presynapses, since tegula afferents in flying locusts have been shown to be responsible for the timing and shape of the repetitively occurring depolarisations in ipsilateral elevator motorneurons during flight (Wolf and Pearson, 1988). On the other hand, the habituation is, in the case of excitatory responses, possibly not owed to adaptation at the spike initiating zone(s) of the DUM neurons, since DUM neurons which habituated to a specific stimulus were still responsive to stimulation of different sensory modalities (own data and Field et al., 2008). It is thus conceivable that the attenuation occurred on the

Table 1.1: Cell numbers and innervation targets of DUM neuron types of the meso- and metahoracic ganglia. Key of abbreviations: 1 Bräunig and Evans, 1994; 2 Bräunig, 1997; 3 Evans and O'Shea, 1977; 4 Hoyle, 1978; 5 Kutsch and Schneider, 1987; 6 Stevenson and Meuser, 1997; 7 Watson, 1984; 8 Whim and Evans, 1988; N Number of cells; M Muscle; Ref. References.

Segment	Cell	N	Known peripheral targets	Ref.
Mesothorax	DUM 1b	1	Ventral longitudinal muscles, spiracle muscle, transversal nerve, salivary glands	1
	DUMDL	1	Dorsolongitudinal flight muscle M81	4,8
	DUM 3	5		
	DUM 3,4	6	N4: M90, M99	5
	DUM 3,4,5	4	N4: M85 N5: Ext. tibiae, flexor tibiae	6
	DUM 5	2		
Metathorax	DUM 1b	1	Ventral longitudinal muscles, spiracle muscle, transversal nerve, salivary glands	1
	DUMDL	1	Dorsolongitudinal flight muscle M112	4,8
	DUM 3	5		
	DUM 3,4	6	N4: M113, M119, M120, M129	5
	DUM 3,4,5	3	N3: M121, M125, M126, M133, M135 N4: M114, M115, M122, M123, M124, M132 N5: M133a, M136	2,6
	DUMETi (5a)	1	M135	3,4,7
	DUM 5b	2		

interneuron level, possibly due to diminishing transmitter release with ongoing stimulation. The strength of habituation may also reflect the amount of processing in interneurons.

Table 1.1 displays an overview of cell numbers and targets of meso- and metathoracic DUM neurons derived from previous publications, on which bases the subdivision of these neurons into "wing" (DUMDL; DUM 3; DUM 3,4) and "leg group" (DUM 3,4,5; DUM 5) neurons. Apart from DUM 5 neurons, individuals of all subtypes were recorded in this study and subsequently identified by intracellular staining. In table 1.2 the data of this study are summarized and compared with previous work.

DUM 1 neurons

Apart from DUM 5 neurons, DUM 1 neurons are the least numerous subgroup with only two individually identifiable neurons, DUMDL (DUM 1a) and DUM 1b. DUMDL has been proposed to be affiliated to the "wing group" neurons, since its innervation targets are the indirect dorsolongitudinal (DL) flight muscles M85/M112 (table 1.1). Previous data have shown that DUMDL responds to touch of antennal sensillae with excitation (Field et al., 2008)(table 1.1). In response to N1C1(a) stimulation DUMDL tended to receive IPSPs in 3 out of 4 recorded cells (fig. 1.1), but latencies varied widely among individual cells, namely from 15 ms, recorded following

stimulation of N1C1 in isolated ganglia, to 120 ms in preparations, where the tegula nerve itself (N1C1a) was excited. The habituation during stimulation sequences of different frequencies (1 to 10 Hz) was prominent, meaning that the inhibitory responses disappeared during ongoing stimulation, such that only the first stimulus/i elicited inhibitory potentials. As a measure for the degree of habituation served the response rate during a stimulus sequence of 10 stimuli, where 1 signifies no habituation. DUMDL neurons had a mean response rate of 0.41 ± 0.27. In cases where habituation to the stimulus would not occur readily, the latencies of consecutive IPSPs increased by up to 25 % during stimulation sequences. Altogether, these data confirm previous results (Duch and Pflüger, 1999), showing evidence for a segmental polysynaptic pathway from tegula afferents to DUMDL.

Interestingly, in an experiment where N1D of the metathorax was recorded in parallel to a mesothoracic DUMDL neuron (figs. 1.1A/B), inhibitory responses of DUMDL to N1C1a stimulation always coincided with marked activity in N1D, possibly indicating the activation of the flight motor. However, these bursts lasted for less than 0.5 seconds in most cases and were not induced reliably. The IPSP response of DUMDL occurred almost synchronously with the onset of enhanced motor neuron activity in this preparation and failed to appear, if the motor neurons did not respond to stimulation (figs. 1.1A/B). Surprisingly, stronger motor bursts were correlated with action potentials in DUMDL (fig. 1.1B). Since the spikes in N1D arrived with a delay of a few milliseconds at the recording site, these seemed to precede DUMDL reactions. This would support the notion that DUM neuron activation is coupled to motor activity, however, the obvious complexity of the response can hardly be resolved by these experiments.

The second DUM 1 neuron, DUM 1b, is one of the least investigated cells of the DUM neuron group. Since its targets are not primarily involved in wing or leg movements, it cannot be assigned to any of the functional DUM neuron subgroups, but has a unique status (table 1.1). Supporting this, in previous studies DUM 1b showed no distinctive activity patterns in response to motor behaviour or sensory stimulation of diverse kind (Burrows and Pflüger, 1995; Baudoux and Burrows, 1998). In the present study two neurons of this type were intracellularly recorded and subjected to TCC stimulation. This was performed with 100 to 200 Hz stimulus trains corresponding to the TCG discharge frequency following activation of wind-sensitive hairs on the forehead (Bicker and Pearson, 1983). Reliably, both DUM 1b neurons fired action potentials in response to TCC stimulation (fig. 1.2A), hinting to an excitatory pathway from TCG to this DUM neuron subtype. The latencies in both cases varied only mildly and the minimal delay recorded was 22 ms. In consideration of the time for the signal to reach the metathoracic ganglion, where both neurons

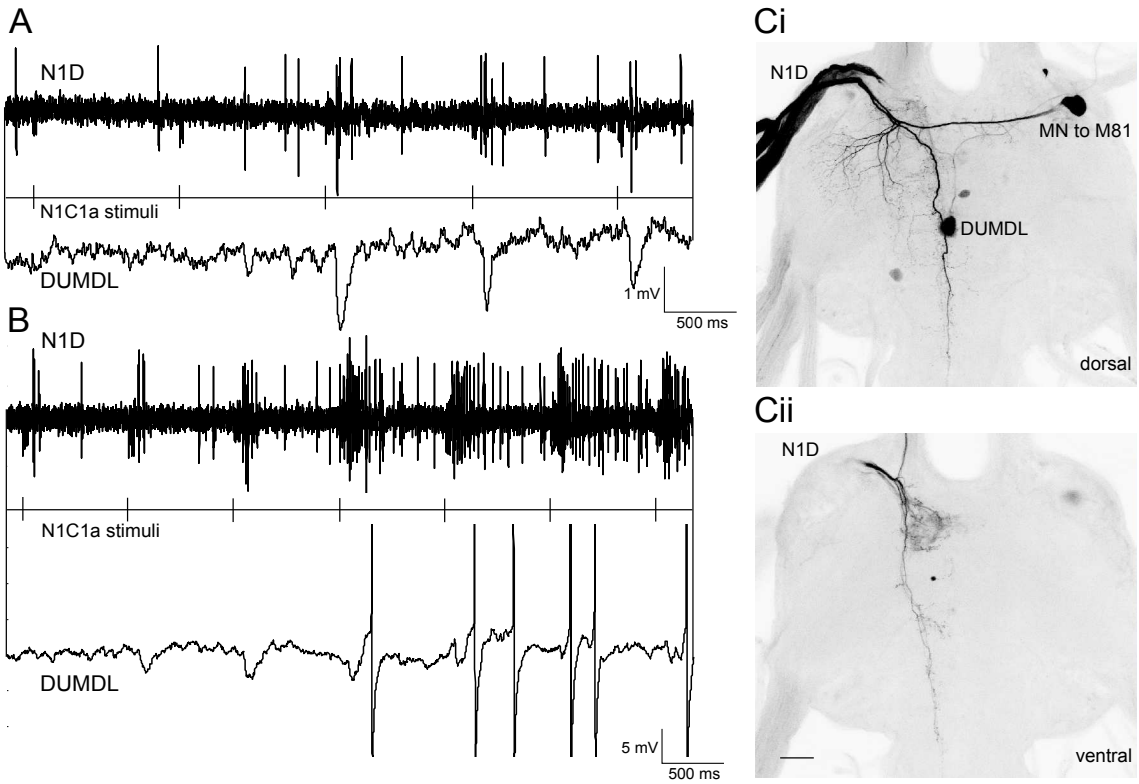

Figure 1.1: Recording of DUMDL in response to N1C1a stimulation and in correlation with N1D activity. **A**: Following N1C1a stimulation with 200 Hz trains at 1 Hz DUMDL receives IPSPs, but only simultaneously with increased N1D activity. **B**: Short bursts of rhythmic activity in N1D following N1C1a stimulation coincide with excitation of DUMDL. **C**: Retrograde nerve staining of N1D with neurobiotin reveals one prominent motorneuron to M82, DUMDL and stretch receptor afferents in the dorsal neuropil of the metathoracic ganglion (Ci). Sensory projections of undetermined provenance are stained within ventral neuropils (Cii). Z-Dimension of entire image stack 245 μm. Scale bar 100 μm.

were impaled (at an assumed average conduction velocity for TCG of 3 ms/mm), the latency within the ganglion may amount to 17 to 18 ms. This delay surely is to long to represent a monosynaptic connection, but, on the other hand, possibly implies only few interneurons conveying the signal. During sequences of constant stimulation, consecutive spikes appeared with a prolonged delay of up to 2.5 times (fig. 1.2C) and failed to appear, especially if the stimulus frequency was increased (fig. 1.2A). However, in these cases EPSPs, which continuously became smaller, were still observed. The habituation, determined by the response rate of on average 0.8 $\pm$ 0.2, was comparably low, but yet indicated that during maintained stimulation at higher frequency the neurons failed to respond.

Fig. 1.2B verifies the identity of one of the DUM 1b neurons with its axon projecting into the recurrent nerve (RN).

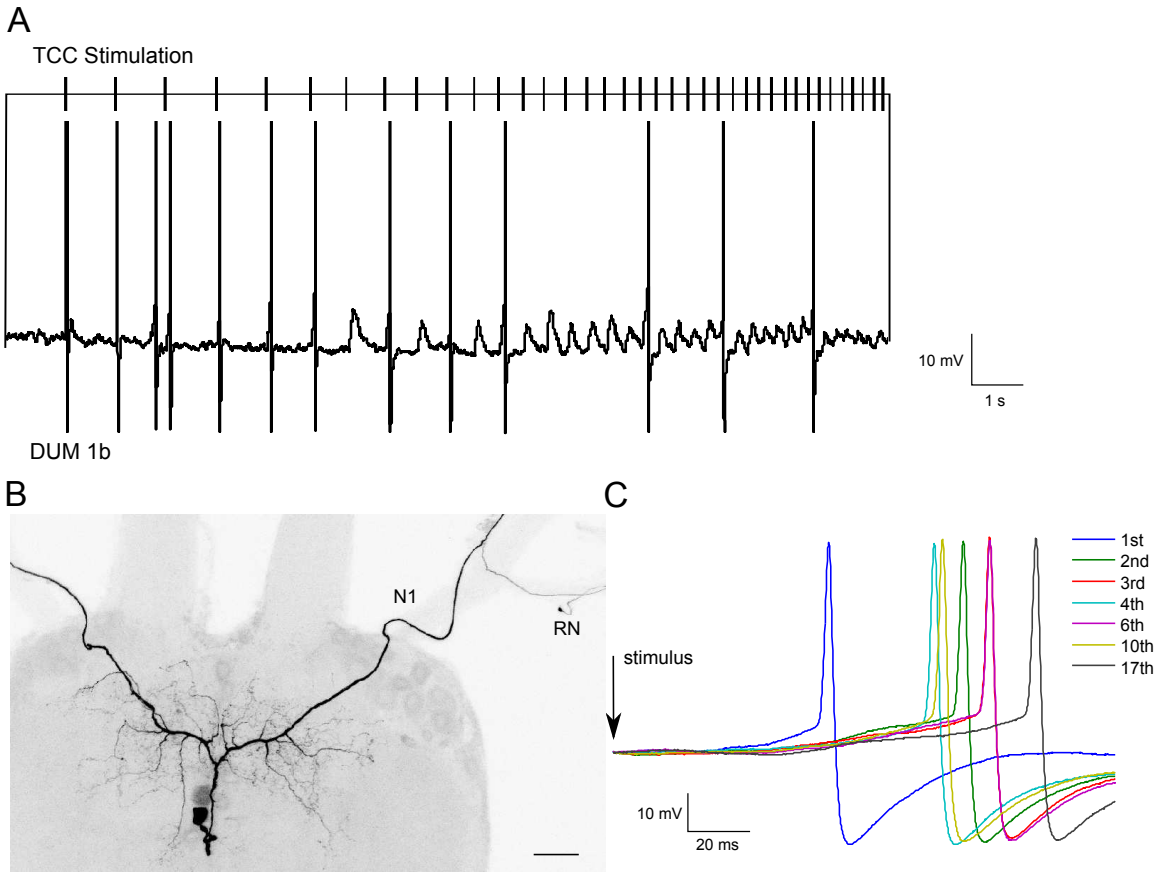

Figure 1.2: DUM 1b response to TCC stimulation. **A**: DUM 1b generates action potentials (APs) following TCC stimulation at approximately 1 Hz, which fail to be elicited with increased stimulation frequency (5-10 Hz). However, EPSPs are still observable. **B**: Identification of a metathoracic DUM 1b neuron by intracellular staining. Compared to DUMDL, DUM 1b has a smaller soma size and an axon in N1A and the recurrent nerve (RN). Scale bar 100 μm. **C**: Overlay of seven successive APs derived from a stimulation sequence of constant stimulation frequency (1 Hz). Note the increase of latency during maintained stimulation.

DUM 3 neurons

Although the innervation targets of DUM 3 neurons are unknown, the information gathered so far favors the notion, that DUM 3 neurons functionally belong to the "wing group" neurons, together with DUM 3,4 neurons and DUMDL (table 1.1). This is supported by the fact, that DUM 3 neurons often have inhibitory potentials in common with simultaneously recorded DUM 3,4 neurons (Baudoux and Burrows, 1998). Interestingly, this population exhibits a distinct anatomical structure, for their middle, "b", branches (see next section) are less developed than those of all other DUM neuron subtypes; a feature, which seems to be compensated by excessive arborisations and sometimes conspicuous branches within the lateral branch groups (fig. 1.3E).

During recordings in semi-intact preparations, the fast and small-amplitude changes in the membrane potential of DUM 3 neurons presumably reflected contin-

uous synaptic drive, and preferentially inhibitory postsynaptic potentials (IPSPs) were encountered. Some of the cells recorded in this study were responsive to touch of the antennae, but in an ambiguous fashion, and no clear picture emerged from these data; this was in accordance to previous data, which either reported of silent DUM 3 neurons following antennal or wind-sensitive head hair stimulation (Duch and Pflüger, 1999) or variable responses dependent on the arousal state of the animal (Baudoux and Burrows, 1998).

The response of DUM 3 neurons to N1C1(a) stimulation confirmed previous data (Duch and Pflüger, 1999) as well. The neurons showing responses (5 of 10 recorded cells) to single stimuli (5-10 Hz) and 100 Hz stimulus trains (1 Hz) received exclusively IPSPs following stimulation of either mesothoracic N1C1 or N1C1a; one of the reactive cells was situated in the metathoracic ganglion. The inhibitory character of the PSPs was verified by current injection into the neuron (fig. 1.3A); depolarisation resulted in amplification of the IPSP amplitude, which at the resting potential amounted to about 3 mV. Increasing the stimulus voltage sometimes evoked larger IPSPs, hinting to the recruitment of additional fibers and a presumably stronger excitement of central postsynaptic INs conveying the signal to DUM neurons.

The latencies from stimulus onset to DUM 3 reaction were not short enough to indicate monosynaptic connections, but suggested at least one IN between afferents and recipient cell (table 1.2). The shortest latency amounted to 11 ms and was observed in a semi-intact preparation with complete CNS; however, on average higher values around 28 ms were registered, especially in the thorax preparations. In one semi-intact preparation, where the connectives between prothoracic and suboesophageal ganglion were cut in between successive stimulation sequences, responses were observed before and after dissection with only a slight latency increase of 11 %, showing that one/the pathway was immanent in the absence of SOG and higher brain centres and thus probably segmental. In general, during the course of a repetitive stimulation of 1 to 10 Hz the latencies tended to prolong mildly by up to 26 %. This may be part of the habituation process observed. The mean habituation for DUM 3 neurons (in terms of the response rate to the first 10 stimuli of a stimulation sequence) was 0.68 $\pm$ 0.35 1.3D. Thus the ability of neurons to follow each stimulus at this frequency was quite weak, supporting the polysynaptic nature of the pathway. The tendency of DUM 3 neurons to habituate showed no obvious dependence of the stimulus frequency applied, but varied among individual neurons.

In summary, the reaction of DUM 3 neurons to tegula stimulation confirmed an inhibitory response. The mediating neurons are assumed to lie within the thoracic ganglia, since the response was registered in isolated thorax preparations as well as after dissection of the neck connectives. However, alternative pathways may exist.

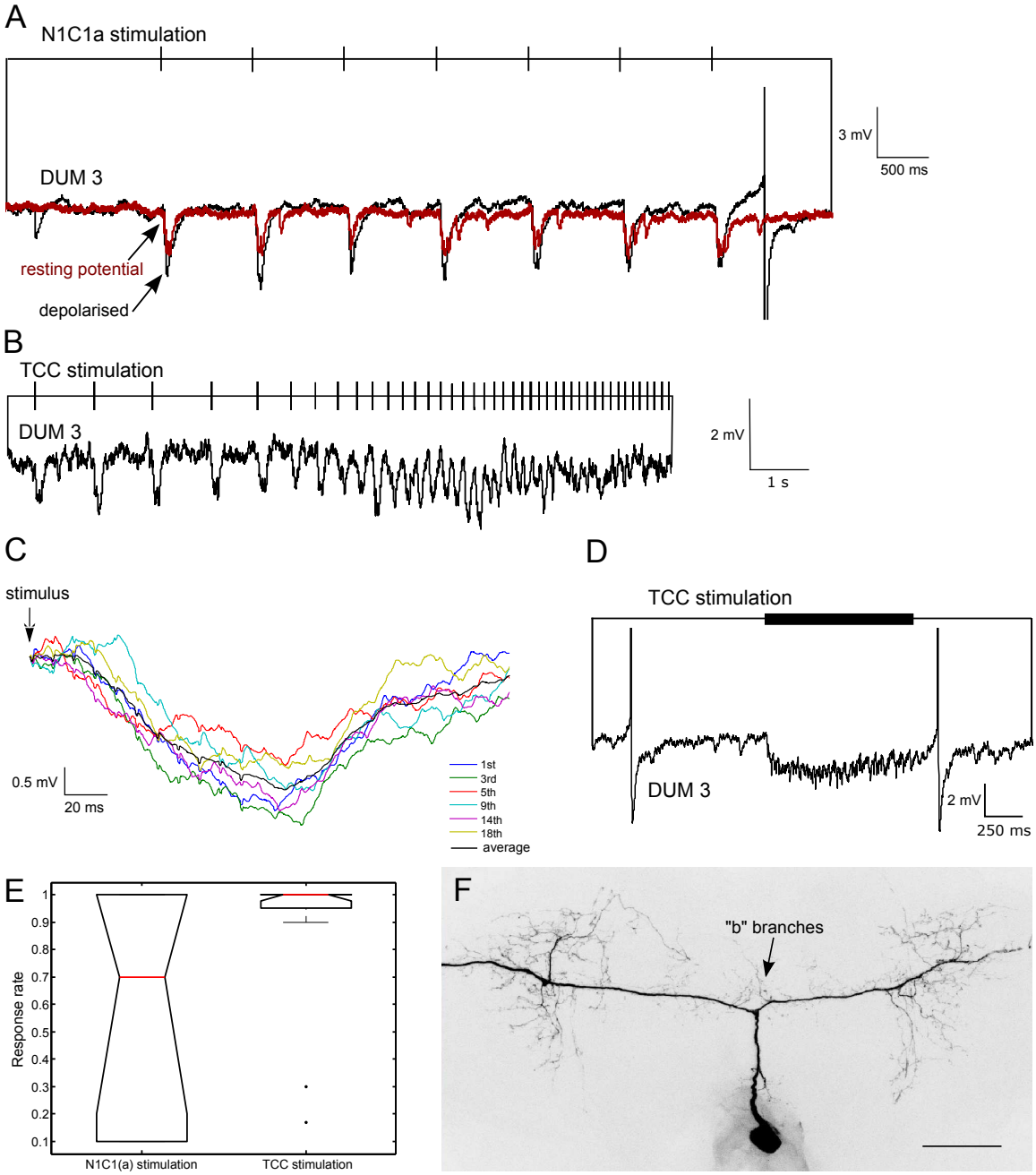

Figure 1.3: DUM 3 neuron responses to N1C1(a) and TCC stimulation. **A**: Representative recording of a mesothoracic DUM 3 neuron receiving IPSPs following tegula nerve stimulation at 1.5 Hz. Depolarisation of the neuron (red trace) leads to amplitude increase and confirms the inhibitory character of the PSPs. **B**: Recording of a mesothoracic DUM 3 neuron reveals IPSPs following TCC stimulation at increasing frequency. Up to a frequency of about 7 Hz the DUM 3 neuron follows single stimuli. **C**: Six superimposed sweeps of successive IPSPs taken from a stimulation sequence of constant frequency (2 Hz) from the same recording as in A. There is only a small decrement in amplitude and a small latency increase. **D**: A DUM 3 neuron shows summation of IPSPs during TCC stimulation at 200 Hz. **E**: Boxplots comparing the response rates of DUM 3 neurons to both stimulation paradigms (during stimulation sequences of 5-10 Hz). They illustrate that habituation during excitation of N1C1(a) is stronger and more variable than habituation during TCC stimulation. $N_{N1C1(a)}$=8 sequences from 3 neurons, N_{TCC}=12 sequences from 3 neurons. **F**: Intracellularly stained mesothoracic DUM 3 neuron showing the prominent lateral but hardly developed "b" branches. Scale bar 100 μm

Stimulation of TCC with 100 to 200 Hz stimulus trains resulted in a similarly uniform response pattern in DUM 3 neurons. Four out of 6 cells tested (table 1.2) were reactive to voltage pulses delivered to TCC and received exclusively IPSPs, either in meso- or metathoracic ganglia. This was verified as described above and a representative recording is displayed in fig. 1.3B. The shortest latency amounted to 12 ms, which - after subtraction of the time for the signal to reach the thoracic ganglia - suggests presumably only one IN mediating the signal, apart from TCG. However, the latency range was variable among the recorded cells. Fig. 1.3C shows the sweeps of 8 successive IPSPs taken from a 2 Hz stimulation sequence for a mesothoracic DUM 3 neuron. In this neuron the IPSPs had similar latencies and amplitudes at the beginning and the end of the sequence, however, the trend for increasingly retarded responses within such a sequence differed among individual cells, showing a maximum increase of 43 % in one neuron. As for the habituation, the observed response rate values ranged predominantly between 0.6 to 1, if the neurons' reaction to the first 10 stimuli of a stimulation sequence was taken into account.

Thus, in some neurons no habituation occurred at this (low) stimulation frequency, as illustrated in fig. 1.3E. However, during flight the TCG neuron discharges with about 2 spikes per cycle (Bacon and Möhl, 1983); at 15-20 Hz, which approximately represents flight frequency, DUM 3 neurons were hardly found to follow single stimuli, which can be also deduced from fig. 1.3B. At maintained high frequency stimulation of 100-200 Hz, the IPSPs were found to summate (fig. 1.3E).

A comparison of the observed response rates for both stimulation paradigms at the same stimulation frequency (fig. 1.3E) revealed that DUM 3 neurons which responded to N1C1(a) excitation were less reliable in their responses and tended to habituate more quickly than those neurons which were exposed to TCC stimulation.

DUM 3,4 neurons

Table 1.1 displays known characteristics for meso- and metathoracic DUM 3,4 neurons, which innervate flight muscles and belong to the "wing group" neurons. Representatively, the DUM 3,4 morphology is illustrated in fig. 2.3A, however, this group comprising six cells per ganglion presumably is not as homogeneous, regarding anatomy and function, as previously supposed. DUM 3,4 neurons in the current study therefore were, if possible, subdivided into DUM 3A,4 and DUM 3AC,4 neurons depending on whether their axon in nerve 3 bifurcated to send collaterals in N3A and N3C (Campbell et al., 1995).

When recording from DUM 3,4 neurons in putatively quiescent animals, the frequency of fast and small-amplitude membrane potential oscillations was in general higher than in DUM 3,4,5 neurons. One possible explanation may be stronger synap-

tic drive, but also intrinsic factors may play a role. DUM 3,4 neurons were moreover frequently found to receive IPSPs; this input often occurs simultaneously in other DUM neurons of the "wing group", which has been revealed previously by double intracellular recordings (Baudoux and Burrows, 1998). In addition, DUM 3,4 neurons were shown to receive inhibition in parallel to several kinds of motor pattern (kicking, flight) or following sensory stimulation (Burrows and Pflüger, 1995), however, the behaviour was not always uniform (Baudoux and Burrows, 1998). Similarly, DUM 3,4 neurons in this study sometimes were excited by sensory stimulation, e.g after touching the antennae as displayed in figure 1.4A.

During the experiments, DUM 3,4 neurons (N=18) were almost exclusively stimulated via nerve N1C1, both in thorax preparations and completely isolated ganglia. Similar to DUM 3 neurons, DUM 3,4 neurons in 8 recordings were clearly inhibited by stimulation of N1C1 (table 1.2). This effect, visualised during depolarisation of a mesothoracic neuron, is illustrated in fig. 1.4B. The action potentials of the neuron were evoked by depolarising current; simultaneous stimulation of N1C revealed IPSPs. However, this finding was only verified for DUM 3A,4 neurons (6 out of 11 cells), while for DUM 3AC,4 neurons (4 out of 6 cells) the nature of the PSPs was not clearly determined in all recordings; thus, apart from inhibitory responses EPSPs are possible as well. The latencies differed considerably between DUM 3A,4 and DUM 3AC,4 neurons (fig. 1.4D), but were also dependent on the stimulus regime applied and the preparation used. If stimulated at 5 to 10 Hz, the minima lay at 10 ms for DUM 3A,4 neurons and at 21 ms for DUM 3AC,4 neurons.

Fig. 1.4C displays the response rates of DUM 3,4 neurons. They were discriminated according to the subtype and, in case of DUM 3A,4 neurons, according to the preparation and the stimulation regime used. Those DUM 3A,4 neurons, which were stimulated in isolated ganglia at 1 Hz (100 Hz trains) tended to show higher latencies than those stimulated in thorax preparations at 5 to 10 Hz. The tendency to habituate to stimuli of either kind was remarkably high in all groups, however in general those neurons that were stimulated at higher frequency habituated more readily (fig. 1.4C). During stimulation sequences of equal length the assessed average response rates were 0.5 for DUM 3AC,4 neurons and 0.72 for DUM 3A,4 neurons. More than half of the sequences examined revealed rapid habituation during the first 3 stimuli; in sequences where this was not the case, the latencies of successive IPSPs almost always increased, with a maximal increase of 68 % in DUM 3AC,4 and 58 % in DUM 3A,4 neurons. No difference was found between 5 and 10 Hz stimulation sequences with respect to habituation.

In summary, DUM 3,4 neurons were predominantly inhibited by N1C1 stimulation; this was true both for DUM 3A,4 and DUM 3AC,4 neurons, however, the

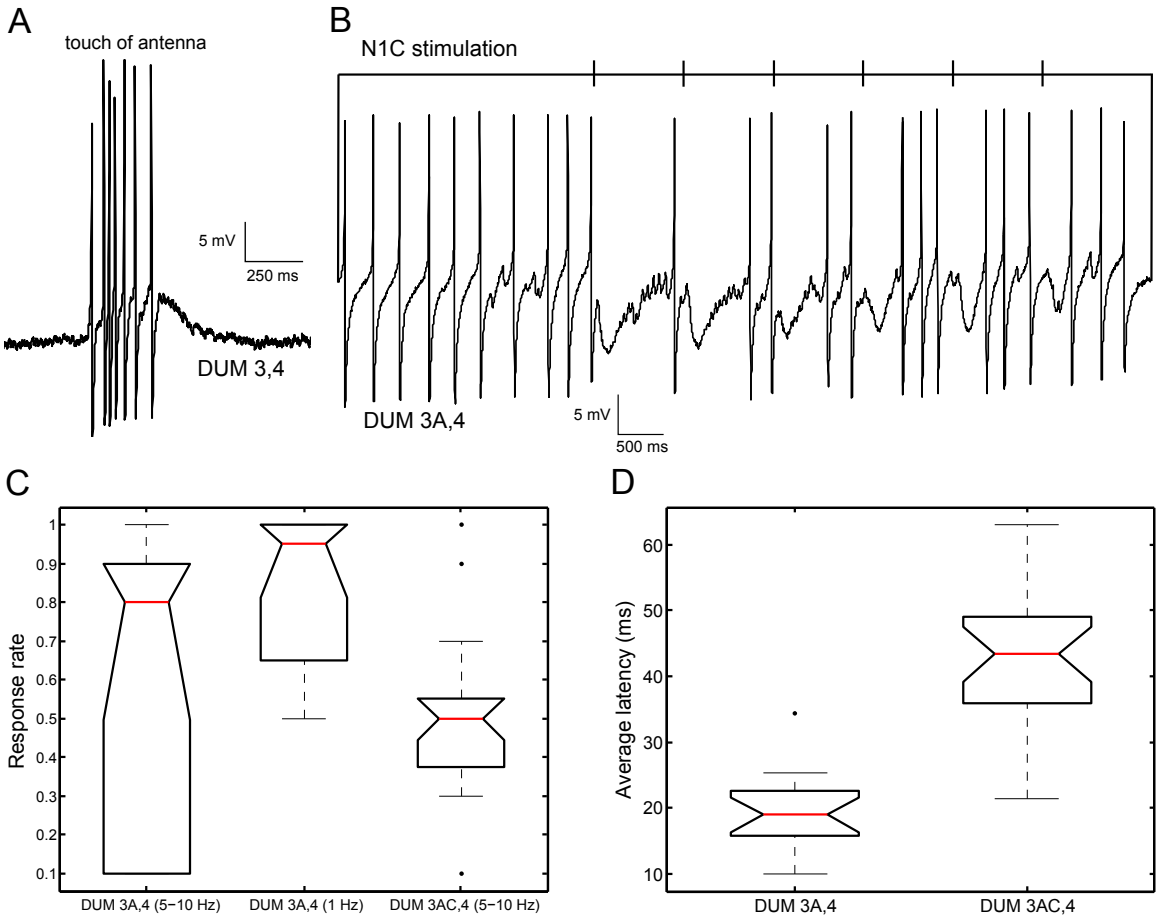

Figure 1.4: DUM 3,4 neuron responses to sensory and tegula stimulation. **A**: A DUM 3,4 neuron fires after antennal touch. **B**: Representative recording of a DUM 3A,4 neuron receiving IPSPs during N1C1 stimulation at 2 Hz. The spikes are due to injection of depolarising current. **C**: Boxplots illustrating response rate distributions of DUM 3,4 neurons during 5-10 Hz (DUM 3A,4 and DUM 3AC,4) and 1 Hz (DUM 3A,4) stimulation sequences. A marked difference was found between DUM 3AC,4 neurons stimulated at 10 Hz and DUM 3A,4 neurons stimulated at 1 Hz. $N_{DUM3A,4at10Hz}$=17 sequences from 3 neurons, $N_{DUM3A,4at1Hz}$=16 sequences from 4 neurons, $N_{DUM3AC,4at10Hz}$=25 sequences from 4 neurons. **D**: Boxplot displaying differing latencies for DUM 3A,4 and DUM 3AC,4 neurons. The latencies were determined as the average of the response latencies to the first 3 stimuli of a stimulation sequence (stimulation frequency between 5 and 10 Hz). $N_{DUM3A,4}$=25 sequences from 4 neurons, $N_{DUM3AC,4}$=17 sequences from 3 neurons.

difference in latencies and the partially ambiguous data record of DUM 3AC,4 neurons may indicate a possible functional segregation of DUM 3,4 neurons.

TCC stimulation was found to elicit responses in DUM 3,4 neurons as well, verified for 3 out of 7 cells of subtype DUM 3A,4. However, 3 tested DUM 3AC,4 neurons were not reactive. The inhibitory character of the PSPs evoked by TCC stimulation is displayed in fig. 1.5A for a mesothoracic DUM 3A,4 neuron. The latencies measured were at minimum about 22 ms, but increased with ongoing stimulation by a maximal factor of 2. In general, prolonged stimulation sequences gradually retarded the latencies. Together with the fact that the response rate to a stimulation frequency of 1 Hz was highly variable and ranged from 0.1 to 0.9, these data imply the existence of

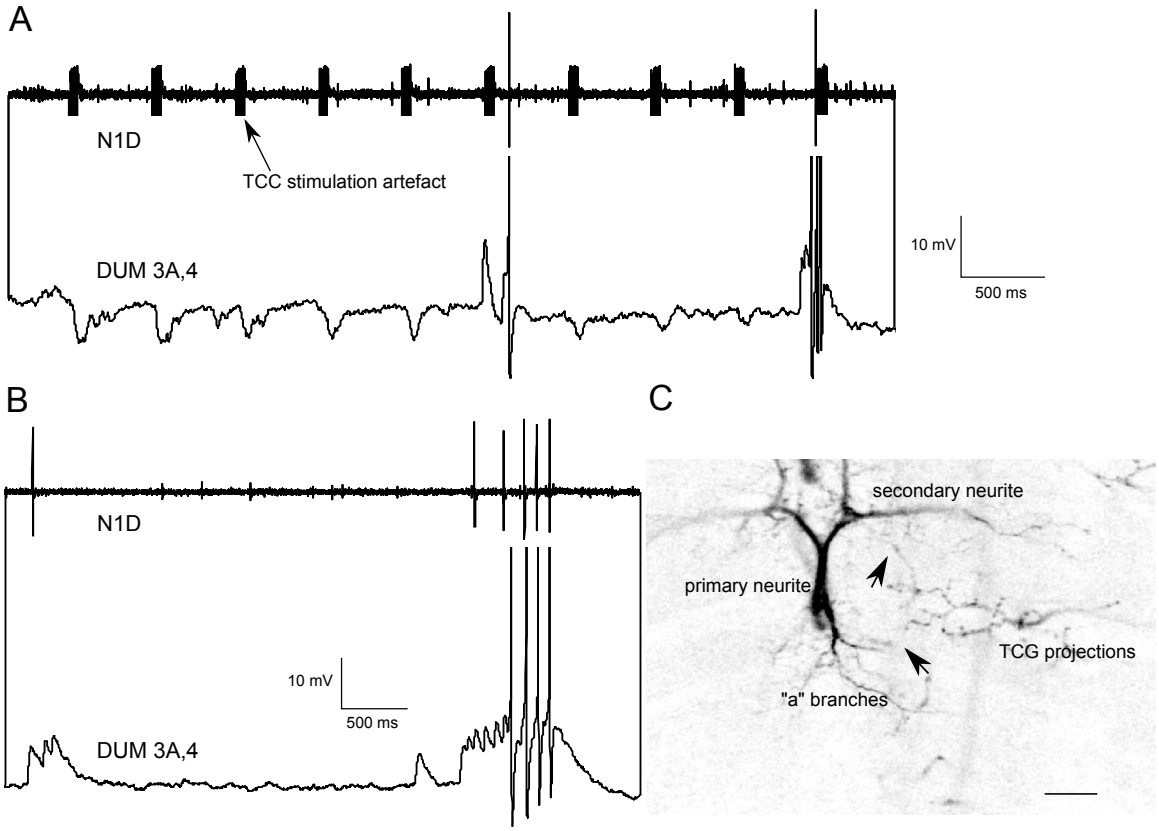

Figure 1.5: DUM 3A,4 neuron response to TCC stimulation. **A**: Stimulation of TCC at 100 Hz trains (arrow indicates the stimulation artefact detectable in the N1D recording) elicits inhibitory potentials in a DUM 3A,4 neuron. Simultaneous recording of N1D reveals correlated activity to the DUM 3A,4 neuron. **B**: Simultaneous recording of the same DUM 3A,4 neuron as in A and N1D showing that action potentials in both traces are highly correlated. **C**: TCG projections lie in vicinity to DUM neuron arborisations. The single optical slice (1 μm width) shows the spatial relation of DUM 3A,4 neuron branches to TCG varicosities (stained via anterograde dye fill of TCC) in the metathoracic dorsal neuropil. Scale bar 50 μm

processing units in between TCG and the DUM neuron. However, an anterograde fill of TCG revealed spatial proximity of its varicosities to DUM neuron branches within the dorsal neuropil of meso- and metahoracic ganglia (fig. 1.5C).

TCC stimulation rarely elicited rhythmic activity in the simultaneously recorded N1D, as would be expected from previous data (Bicker and Pearson, 1983), even if the stimulation was sufficient to evoke a DUM neuron response (fig. 1.5A). Interestingly, however, one DUM 3A,4 neuron showed activity strongly corresponding to that of N1D. Fig. 1.5B reveals that EPSPs and spikes in DUM 3A,4 coincided with action potentials of a prominent unit in N1D. Spikes appeared almost synchronously, the delay between both amounted to less than 10 ms. In consideration of the time for the action potentials in N1D to reach the recording site, this could indicate simultaneous input to (motor) neurons innervating flight muscles via N1D and to DUM 3A,4. Until now, DUM 3,4 neurons have not been suggested to be positively coupled to flight related behaviour, therefore this finding of simultaneous DUM 3,4 and flight

motor unit excitation again stresses the notion that this population may be more divergent than previously reported.

DUM 3,4,5 neurons

This population is, in contrast to the precedingly treated neurons, constituent of the so called "leg group", for its peripheral targets include predominantly leg muscles (table 1.1). In electrophysiological recordings these cells not only respond with EPSPs to all kinds of sensory stimulation (table 1.2), but also are rhythmically active in parallel to motor patterns. These include not only those involving leg muscles, such as kicking and walking, (Burrows and Pflüger, 1995) but also flight (Duch and Pflüger, 1999). With other cells of the "leg group", the DUM 5 neurons, they were previously shown to have many EPSPs and action potentials in common (Baudoux and Burrows, 1998). Fig. 1.6A confirms part of these findings with recordings of individual DUM 3,4,5 neurons displaying reactivity to wing hair stimulation (fig. 1.6A, upper trace), as well as rhythmical activity possibly in parallel to a slow motor pattern like walking (fig. 1.6A, lower trace). Even without intentional stimulation EPSPs were often encountered in these neurons.

In contrast to previous findings (Duch and Pflüger, 1999), the stimulation of N1C1(a) elicited responses in DUM 3,4,5 neurons in thorax preparations (see Methods), indicating a segmental pathway from the tegula to DUM 3,4,5 neurons. The majority of the reactive cells (6 out of 11 cells tested) received excitatory input and generated EPSPs and even action potentials (fig. 1.6B). Two cells were inhibited, however, the neurobiotin staining in these preparations labeled further cells in addition to the DUM 3,4,5 neuron, hence the identity of the recorded neuron remained ambiguous. The latencies of the responses varied among individual neurons with a mean latency of 39 ms; with shortest latencies of 19 ms, these findings again indicated a polysynaptic pathway. During stimulation sequences at 10 Hz as shown in fig. 1.6D), habituation readily occurred, thus, typical for the habituation process, its strength depended, among other factors, on the stimulus regime applied. Thus, the average response rate (as a measure of habituation) at 1 Hz stimulation sequences (100 ms 100 Hz trains) was about 0.6, whereas at 5-10 Hz stimulation frequency it was only about 0.25, meaning that in these sequences the response disappeared after the initial 3 stimuli. This difference is illustrated for all stimulation sequences of DUM 3,4,5 neurons in fig. 1.6D. In cases where habituation was less prominent, consecutive spikes occurred with a delay. Fig. 1.6C displays data from two different neurons, stimulated at either 1 (i) or 2.5 Hz (ii); it shows for 4 consecutive spikes that latencies increased during maintained stimulation.

The responses of DUM 3,4,5 neurons to N1C(1a) stimulation were predominantly

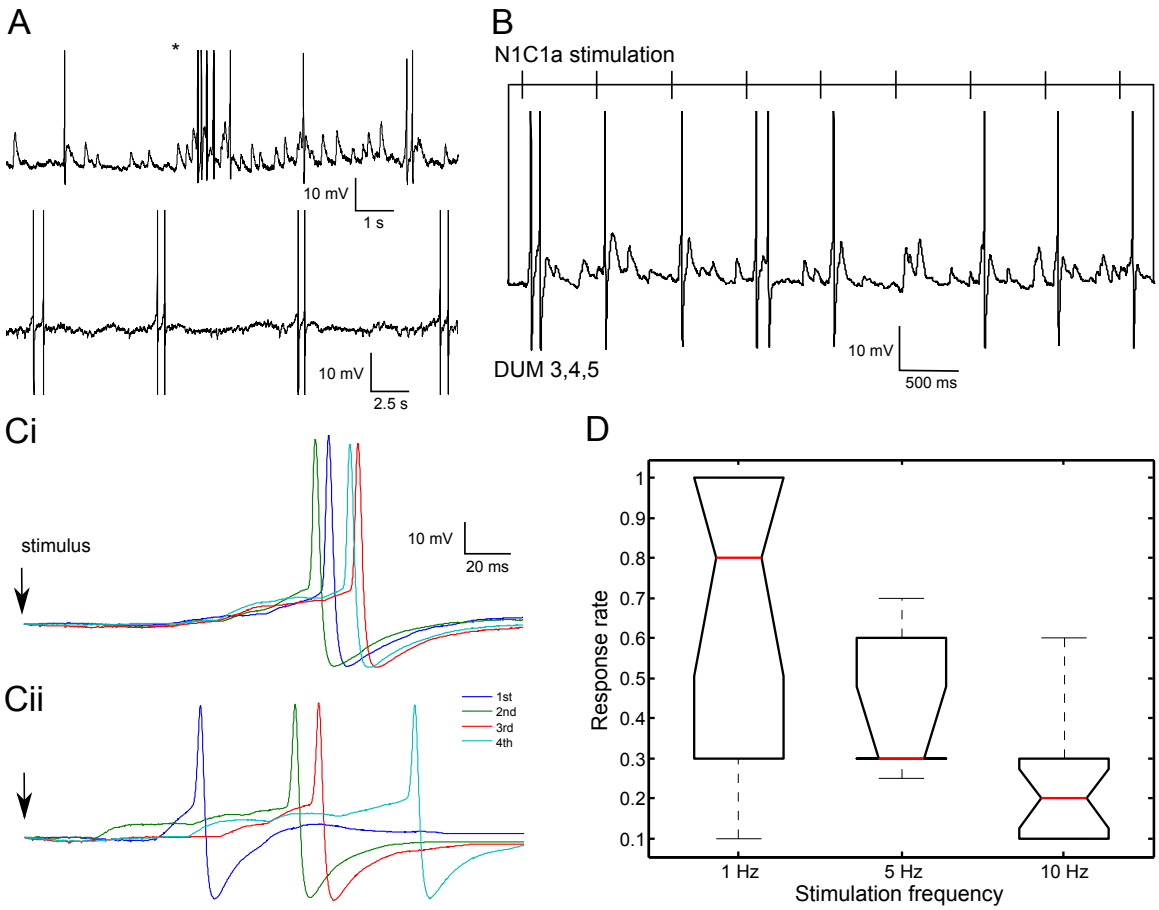

Figure 1.6: DUM 3,4,5 neurons are excited by N1C1(a) stimulation. **A**: Recordings of DUM 3,4,5 neurons exemplarily show (i) PSPs and action potentials in response to wing hair stimulation (asterisk) and (ii) rhythmical spiking presumably in parallel to a slow motor pattern like walking. **B**: Representative recording of a DUM 3,4,5 neuron showing spikes in response to stimulation of N1C1a. **C**: Latency increase during N1C1a stimulation. Overlays of four successive spikes during stimulation sequences of (i) 1 Hz and (ii) 2.5 Hz of two different DUM 3,4,5 neurons show increasingly retarded spikes, especially for (ii), where the stimulation frequency is higher. **D**: Boxplots displaying response rates of DUM 3,4,5 neurons reveal markedly stronger habituation during stimulation sequences of higher frequency. N_{1Hz}=14 sequences from 4 neurons, N_{5Hz}=7 sequences from 3 neurons, N_{10Hz}=18 sequences from 5 neurons.

observed in decapitated and deafferentated preparations, but were elicited in one preparation with intact CNS as well. An intersegmental pathway within the thoracic ganglia was obvious, since metathoracic DUM 3,4,5 neurons were reactive to stimulation of either meta- or mesothoracic N1C1(a). A comparison of activity in the simultaneously recorded nerve 1D and one DUM 3,4,5 trace revealed no obvious correlation, but DUM 3,4,5 activity seemed in general high, if there was activity in the synchronously recorded N1D. However, since actual rhythmic pattern in N1D was not evoked in these samples, this was not examined in detail.

In summary, DUM 3,4,5 neurons showed excitatory responses following N1C1(a) stimulation, which suggests the existence of a thoracic segmental pathway from tegula afferents to DUM 3,4,5 neurons.

TCC stimulation elicited no responses in DUM 3,4,5 neurons, however, the sample size (N=2) was to small to allow for speculations.

Table 1.2: Summary of thoracic DUM neuron responses to N1C1(a) and TCC stimulation and to other sensory modalities. DUM 3,4 neurons comprise DUM 3A,4 and DUM 3AC,4 neurons. Nerve 2C (N2C) holds afferents of a myochordotonal and a posterior joint chordotonal organ (Bräunig et al., 1981). Key of abbreviations: COs Chordotonal organs, N Responsive neurons (numbers in brackets: total cell number tested) or Nerve (Stimulation), Ref. References: 1 this study 2 Duch and Pflüger, 1999; 3 Field et al., 2008; 4 Morris et al., 1999; x Unspecified number of cells.

Cell	Stimulation site	N	Response	Latency (ms)	Ref.
DUMDL	N1C1(a)	3 (4)	Inhibition	≥ 15	1
	N1C	2	Inhibition	≥ 8	2
	Cuticular sensillae	1 (1)	Inhibition/Excitation	≥ 60	3
	N2C	(3)			4
DUM 1b	TCC	2 (2)	Excitation	≥ 22	1
DUM 3	N1C1(a)	5 (10)	Inhibition	≥ 12	1
	N1C	5	Inhibition	≥ 8	2
	TCC	4 (6)	Inhibition	≥ 12	1
	Campaniform sensillae	1 (4)	Weak Excitation	≥ 60	3
	N2C	x (x)	Inhibition	≥ 15	4
DUM 3,4	N1C1(a)	12 (18)	Inhibition/Excitation?	≥ 10	1
	N1C	8	Inhibition	≥ 8	2
	TCC	3 (10)	Inhibition	≥ 27	1
	Cuticular sensillae	5 (26)	Inhibition	≥ 20	3
	N2C	x (x)	Inhibition	≥ 15	4
DUM 3A,4	N1C1(a)	6 (11)	Inhibition	≥ 10	1
	TCC	3 (7)	Inhibition	≥ 27	1
DUM 3AC,4	N1C1(a)	4 (5)	Inhibition/Excitation?	≥ 21	1
	TCC	(3)			1
DUM 3,4,5	N1C1(a)	6 (11)	Excitation	≥ 19	1
	N1C	(x)			2
	TCC	(2)			1
	Cuticular sensillae	10 (20)	Excitation	≥ 20	3
	COs	3 (20)	Excitation		3
	Compound eyes	7 (20)	Excitation		3
	N2C	7/3 (14)	Excitation/Inhibition	≥ 15	4
DUM 5	N1C	(x)			2
	Cuticular sensillae	5 (14)	Excitation	≥ 20	3
	COs	2 (14)	Excitation		3
	Compound eyes	4 (14)	Excitation		3
	N2C	12 (15)	Excitation	≥ 15	4

3.2 Distribution of putative inhibitory input synapses on selected branches of DUM 3,4 and DUM 3,4,5 neurons

How thoracic DUM neurons are putatively integrated into central circuits has been developed on the basis of physiological data, however, visualising presumable presynaptic contacts with the help of immunocytochemistry can provide a more complete view. Intracellular recordings from thoracic DUM 3,4 and DUM 3,4,5 neurons revealed that DUM 3,4 neurons, in contrast to DUM 3,4,5 neurons, frequently receive inhibitory input, either in supposedly quiescent animals or in response to sensory stimulation and motor behaviour (see 3.1). Whether this differential activity and activation of "wing group" and "leg group" DUM neurons is also reflected in the amount of inhibitory input synapses on the dendritic field of DUM 3,4 and DUM 3,4,5 neurons is subject of the following co-localisation analysis.

Antibody characterisation

In order to unambiguously label presynaptic loci for the identification of putative inhibitory synapses, a monoclonal antibody against synapsin I (SynI) was applied as a marker (Klagges et al., 1996), for synapsins are abundant and ubiquitous synaptic vesicle phosphoproteins (Südhof, 2004). Fig. 2.1A displays a single optical slice with SynI-immunoreactivity (SynI-ir) in the neuropil of the mesothoracic ganglion appearing as distinct puncta of 0.3 to 3 μm in diameter. Characteristically the staining was evenly distributed throughout the neuropil, but lacking in tracts (not shown).

Although not the only transmitter eliciting inhibitory responses in CNS neurons, γ-amino butyric acid (GABA) is supposed to be the main inhibitory transmitter in the invertebrate CNS (Pitman, 1971; Anthony et al., 1993). Alternatively to a monoclonal antibody to GABA, which showed excellent labeling of GABAergic somata in the cortex of a wholemount ganglion, but performed poorly within the depth of the neuropil (fig. 2.2A), even on vibratome sections, an antibody to the enzyme glutamic acid decarboxylase (GAD 65/67) furnished satisfactory results in neuropil areas (fig. 2.1B). GAD catalyses the main pathway in biosynthesis of GABA by mediating the transformation of L-glutamate to GABA and was thus expected to be reliably confined to GABAergic neurons. This was subject of a comparison of the somata labelled with either of the antibodies. Fig. 2.2B representatively displays GAD-ir on the most dorsal horizontal section of the metathoracic ganglion. In addition to an even neuropil staining, several clusters of mainly small cell bodies were distinguishable and strongly resembled the GABAergic somata described by (Watson, 1986), as e.g. the median dorsal cluster situated posteriorly to the DUM neuron region (median dorsal group MDG in fig. 2.2B). GABA-ir revealed somata groups of similar size and position (fig. 2.2A). The size of the somata within the peripheral clusters (lateral dorsal group

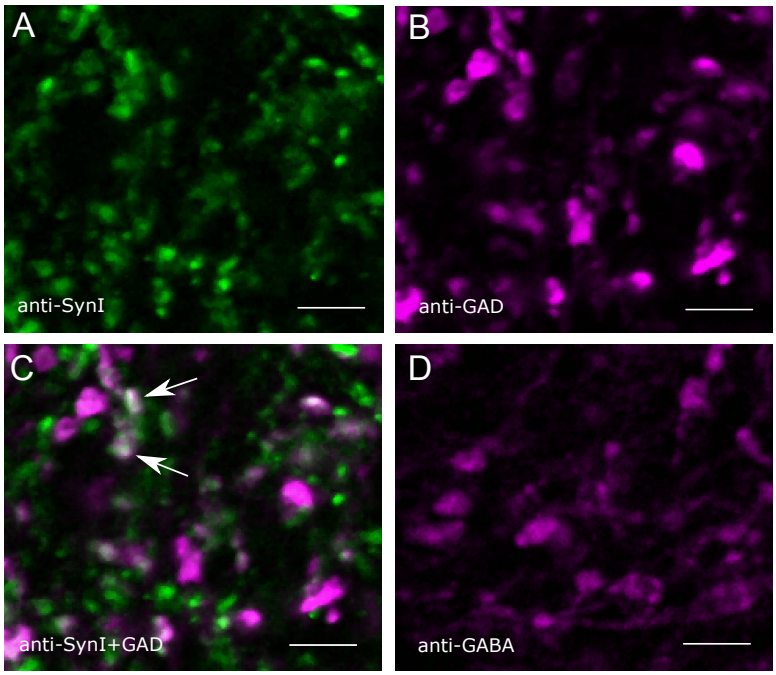

Figure 2.1: High resolution confocal images of SynI- and GAD-immunoreactivity (SynI-/GAD-ir) in the dorsal neuropil of the mesothoracic ganglion. **A**: Single optical slice showing SynI-ir as fine meshwork and distinct puncta of 0.3 to 3 μm in diameter. **B**: GAD-ir on the same optical slice as in A; GAD-ir exhibits larger puncta compared to SynI. **C**: Overlay of A and B, i.e. SynI-ir (green) and GAD-ir (magenta), indicates loci of co-localisation and thus putative GABAergic synapses (arrows pointing to white areas). **D** Different optical slice as in A,B,C showing GABA-ir of similar, but more fibrous appearance as GAD-ir. Z-dimension of all slices 0.3 μm, scale bars for all slices 2 μm

LDG) ranged between 20-40 μm in diameter and could thus hardly be mistaken for the considerably larger glutamatergic motoneurons (Watson and Seymour-Laurent, 1993). Further evidence provided the only larger diameter somata (around 60 μm) on the ventral surface of the ganglion (fig. 2.2C), which most probably represent the GABAergic common inhibitor (CI) neurons (Watson et al., 1985; Watson, 1986).

Puncta of GAD-ir in the neuropil had a less delicate appearance than those of SynI-ir (fig. 2.1B) and were comparable to GABA-ir pattern (fig. 2.1D), which, however, was less intense and more frequently stained also fibers. The overlay of anti-SynI and anti-GAD staining displayed in fig. 2.1C shows overlap of both markers in some areas indicating colocalisation (arrows) and thus the presence of putative GABAergic synapses.

DUM neuron anatomy and branch selection

Only a subset of DUM neuron branches, the so called "b" branches, was investigated to reveal its putative input synapses, since it enabled the evaluation of at least three neurons per group. Despite anatomical incongruities between DUM neuron subtypes and individual aberrations from the bilaterally symmetrical architecture, individual DUM neuron branches can in general be reliably identified and were named with

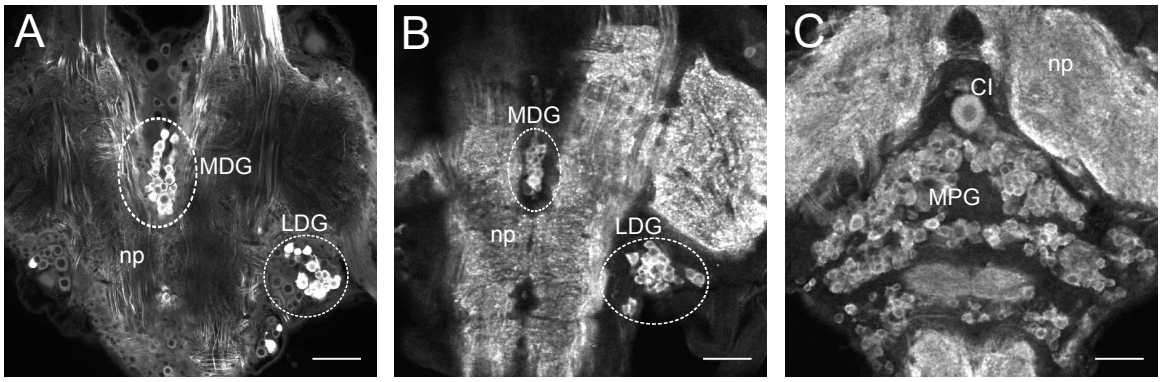

Figure 2.2: GABA- and GAD-immunoreactivity on the dorsal surface of the metathoracic ganglion stain similar somata clusters. **A**: GABA-ir highlights cell clusters of the median dorsal group (MDG) and lateral dorsal group (LDG) (Watson, 1986), the neuropil (np) lacks staining. Z-Dimension of single optical slice 1 μm. **B**: GAD-ir labels similar groups of neurons as GABA-ir (A) and intensely stains the neuropil. **C**: GAD-ir on the ventral side of the metathoracic ganglion reveals groups of cells similar to those described as GABAergic by Watson (1986), like the medial posterior group (MPG) and one of the common inhibitor neurons (CI). Z-Dimension of single optical slices in B and C 1.3 μm, all scale bars 100 μm

letters from "a" to "d" (Watson, 1984).

Fig. 2.3 shows aligned image stacks in dorsal, frontal and lateral views of two representative mesothoracic DUM 3,4 and DUM 3,4,5 neurons with the respective branch regions labeled accordingly. While "a" branches arise exclusively from the primary neurite, branches of groups "b" to "d" diverge from the lateral neurite, with "b" branches being the most centrally and "d" branches the most laterally situated groups. However, as illustrated in fig. 2.3A, DUM 3,4 neurons do not form explicit "d" branches. The "b" branches are most conspicuous: Branching off the secondary neurite next to the bifurcation zone, they advance anteriorly at both sides of the midline (Fig. 2.3Ai/Bi). The main branch forms two to four prominent collaterals, which in turn give rise to finer arborisations; these extend also more laterally and ventrally. In relation to a framework of ganglionic structures (Tyrer and Gregory, 1982; Pflüger and Watson, 1988; Kononenko and Pflüger, 2007), they were found to be limited in their lateral extension to the area between the dorsal intermediate tracts (DIT). As for the ventral spread of "b" branches, DUM 3,4,5 neurons run deeper into the core of the neuropil (fig. 2.3Bii/Biii) than DUM 3,4 neurons, which remain confined to the dorsal surface (fig. 2.3Aii/Aiii). In the metathoracic ganglion the branches of DUM 3,4,5 expand into ventral neuropil areas beyond dorsal commissure IV (DCIV), while those of DUM 3,4 neurons do rarely pass this border. However, the majority of "b" branch ramifications cover the same dorsal areas in both neuronal subtypes. "B" branches are, as illustrated in fig. 2.3, unlike the more lateral DUM neuron branches, prominently developed in both subgroups, of comparable size and less intermingled with processes from other branch groups, features which favored

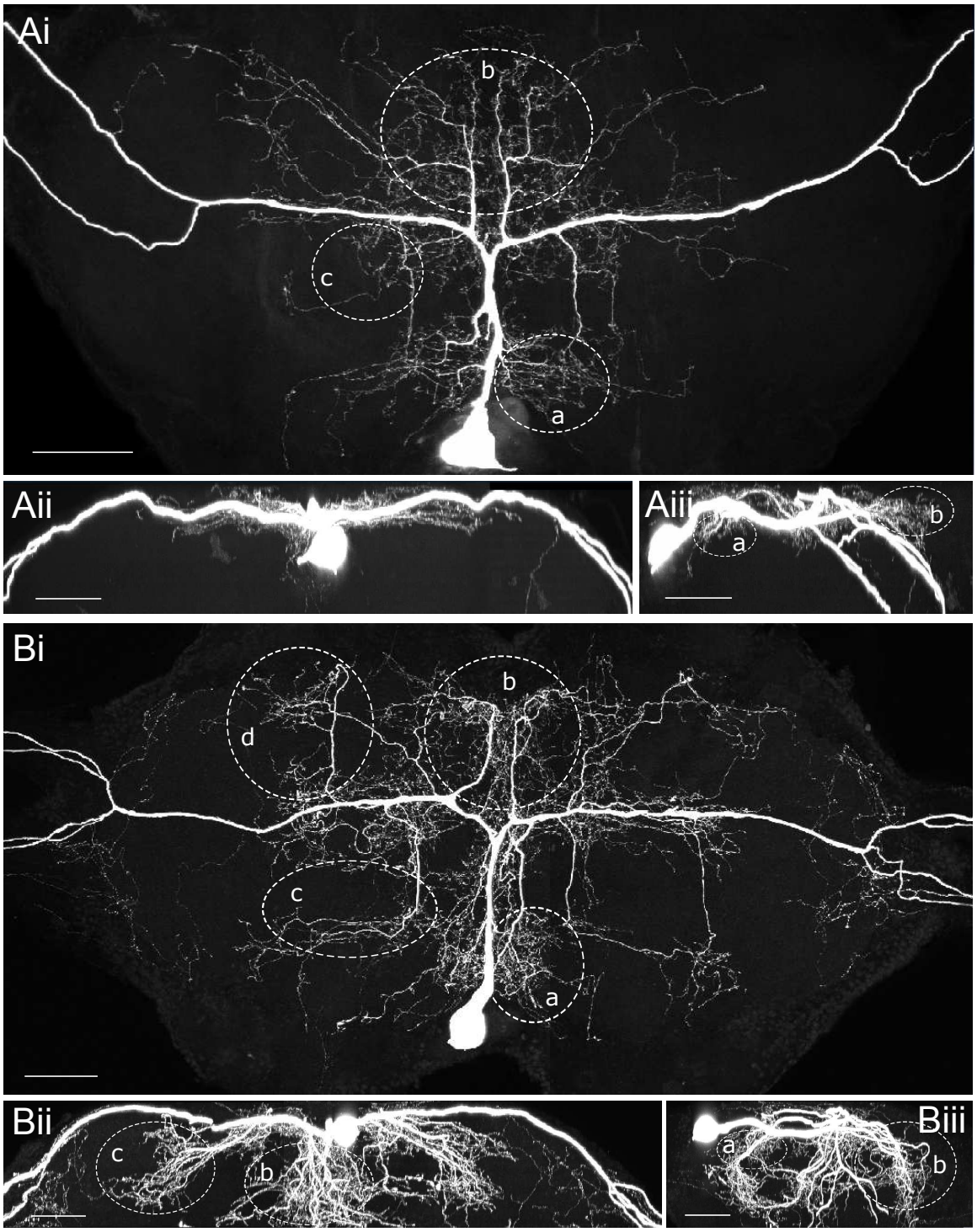

Figure 2.3: Anatomical structure of intracellularly stained DUM 3,4 and DUM 3,4,5 neurons with ellipses encircling the regions of branches marked with letters from "a" to "d". **A**: Confocal image stack of an intracellularly stained DUM 3,4 neuron in dorsal (Ai), frontal (Aii) and lateral view (Aiii). DUM 3,4 neurons do not possess explicit "d" branches; their dendritic arborisations are mainly confined to the dorsal surface (Aii). **B**: Confocal image stack of an intracellularly stained DUM 3,4,5 neuron in dorsal (Bi), frontal (Bii) and lateral view (Biii). Note that extensive arborisations reach into more ventral regions of the ganglion (Bii/Biii). All scale bars 100 μm

their selection for the current evaluation.

However, extrapolation of data restricted to only a part of the dendritic tree presupposed an even distribution of GAD/SynI-immunopositive labels throughout the neuropil. This has been proved by the inspection of own data (3.2) and of previous observations regarding the (motor) neuropils of *Manduca sexta* (Meseke et al., 2009b) and locusts (Watson and Laurent, 1990).

Putative inhibitory input sites on "b" branches of DUM 3,4 and DUM 3,4,5 neurons

In order to identify presynaptic sites to DUM neuron dendrites, GAD/SynI-immunopositive labels were mapped onto the surface of the reconstructed neurons (see Methods 2.7). This procedure is based on the assumption that a synaptic terminal's width, including active zone, reserve vesicle pool and synaptic cleft is estimated to span about 220-320 nm (Rollenhagen and Lübke, 2006), thus, images gained by fully exploiting the resolving power of confocal microscopy (voxel dimensions 0.1x0.1x0.3 μm) should allow for reliable estimations on the scale of synapses (Evers et al., 2005; Hohensee et al., 2008).

Fig. 2.4A shows a single dendrite of the skeleton tree consisting of spherical vertices and fitted to the contour of the intracellularly stained neuron. After reconstruction in idealized shape, this skeleton was transformed into the more realistic surface (for details see Methods 2.7 or Schmitt et al., 2004). Subsequently, within a distance of 0.3 μm to the surface all double-staining of GAD-ir and SynI-ir (above threshold) was considered and projected onto the neuron's surface. The resulting distribution was visualised in a colour coded mode (fig. 2.4B), where warmer/brighter colours of surface areas indicated higher staining intensities in the region next to the respective surface triangle and thus the probable existence of a (GABAergic) presynaptic profile (arrow in fig. 2.4B).

To gain insight into the integrity of the data, absolute length and surface extension of the reconstructed "b" branch trees (N=3 for DUM 3,4 neurons, among which two DUM 3(A),4 neurons and one DUM 3(AC),4 neuron; N=4 for DUM 3,4,5) were initially compared. The mean absolute dendritic length for both groups was found to amount to 5.8±1.3 mm (DUM 3,4) and 4.8±2.1 mm (DUM 3,4,5), respectively, suggesting minor differences in the overall "b" branch tree size. This held also true for the absolute surface size, which accounted for 10.7±2.7 mm^2 (DUM 3,4) and 9.2±4.2 mm^2 (DUM 3,4,5), respectively. Thus the variability in size among the DUM 3,4,5 samples were greater than for the branches of DUM 3,4 neurons. It has to be added that probably none of the samples provided a measure of the absolute "b" branch tree extension of the respective neuron, since not all dendritic processes could be reliably included into the evaluation due to the fragmentation of the stained neuron

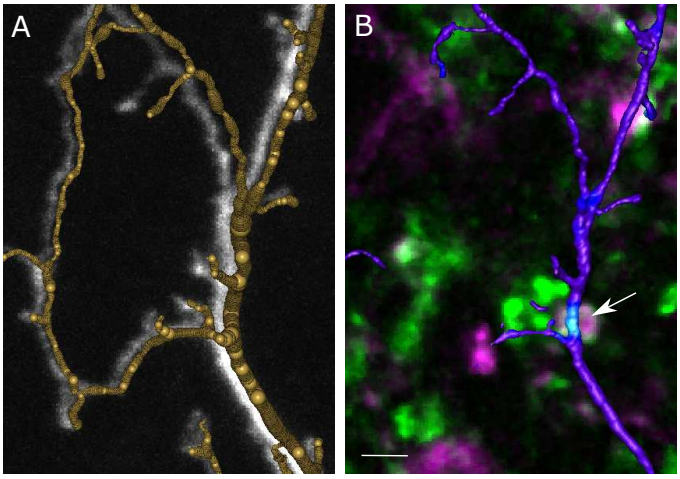

Figure 2.4: Dendrite reconstruction and surface mapping of putative GABAergic input synapses. **A**: Reconstructed branch and corresponding confocal image stack (z-dimension 20 μm) of the intracellularly stained neuron. **B**: Realistic surface generation of the reconstructed dendrite shown in A. Within a distance of 0.3 μm all positive double staining of SynI- and GAD-ir is mapped onto the dendritic surface and visualized in a colour coded mode. Warmer colours indicate higher staining intensities next to the respective surface element. The arrow points to a surface area of putative inhibitory input, the underlying optical slice (0.3 μm width) shows co-localisation of SynI (green)- and GAD (magenta)-ir. Scale bars 2 μm.

on sections. It is, however, probable that, independently of the observed differences in overall length, there is natural variability, since also the shape of the branches was quite variable among all DUM neurons ever stained (personal observation). To also yield a measure of the variability in the amount of putative input sites, the portions of synaptic input sites were determined for equal-sized subsurfaces, which, however, did not necessarily correspond to branch-descendants of the same tree root, but rather to branches assigned to neighbouring neuropil regions. Fig. 2.5B shows a reconstructed "b" branch tree and the corresponding original data of the aligned confocal images (fig. 2.5A). It representatively illustrates the subdivision into equal surface partitions.

For the evaluation it was not attempted to count individual synaptic contacts, since reliable estimations of an anatomical synapse's size and its actual apposition zones is allocable only from electron microscopy data. Instead the overall surface covered by putative input sites of every examined dendritic field was set in relation to this dendritic field's absolute surface, yielding the percentage of the surface area covered by putative synapses. The values obtained from the smaller "b" branch partitions went equally into the total evaluation.

Fig. 2.6Ai displays the proportions of the putative synaptic input area per tree for both neuronal subtypes. For DUM 3,4 neurons it shows a significantly higher percentage of putative synaptic input sites, namely 14.2±4.6 % in contrast to only 8.7±3.2 % for DUM 3,4,5 neurons, implying that DUM 3,4 neurons in this area might be in contact with more presynaptic profiles than DUM 3,4,5 neurons. The same data

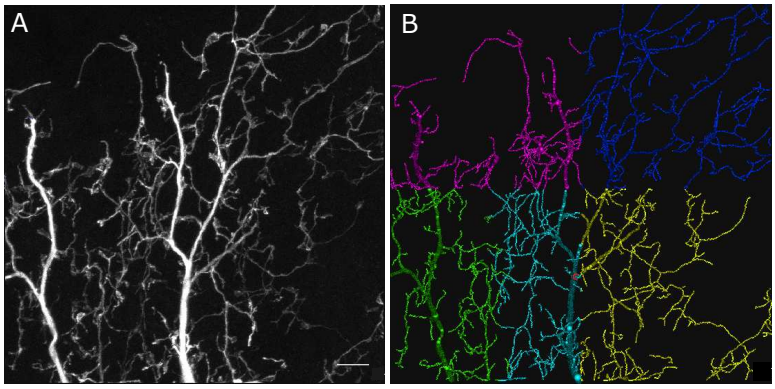

Figure 2.5: Subdivision of reconstructed "b" branches into equal-sized surface partitions. **A**: Confocal image stack showing "b" branches of a DUM 3(A),4 neuron. Z-dimension 36 μm. **B**: Reconstruction of the "b" branches displayed in A, with different colours ("materials" in Amira 4.1.1) marking equal-sized subsurfaces, representative illustration. Scale bar for A and B 10 μm

is displayed in fig. 2.6Aii, this time itemised for the individual samples (A for DUM 3,4 neurons and B for DUM 3,4,5 neurons). No strict separation of the groups was evident, with two samples (A3 and B2) showing rather similar, intermediate values. However, the fact that the branches from sample A3 (fig. 2.6Aii) belonged to a DUM 3AC,4 neuron, may fit in with the previously suggested notion that DUM 3,4 neurons do not compose a homogeneous population.

Regarding putative GABAergic input, there was only a small bias towards a larger area of GABAergic input for DUM 3,4 neurons, with 4.1±1.5 % versus 3.2±1.8 % for DUM 3,4,5 neurons (fig. 2.6Bi). Accordingly, the individual samples hardly showed a group specific separation (fig. 2.6Bii). The division of the amount of anti-GAD by anti-SynI+GAD staining yielded a measure of the GABAergic share of all putative synaptic input area; this value did not differ significantly between both groups, being 0.29±0.13 for DUM 3,4 and 0.36±0.08 for DUM 3,4,5 neurons. In both cases about a third of all putative synaptic input sites were thus found to be of GABAergic origin. However, these data implied that the proportion of non-GABAergic input sites, which may predominantly include putative excitatory synapses, lay twice as high for DUM 3,4 neurons, with about 10 %, as for DUM 3,4,5 neurons, with about 5 %.

To answer the question, whether these observations reflected differences in neuropil staining, the density of SynI-ir and SynI+GAD-ir in the neuropil was assessed for the image stacks from DUM 3,4 and DUM 3,4,5 neurons separately. For this purpose three cubes of corresponding dimension were selected within evenly stained regions of the neuropil for each DUM neuron sample. The threshold values for immunopositive staining were adopted from the co-localisation analysis. In Fig. 2.7A the amount of anti-SynI labels within the neuropil are compared for the image stacks of DUM 3,4 and DUM 3,4,5 neurons, showing distributions with medians of 21.6±6,2 % (DUM 3,4) and 20±8,2 % (DUM 3,4,5). Co-localised labels of GAD- and SynI-

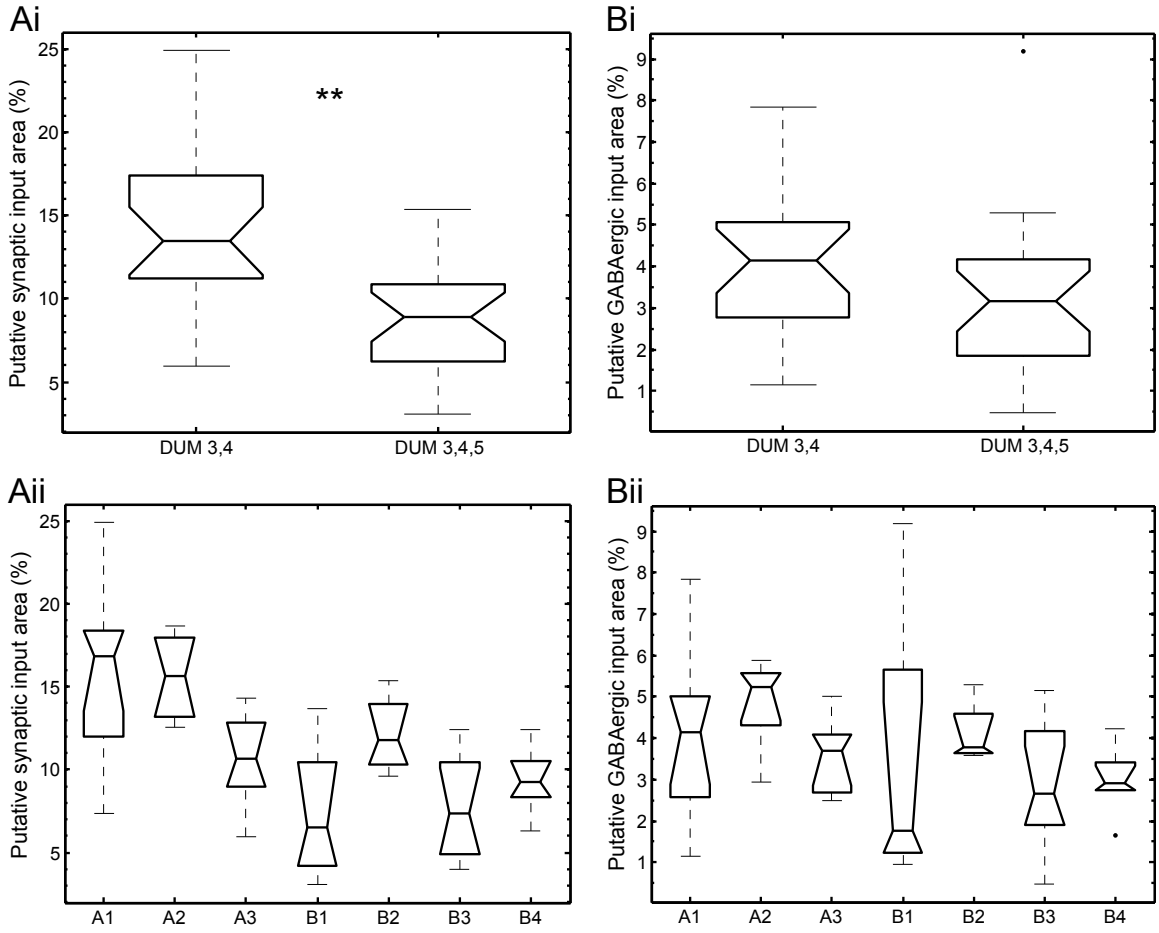

Figure 2.6: Putative synaptic and GABAergic input area on "b" branches of DUM 3,4 and DUM 3,4,5 neurons. **A**: Boxplots showing that the putative synaptic input area is greater for DUM 3,4 with 14.2±4.6 % of the surface than for DUM 3,4,5 neurons with 8.7±3.2 % (Ai). In Aii the data is itemized for individual neurons (A1-A3: DUM 3,4; B1-B4: DUM 3,4,5). Note that sample A3 represents a DUM 3AC,4 neuron. N of subsurfaces included: $N_{DUM3,4} = 22$, $N_{DUM3,4,5} = 25$. Kolmogorov-Smirnoff-Test,**$p<0.01$. **B**: Boxplots displaying the putative GABAergic input area for DUM 3,4 and DUM 3,4,5 neurons. There is only a small tendency of greater input surfaces on DUM 3,4 neuron dendrites with 4.1±1.5 % versus 3.2±1.8 % for DUM 3,4,5 neurons (Bi). The individual samples thus distribute more uniformly than in Aii (Bii). N as in A.

ir covered 4.5±1.9 % (DUM 3,4) and 4.9±2.6 % (DUM 3,4,5) of the neuropil (fig. 2.7B). These relations were reflected in a GAD/SynI+GAD-ratio of 0.21±0.1 (DUM 3,4) and 0.25±0.1 (DUM 3,4,5), indicating that about a fifth to a fourth of the putative synaptic terminals were presumably GABAergic (fig. 2.7C). These data displayed a certain variability among samples, however, did not indicate a correlation of neuron specific synaptic input sites to the neuropil staining density, since the above stated relations (fig. 2.6) were not reflected in the neuropil.

To test whether the putative input synapses appeared randomly distributed or preferentially targeted higher order branches of smaller diameter at the periphery of the dendritic field, the "b" branches and their putative input synapse coverage were

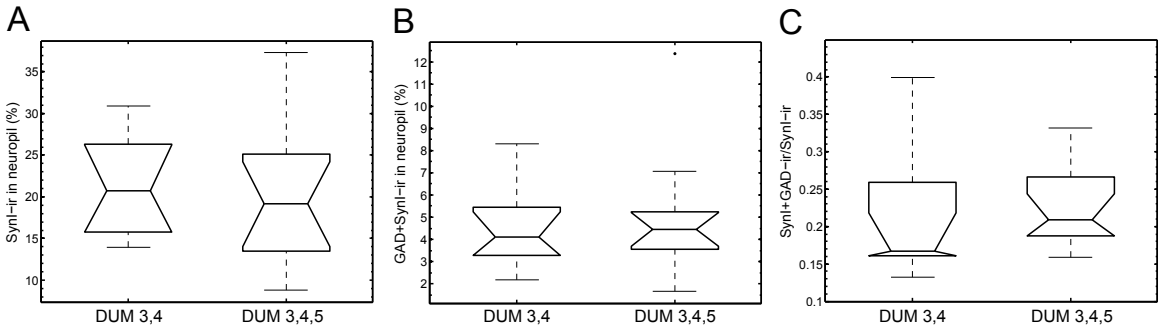

Figure 2.7: Proportion of neuropil volumes covered by SynI- and SynI+GAD-immunolabels. **A**: The average percentage of neuropil covered by SynI-staining lies within the same range for DUM 3,4 and DUM 3,4,5 samples. **B**: The percentage of neuropil covered by SynI+GAD-staining, i.e. putative GABAergic synapses, is shown for DUM 3,4 and DUM 3,4,5 samples and reveals no difference of the medians. **C**: Share of putative GABAergic (SynI+GAD-ir) terminals of all putative synapses identified by SynI-ir for DUM 3,4 and DUM 3,4,5 samples. No significant differences were revealed for DUM 3,4 and DUM 3,4,5 samples, however, a slight tendency to a higher GABAergic share for DUM 3,4,5 samples was visible. Number of image stacks examined: $N_{DUM3,4}$=9, $N_{DUM3,4,5}$=13.

categorised with respect to the radius of the individual dendrite segments. The statistical data available for the reconstructed trees showed that 86 % of the branches comprised dendrites with radii less than 0.5 μm and that more than 70 % (72 % for DUM 3,4 and 73 % for DUM 3,4,5 neurons) did not exceed 0.3 μm (fig. 2.8A). Although the lack of a greater amount of thicker (low-order) dendrites rendered a respective evaluation less comprehensive, the data affirmed a bias in synapse distribution with less presynaptic profiles in touch with branches of greater diameter (fig. 2.8B). This applied both to DUM 3,4 and DUM 3,4,5 neurons. Regarding the radius classes from 0.1 to 0.5, which held the abundant majority of branches, no significant differences in the amount of either putative synaptic or putative GABAergic input sites were revealed within either the DUM 3,4 or the DUM 3,4,5 neuron pool (fig. 2.8C/D), thus within this radius range, the distribution seemed to be quite uniform. However, the tendency of DUM 3,4 neurons to excel DUM 3,4,5 neurons in the amount of putative input synapses was again clearly discernible and significant for radii ranging between 0.3 and 0.4 μm (fig. 2.8C, Wilcoxon-Rank-Sum-Test, $p<0.01$). Within the same intervall, this tendency was apparent for the amount of putative GABAergic input sites as well, whereas for the other branch radius classes a difference between the neurons was not obvious (fig. 2.8D).

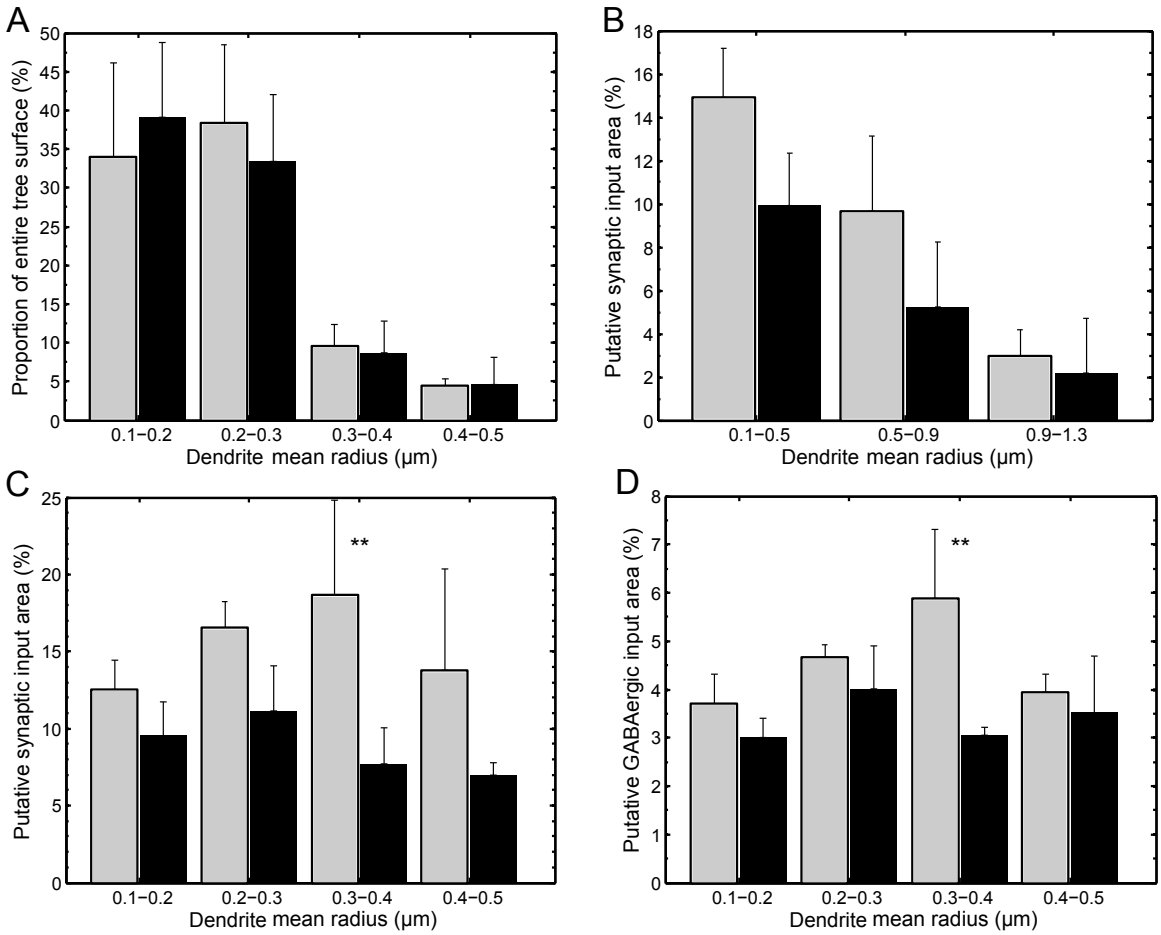

Figure 2.8: Putative synaptic and GABAergic input area for different branch radii of DUM 3,4 (grey bars) and DUM 3,4,5 (black bars) neurons. **A**: Surface proportions per dendrite radius class for DUM 3,4 and DUM 3,4,5 "b" branches with more than 80 % of the examined dendrites having radii less than 0.5 μm. **B**: Putative synaptic input area for three branch radius classes from 0.1 to 1.3 μm showing that low-order dendrites receive less input. However, note that less than 20 % of the examined branches had radii above 0.5 μm. **C**: Putative synaptic input area for dendrites of four branch radius classes between 0.1 to 0.5 μm reveals larger values for DUM 3,4 neurons, with significant differences for branches of radii between 0.3 and 0.4 μm. Wilcoxon-Rank-Sum-Test,**p<0.01. **D**: Putative GABAergic input area on dendrites of branch radius classes 0.1 to 0.5 μm does not differ between DUM 3,4 and DUM 3,4,5 neurons, however, for branches of 0.3 to 0.4 μm radius DUM 3,4,5 neurons receive less putative GABAergic input. Wilcoxon-Rank-Sum-Test,**p<0.01. $N_{DUM3,4}$=3, $N_{DUM3,4}$=4.

3.3 Distribution and modulatory function of octopamine and tyramine in the periphery

Distribution of neuromodulatory fibers on M85/M114

Due to its small size and DUM neuron innervation the pleuroaxillary flight steering muscle M85(mesothorax)/M114(metathorax) provided a good means for the visualisation of neuromodulatory varicosities on skeletal muscle and served to highlight some of their anatomical properties. Fig. 3.1A displays the pattern of octopamine-immunoreactivity (OA-ir) on M 85. Both muscle parts a and b, which receive slightly different innervation by motor neurons (Meuser and Pflüger, 1998), but share innervation of DUM 3,4,5a (Stevenson and Meuser, 1997), were evenly covered by varicosities of neuromodulatory origin (fig. 3.1A). The octopaminergic innervation prevailingly proceeded in parallel to single muscle fibers throughout all muscle layers and along the entire muscle length. Octopaminergic varicosities appeared as chains of loosely arranged boutons; the latter varied in their size, were often elliptic in shape and had a mean diameter of 1.7 ± 0.55 μm (fig. 3.1B). In some cases not only boutons, but also fibers were stained, indicating the presence of the biogenic amine in this cellular compartment. Thanks to the availability of a reliable antibody to tyramine (Kononenko et al., 2009) the occurrence of tyramine on skeletal muscle was verified. As displayed in fig. 3.1C, tyramine-immunoreactivity (TA-ir) turned out to be exclusively confined to varicosities that were also shown to be octopaminergic. The TA-ir in general was less intense than the OA-ir. However, since boutons were clearly labelled, it may be assumed that both transmitters were concentrated in synaptic vesicles. This co-localisation of octopamine and tyramine furthermore was confirmed for the second posterior tergocoxal muscle M91/M120, which in contrast to M85/114 is innervated by a DUM 3,4 neuron. This differential innervation was verified by retrograde staining of the M120 motor nerve N4D2 and is shown in fig. 3.3.

Motor neuron terminals were visualized for comparison using anterograde neurobiotin staining of N4D4. This approach in most cases revealed axons and terminals of the larger diameter neurons (two motor neurons and the common inhibitor neuron), whereas the few smaller diameter neurons innervating this muscle (Pflüger et al., 1986; Stevenson and Meuser, 1997), to which belongs also the DUM 3,4,5 neuron, became barely stained, unless the incubation time did not exceed 24 hours. These terminals, in contrast to neuromodulatory boutons, consisted of large densely packed accumulations mostly aligned in parallel to muscle fibers (3 to 8 μm in diameter, fig. 3.2A, which they completely covered in a compact meshwork, as typical for insect muscle. To examine the presence of typical synaptic proteins in motor neuron terminals, counterstaining of the dye filled motor axons with either one of two synaptic markers, namely an antibody to synapsin I, which occurs associated with synaptic

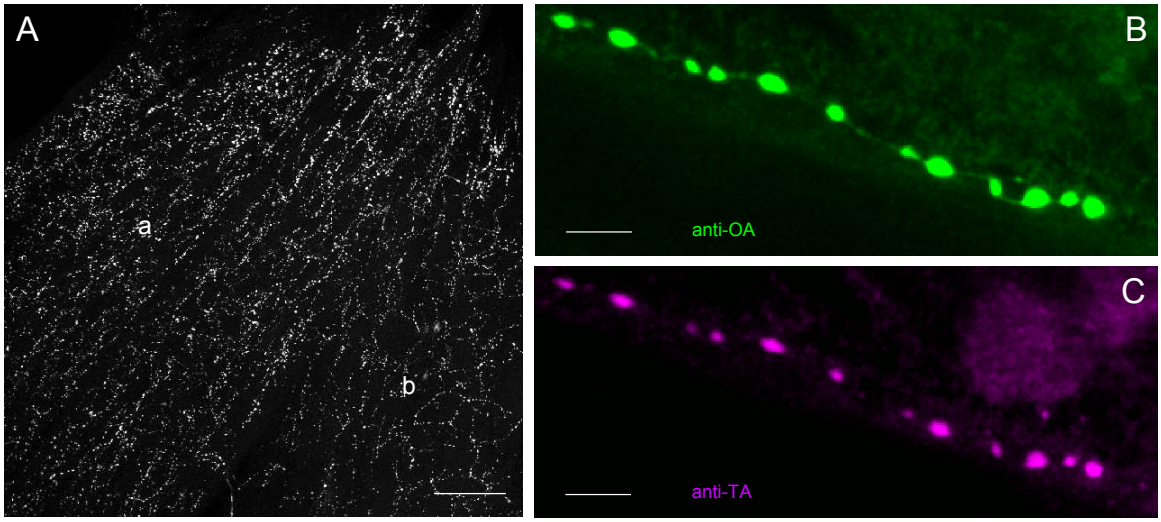

Figure 3.1: Octopamine and tyramine are co-localised on the locust flight steering muscle M85. **A**: OA-ir reveals evenly distributed chains of varicosities on muscle parts a and b of M85. Z-Dimension of image stack 30 μm, scale bar 100 μm. **B,C**: Co-localisation of OA-ir (B) and TA-ir (C) in boutons on M85. Z-Dimension of image stacks 11 μm, scale bar 5 μm

vesicles and to NC82, a protein which is part of the active zone complex, was performed. Fig. 3.2C shows that double-labelling of axons (neurobiotin) and terminals with anti-synapsin I resulted in a clear compartmentalisation and highlighted entire motor terminals. NC82 labelling, differently to synapsin I, yielded distinct puncta which presumably corresponded to the position of active zones within the large terminals (fig. 3.2B). The identity of the transmitter(s) stored in single motor terminals could not unambiguously be determined in this study due to difficulties regarding antibody penetration and specificity (anti-glutamate and anti-GABA); however, it is probable drawing on other studies and own preliminary data (not shown) that the motor neuron terminals contain and release glutamate, while the common inhibitor neurons are GABAergic (Usherwood et al., 1968; Usherwood and Grundfest, 1965).

As for the neuromodulatory varicosities, synapsin I counterstaining yielded positive results as well. Fig. 3.3F reveals the detection of this synaptic protein in TA-immunoreactive boutons, however, compared to the anti-synapsin I staining intensity in motor terminals, its presence was quite weak, probably hinting to a smaller amount of synapsin I in neuromodulatory boutons.

In double-stainings of motor terminals and neuromodulatory varicosities (OA-ir), these fibers of different provenance often lay in immediate vicinity, with the smaller neuromodulatory fibers either following the motor axons/terminals or even virtually enwinding the latter (fig. 3.3A). This conspicuous arrangement is schematically illustrated in fig. 3.3D. The high resolution image (fig. 3.3B) clearly shows that the distance between motor terminals and octopaminergic boutons was often less than 300 nm, thus both structures can be suggested to maintain synaptic contacts. This

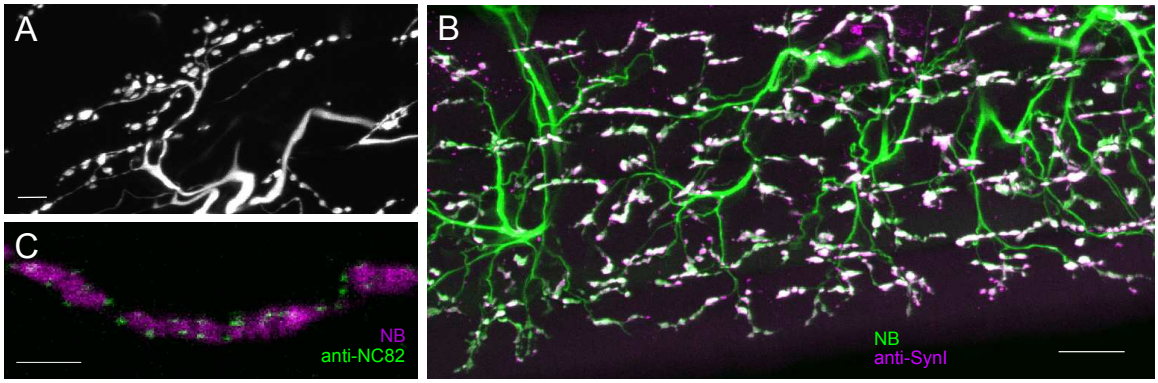

Figure 3.2: Motor neuron terminals on M85 stain with antibodies to synaptic markers. **A**: Typical appearance of motor neuron terminals on M85. Terminals are aligned in parallel to fibers and cover the entire muscle. Z-Dimension of image stack 10 μm, scale bar 10 μm. **B**: Labelling of M85 with anti-synapsin I (magenta) highlights neurobiotin(NB)-stained motor terminals. Z-Dimension of image stack 30 μm, scale bar 20 μm. **C**: Immunoreactivity to the synaptic protein NC82 (green) can be located in motor terminals (green, NB-labelled) as distinct puncta presumably representing active zones. Z-Dimension of image stack 30 μm, scale bar 5 μm.

holds true if the width of the synaptic cleft (of about 15 nm) plus presynaptic membrane and vesicle pool is estimated to amount to 200 to 300 nm (see preceding section 3.2).

Taken together, these data provide evidence for exclusive co-localisation of octopamine and tyramine on insect skeletal muscle and illustrate the distribution pattern of octopaminergic/tyraminergic fibers in alignment with motor neuron terminals.

OA- and TA-ir in dependence on behavioural experience

To investigate whether the peripheral neuromodulator amounts measured by OA- and TA-ir reflected the behavioural state of the animals, adult locusts of either sex were separated into three groups and subjected to different treatment. The control group (N=6) was left undisturbed, whereas the other two were either tethered to perform steady flight (N=5) or exposed to stress (N=4) (see Methods 2.3) prior to tissue fixation and subsequent immunocytochemistry. Fig. 3.4D representatively illustrates OA-ir on muscle tissue of control and stress treated animals. A quantitative analysis of octopamine and TA in boutons was basically performed by selecting representative chains of stained varicosities from each muscle examined (Number of muscles examined: Control: N=9, Flight: N=8, Stress: N=7) and measuring their volume threshold-dependently in consideration of the grey value histogram to part background from staining (see Methods 2.7).

Figs. 3.4A/B show the frequency distributions of the assessed volumes of octopaminergic and tyraminergic boutons. Regarding the size of octopaminergic boutons within the control group, the majority of boutons had volume sizes between 0.1 and 2.2 μm^3. This corresponded well to the average bouton diameter of 1,7 μm (see

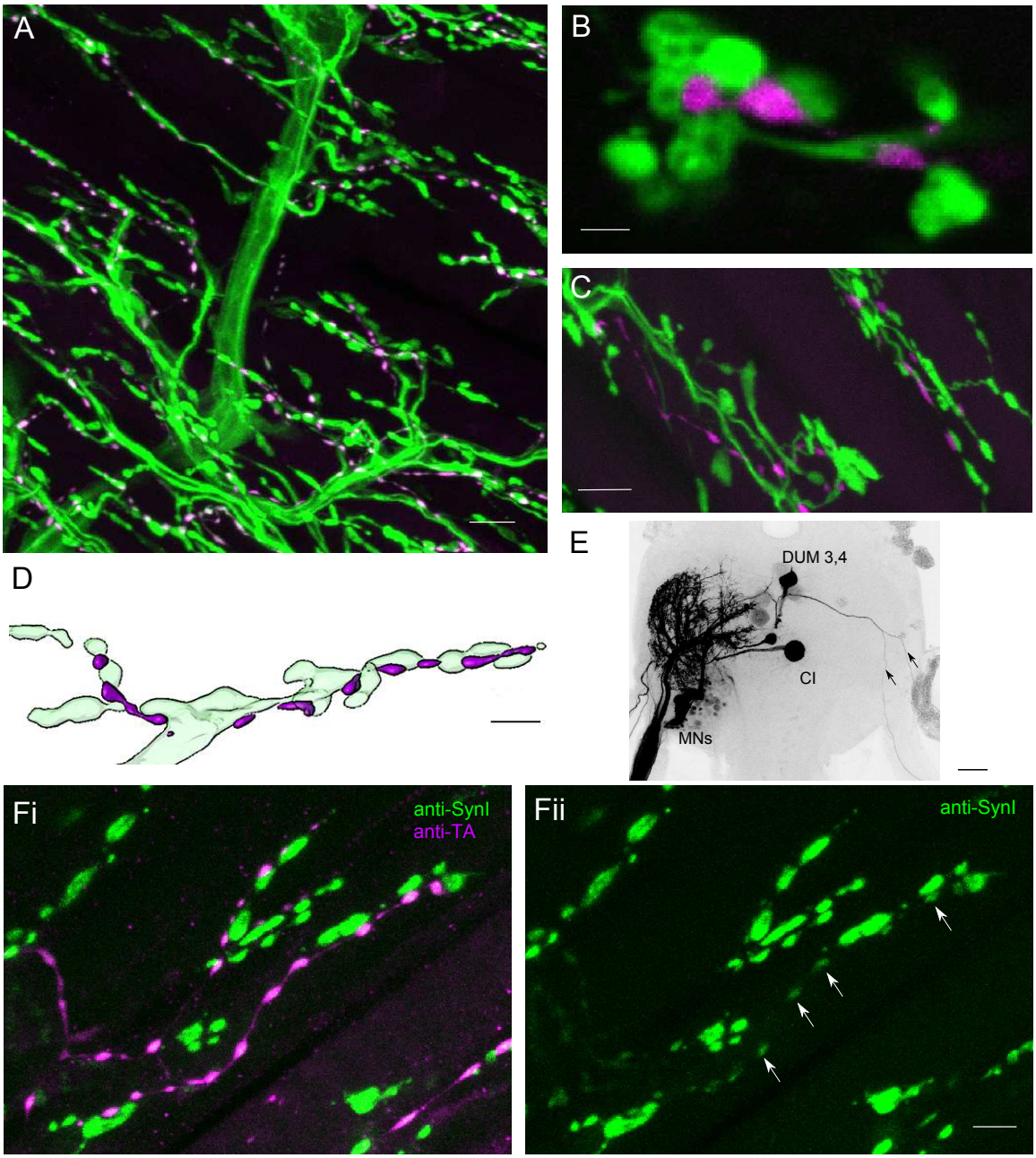

Figure 3.3: Octopaminergic/tyraminergic fibers run in immediate vicinity to motor neuron axons and terminals on M85. **A**: Octopaminergic varicosities (magenta) follow the path of neurobiotin(NB)-labelled (motor) neurons of N4D4 (green). Z-dimension of image stack 100 μm, scale bar 10 μm. **B**: Individual octopaminergic boutons (magenta) are tightly enclosed by motor neuron terminals (green); the distance between both structures is less than 300 nm. Single optical slice of 1 μm width, scale bar 2 μm. **C**: Octopaminergic varicosities (magenta) follow motor terminals (green) on M120. Z-dimension 32 μm, scale bar 10 μm. **D**: Schematic illustrating the typical arrangement of neuromodulatory varicosities (magenta) enwinding motor terminals (green). Scale bar 5 μm. **E**: A DUM 3,4 neuron innervates the metathoracic bifunctional elevator M120 as revealed by retrograde neurobiotin staining of N4D2. Arrows indicate the axons exiting the ganglion via N3 and N4. CI Common Inhibitor neuron, MNs Motorneurons of M120. Z-dimension 316 μm, scale bar 100 μm. **F**: Double-labelling with anti-synapsin I (green) and anti-tyramine (magenta) shows the characteristic octopaminergic/tyraminergic fibers in proximity to motor terminals (green, Fi). The same stack with anti-synapsin I staining alone reveals only weak labelling of OA/TA-ir boutons (Fii). Z-dimension of image stacks 10 μm, scale bar 5 μm

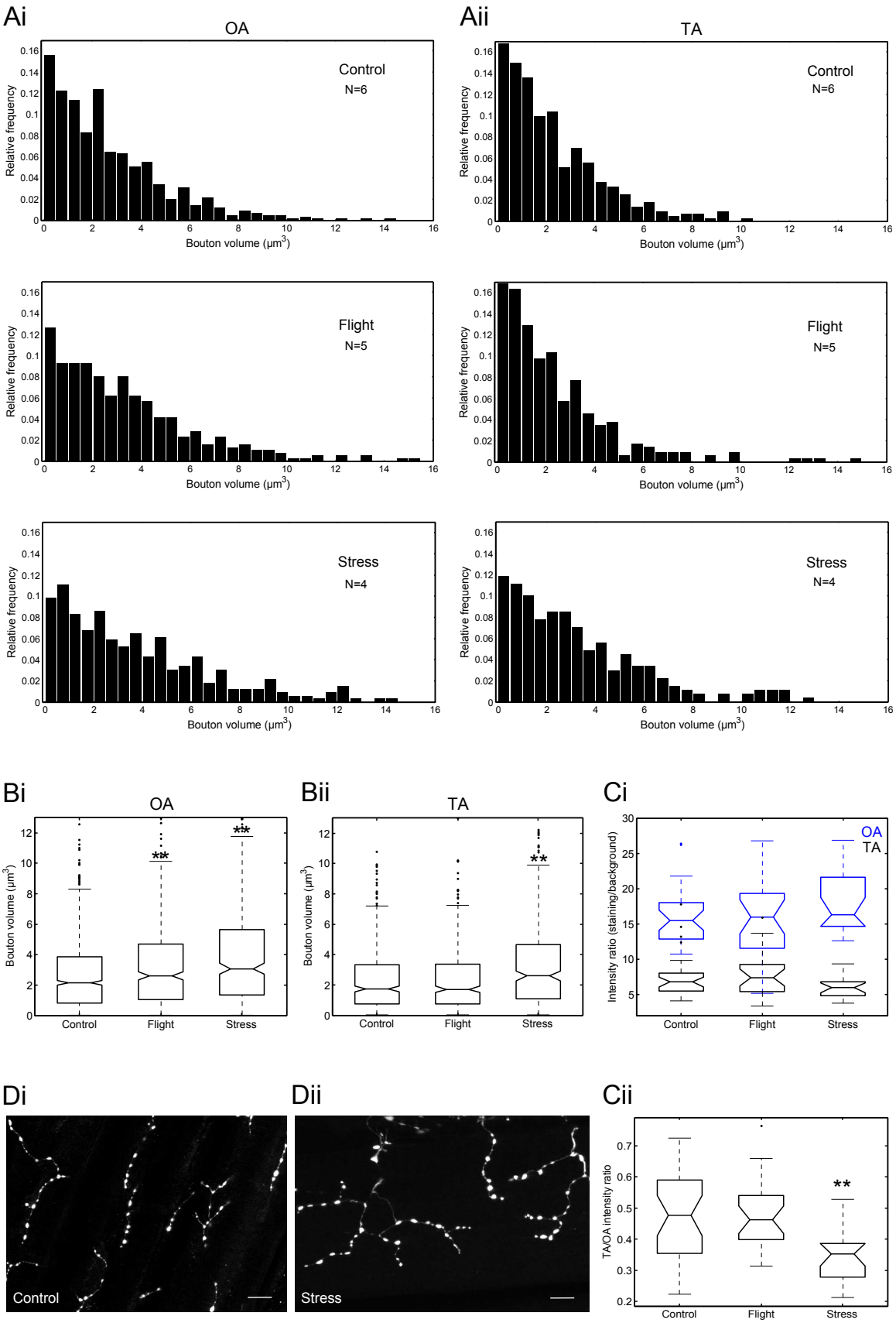
Ai
OA
Control
N=6
Flight
N=5
Stress
N=4
Relative frequency
Bouton volume (μm3)
Aii
TA
Control
N=6
Flight
N=5
Stress
N=4
Relative frequency
Bouton volume (μm3)
Bi
OA
Bouton volume (μm3)
Control
Flight
Stress
**
Bii
TA
Bouton volume (μm3)
Control
Flight
Stress
**
Ci
OA
TA
Intensity ratio (staining/background)
Control
Flight
Stress
Di
Control
Dii
Stress
Cii
TA/OA intensity ratio
Control
Flight
Stress
**

3.3), in consideration of the volume of an ellipsoid body $V_e = \frac{4}{3}\pi r_1 r_2 r_3$, where r_1-r_3 designate the respective half diameters. When comparing the octopamine control distribution to the distributions representing flight-experienced and stress-exposed animals (fig. 3.4A), there seemed to be a mild bias within the latter distributions towards larger bouton volumes. Thus lower relative frequencies were found within the above mentioned range from 0.1 to 2.2 μm^3, but higher ones for greater bouton volumes. This impression was reflected in the significantly different medians of the respective groups (fig. 3.4C), with the stress-exposed group exhibiting the largest difference (median 2.57 μm^3) to the control group. The same held true for tyramine-immunoreactive boutons, where the boutons of stress-exposed animals again showed a significantly biased distribution (median stress 2.4 μm^3 versus control 1.9 μm^3). However, evaluating TA-ir, the group which had experienced flight was not different from the control. Interestingly, although the median of the bouton distribution for the TA-ir control group lay below the one for the OA-ir control group, corroborating the general observation of weaker TA-ir versus OA-ir, the stress group median for the tyramine bouton volume distribution was in the range of the one measured for octopamine (see fig. 3.4C).

To additionally test whether the OA- and TA-ir, respectively, was comparable among different muscle tissue preparations, the relative staining intensities were assessed for the different groups. For this purpose the average intensity of the immunopositive staining was divided by the average background staining per image stack (see Methods 2.7). The results are displayed in fig. 3.4Di and clearly show the gap between the intensity ratios for OA-ir (blue), which were around 15, and TA-ir (black), which were in the range of 6, indicating a higher signal-to-noise ratio for OA-ir and thus qualitative differences between both antibody stainings. However, among differently treated groups the ratios for OA-ir and TA-ir, respectively, did not differ significantly, although for OA-ir they tended to be higher in stress-exposed an-

Figure 3.4 : Size of OA- and TA-immunoreactive boutons on M85 in dependence of behavioural experience. **A**: Frequency distributions of octopaminergic boutons (i) show that flight experienced and stress treated animals display a shifted size distribution towards larger boutons in comparison to the control group. As for TA-ir boutons, this tendency is only obvious for boutons of stress treated animals (ii). Histogram bars represent the relative frequency of boutons for intervals of 0.5 μm^3, N number of animals tested, Number of boutons examined (OA/TA): Control=423/262, Flight=225/212, Stress=183/158. **B**: Boxplots confirming significant differences between the octopaminergic (i) and tyraminergic (ii) bouton volume distributions shown in A. N as in A, Kruskal-Wallis-Test, $^{**}p<0.01$. **C**: The relative OA/TA-ir intensities of control and behaviourally treated groups reveal no differences among groups, although the signal-to-noise ratio of OA-ir in boutons (blue) is generally higher than that of TA-ir in boutons (black)(i). However, the ratio of these relative intensities (TA/OA) is significantly smaller for stress-exposed animals than for the control and flight groups (ii). Number of image stacks examined: Control=33, Flight=26, Stress=19. Kruskal-Wallis-Test, $^{**}p<0.01$. **D**: Representative confocal image stacks display bouton appearance of control (i) and stress-exposed animals (ii). Z-dimension of image stacks 11 μm, scale bar 10 μm. OA octopamine TA tyramine.

imals compared to the control, whereas the opposite seemed to be true for tyramine in stress-exposed animals (fig. 3.4Di). This bias became more apparent, when the TA/octopamine ratio of these relative intensities was assessed (fig. 3.4Dii).

In summary, these data indicate that octopamine and tyramine contents in neuromodulatory boutons show a subtle plasticity dependent on the behavioural pretreatment of the animals.

Effects of tyramine on muscle performance

The fact that tyramine is present in neuromodulatory varicosities and presumably concentrated in vesicles, can be considered one prerequisite for a possible role as independent transmitter in the peripheral nervous system. In the following experiments, the influence of tyramine on M85/M114 contraction properties was examined via muscle mechanograms (see Methods 2.5) and compared to the octopamine effect. Only relative changes were recorded, all measurements refer thus to the initial control status of the respective muscle prior to application of any substance.

TA application to continuously stimulated (1 Hz) isolated muscles (M85/114), which were perfused with locust saline at constant temperature (21-22°C), evoked a dose-dependent increase of muscle performance, which qualitatively resembled the modulation by octopamine, but was less efficient (fig. 3.5D). At a concentration of 10 μM tyramine, individual twitch amplitudes increased slightly by on average 6.7 % compared to the control (fig. 3.5A, N=8). This was considerably less than the approximate 10.6% increase elicited by octopamine application at a concentration of 1 μM (N=10). At this concentration, the tyramine effect was not longer evident (N=15). Similarly, 10 μM tyramine caused an only minor acceleration of the contraction rate of individual muscle twitches by 4 %, compared to a 7 % increase due to application of 1 μM octopamine. 1 μM tyramine was on average not potent to evoke any effect, however, in some preparations a slight increase was evident (figs. 3.5B/D). Regarding the relaxation rate of muscle twitches, the effect of tyramine was most conspicuous: 10 μM tyramine was able to elicit increases of on average 49 % compared to on average 67 % by 1 μM octopamine (fig. 3.5C). Even lower concentrations of tyramine (1 μM) still had an effect of about 9 %. At concentrations of 0.1 μM and less no increase of the examined parameters was observed (data not shown). Fig. 3.5D illustrates a typical time course showing the increase in contraction and relaxation rate due to successive 1 μM octopamine and tyramine application. Not only the differences in potency are clearly discernible, but also the typical slow and longlasting effects. Thus, the maximum increase was observed 3-5 minutes after application, whereas it took about 15 minutes for the effect to cease.

Since tyramine seemed to mimic the octopaminergic effect, tyramine-dependent

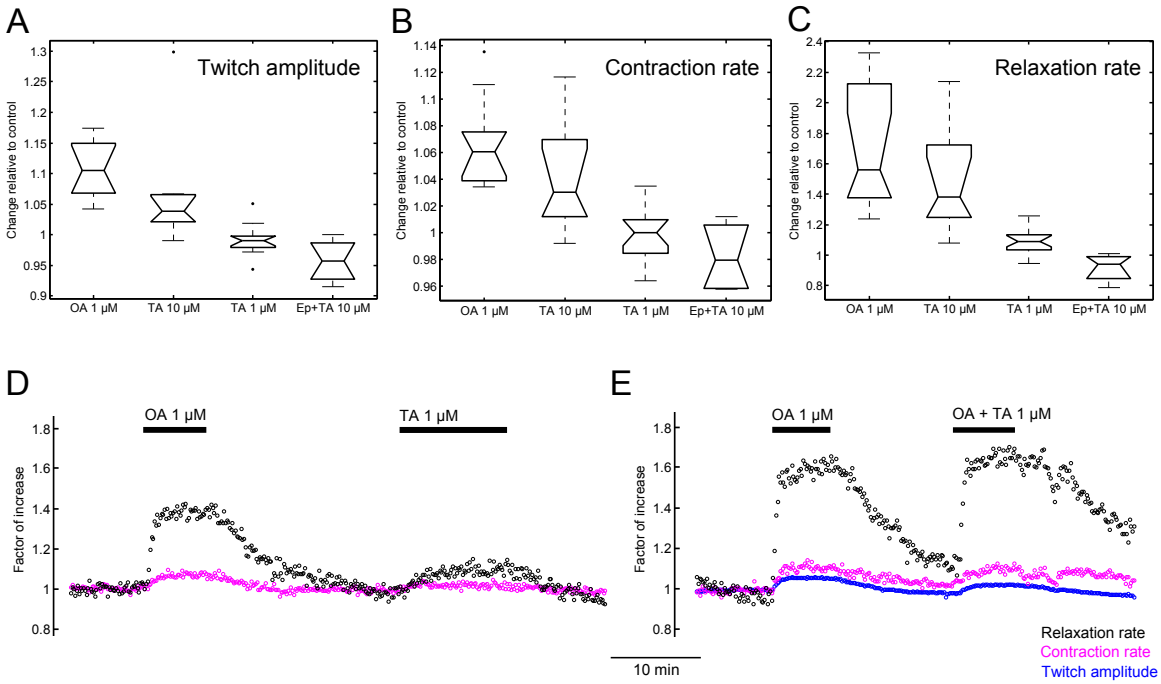

Figure 3.5: Effects of tyramine and epinastine on muscle properties. **A,B,C**: 10 μM TA increases the twitch amplitude (A), the contraction rate (B) and the relaxation rate of single muscle twitches (0.5 Hz stimulation) to a similar extent as 1 μM OA. At 1 μM TA, only a slight increase of the relaxation rate is observed (C), whereas twitch amplitude and contraction rate are hardly affected. Application of 10 μM epinastine together with 10 μM TA completely abolishes the effects (far right boxplot). N(1 μM TA)=10, N(10 μM TA)=8, N(1 μM TA)=15, N(10 μM TA+10 μM Ep)=4. Ep epinastine, OA octopamine, TA tyramine. **D**: Representative time course showing increase of contraction and relaxation rates of individual muscle twitches (evoked at 1 Hz) in response to 1 μM OA, diminishing of the effect due to washout and 1 μM TA application. TA is only half as potent as OA in enhancing the named parameters. Each circle corresponds to data from an individual muscle twitch and was normalised to the initial value prior to substance application. OA octopamine, TA tyramine. **E**: Time course showing increase of twitch amplitude, contraction and relaxation rates in response to 1 μM OA and 1 μM OA+TA application, indicating that the accumulative application of OA and TA does not enhance the response of OA alone. Each circle corresponds to data from an individual muscle twitch and was normalised to the initial value prior to substance application. OA octopamine, TA tyramine.

modulation of muscle properties may be mediated via specific octopamine-receptors (OARs) for which tyramine shows a lower affinity. If this was the case, simultaneous application of octopamine and tyramine would be assumed to result in a competitive effect instead of in further increase of muscle performance. Preliminary data indicated that there was no obvious enhancement of 1 μM application of octopamine and tyramine compared to 1 μM octopamine alone as representatively displayed in fig. 3.5E. However, the sample size was to small to quantify the probably subtle effect accordingly.

To further test if OARs were responsible for the tyramine-mediated increase of muscle performance, a potent antagonist of neuronal OARs, epinastine (Roeder et al., 1998), was applied together with tyramine in equal concentrations of 10 μM (N=4). As illustrated in fig. 3.5A,B,C for all parameters investigated, epinastine at this

concentration completely abolished the tyraminergic effect and often led to a slight decrease in muscle performance. Preliminary data indicated that epinastine at lower concentrations (1 μM) was still able to prevent the 10 μM tyramine effect.

In summary, these data show that tyramine affects the performance of M85/114 qualitatively similarly to octopamine, however, its potency is considerably weaker. These observations together with the fact that the tyramine effect is blocked by the OAR antagonist epinastine, render the effect likely to be mediated by OARs.

4 Discussion

Differential activation of DUM neurons by flight-relevant pathways

Following N1C1(a) and TCC stimulation, intracellularly recorded pterothoracic DUM neurons were demonstrated to be subject to subtype specific excitation or inhibition. More precisely, "wing group" neurons, i.e. DUMDL, DUM 3 and DUM 3,4 neurons, were inhibited, whereas DUM 3,4,5 neurons were excited due to N1C1(a) stimulation in preparations lacking brain and SOG, thus via a segmental polysynaptic pathway. TCC stimulation, i.e. presumable activation of the tritocerebral giant (TCG) interneuron, elicited inhibitory responses in DUM 3 and DUM 3,4 neurons via polysynaptic connections, while DUM 1b neurons received excitatory input.

The tegula, an exteroceptor at the wing base (Altman et al., 1978; Kutsch et al., 1980), has been shown to deliver phasic input to flight motor neurons and interneurons during wing downstroke and to be responsible for the shape and timing of elevator depolarisations (Neumann et al., 1982; Wolf and Pearson, 1988). In accordance with previous results by Duch and Pflüger (1999), "wing group" DUM neurons almost exclusively received inhibitory input due to tegula stimulation via a segmental, polysynaptic pathway (figs. 1.1A/B, 1.3A, 1.4B). In contrast, "leg group" neurons, i.e. only DUM 3,4,5 neurons in the present study, were found to fire action potentials in response to stimulation (fig. 1.6B). These observations, together with the in general longer latencies for "leg group" neurons (table 1.2) clearly indicate differential control of DUM neuron subsets following tegula excitation. The excitatory pathway to DUM 3,4,5 neurons may thus involve more synapses than the inhibitory pathway for "wing group" neurons. Similar results were found for "wing" and "leg group" coupling to internal proprioceptors (Morris et al., 1999).

The fact that N1C1(a) input to DUM neurons passed the connectives between meso- and metathoracic ganglia in either direction, fits in with tegulae afferents conveying signals to motorneurons in the adjacent pterothoracic ganglion via intersegmental interneurons (Pearson and Wolf, 1988). Since these latter connections are considerably faster (about 7 ms versus at least 15 ms for DUM 3,4,5 neurons), they can, however, not be assumed to be identical for DUM 3,4,5 neurons. Surprisingly, the responsiveness of DUM 3,4,5 neurons is not in accordance with the study of Duch and Pflüger (1999), where DUM 3,4,5 neurons remained silent during nerve stimulation. It is unlikely that the segmental pathway revealed in this study was suppressed in the semi-intact preparation comprising brain and suboesophageal ganglion (SOG) used by Duch and Pflüger (1999), since in the present study one semi-intact preparation showed responses as well. However, the suboesophageal ganglion (SOG) has been proposed to play a major role in the processing of sensory information, as

cutting the neck connectives led to loss of abdominal sensory input to DUM neurons (Duch et al., 1999; Field et al., 2008). A more likely explanation in this case, however, may be that the DUM 3,4,5 neuron population itself is under differential control; there are three neurons in the meta- and four neurons in the mesothoracic ganglion, which have been shown to exhibit anatomical differences (Campbell et al., 1995; Bräunig, 1997; Stevenson and Meuser, 1997). A differential recruitment during sensory stimulation and motor behaviour has been also stressed by Morris et al. (1999). Supportively, only about the half of the tested cells were responsive to stimulation. In addition, the responsiveness for a given neuron may change with the internal or arousal state of the animal, which has especially been reported for "wing group" neurons so far (Baudoux and Burrows, 1998). Finally, it is still possible that stimulation of the tegula nerve resulted in wing nerve excitation via current spread, however, due to the selective and subtle stimulation, this is hardly probable.

The DUM 3,4,5 neuron response to tegula stimulation matches with the positive coupling of these neurons to (i) wind-sensitive pathways (Duch and Pflüger, 1999), (ii) flight muscle contractions via internal proprioceptors (Morris et al., 1999) and (iii) the central flight motor (Duch and Pflüger, 1999). The specific significance of this pathway is subject to speculation, since the habituation of DUM 3,4,5 neurons was strong and tegula input was only effective in eliciting few action potentials. This is in accordance with input from chordotonal organs (Morris et al., 1999) and other sensory organs (Field et al., 2008), where the excitatory input to DUM 3,4,5 neurons diminished with repeated stimulation. It was also noted that antidromic stimulation at 10-20 Hz failed to elicit spikes after 5 to 10 minutes in these neurons (Duch and Pflüger, 1999). These data render it unlikely that cycle-to-cycle tegula input during flight (Wolf and Pearson, 1988) continuously activates DUM 3,4,5 neurons. Thus, this pathway is suggested to only be relevant at the onset of flight. Activity of DUM 3,4,5 during flight could either result in targeted octopamine release and thus modulation of leg muscles, which are involved in ruddering movements, or in systemic octopamine release from neurohaemal-like release sites on peripheral nerves (Bräunig, 1997). DUM 3,4,5 neurons could thus contribute to the high haemolymph octopamine levels observed during the first period of flight (Goosey and Candy, 1980; Orchard et al., 1993) with implications both for metabolism and flight muscle performance (Candy, 1978; Mentel et al., 2003).

As for "wing group" DUM neurons, the inhibitory input has been proposed to be sufficient in duration and amplitude to prevent these neurons during flight from spiking (Duch and Pflüger, 1999) and thus from releasing octopamine. Although the observed habituation for "wing group" neurons in this study suggests decreasing influence of tegula input during sustained stimulation (figs. 1.4C), the actual inhibition

of these DUM neurons may be less labile under natural conditions. The almost completely deafferentated preparation used in this study served only to elucidate microcircuits within the thoracic segments. Moreover, the stimulus regime applied did not exactly mimic authentic discharge of sensory afferents, thus parameters such as habituation and latency increase may also vary depending on discharge intervals and coincident input. Finally, there is evidence from semi-intact preparations, that a great deal of sensory information is pre-processed in the SOG before passed on to DUM neurons (Duch et al., 1999; Field et al., 2008). Thus the convergence of sensory input from diverse body parts (head, wings, legs, abdomen) plus central negative coupling to the flight motor (Duch and Pflüger, 1999) may result in sustained inhibition of "wing group" neurons during flight. This continuous inhibition and consequent decrease of octopamine in flight muscles has been shown to promote the decrease of fructose 2,6-bisphosphate (Mentel et al., 2003) and thus could contribute to the observed switch from carbohydrate metabolism to lipid oxidation during long-term flight (Wegener et al., 1986; Blau and Wegener, 1994).

There are some indicators in the present study that DUM 3,4 neurons form a heterogeneous population and possibly are functionally separated into DUM 3A,4 and DUM 3AC,4 neurons (Campbell et al., 1995). First, the considerably longer latencies for DUM 3AC,4 neurons (fig. 1.4D) in comparison to DUM 3A,4 neurons may hint to differential control/pathways. Second, the habituation of DUM 3AC,4 neurons tended to be slightly stronger than for DUM 3A,4 neurons (fig. 1.4C), indicating more labile synapses and/or enhanced processing. Third, the responses of DUM 3AC,4 neurons to N1C1 stimulation were not as reliable as those of DUM 3A,4 neurons, in that they sometimes showed responses which resembled EPSPs; however, this was not verified in last detail. In previous studies DUM 3,4 neurons were shown to respond ambiguously to sensory stimulation of leg or head sensillae (Baudoux and Burrows, 1998; Duch et al., 1999) in that they were either hyperpolarised or depolarised above spike threshold, often depending on whether the locust was in a quiescent state or active. Although the respective coupling to central motor commands may be sufficient to explain this phenomenon, it is possible that the neurons' affiliation to either of the DUM 3,4 subgroups may play a role as well. Supporting a functional segregation, Mentel et al. (2003) noted that DUM 3AC,4 neurons, but not DUM 3A,4 neurons were spontaneously active during leg levator activity.

Further evidence of differential DUM 3,4 activation provided a recording where a DUM 3A,4 neuron was clearly activated in synchrony with motor units recorded in N1D (figs. 1.5A/B). These units either represent the mesothoracic motor neurons innervating M112 or the individual metathoracic motor neuron innervating the same muscle (fig. 1.1Ci, (Bentley, 1970; Tyrer and Altman, 1974)) and thus are depressor

motor neurons. Interestingly, DUM 3,4 neurons have not been demonstrated before to be other than negatively coupled to flight motor neuron activity. However, the activity recorded in N1D was arrhythmic, thus so far does not contradict the inhibition of DUM 3,4 neurons during flight (Duch and Pflüger, 1999). The observed coincident firing might be due to some common input either of sensory or local provenance, without activation of the central flight motor.

Interestingly, the experiments performing TCC stimulation strongly suggest that DUM 3 and DUM 3A,4 neurons receive input from TCG. TCG itself receives direct input from wind-sensitive hairs on the facial setae, from the antennae and in addition some visual input (Bacon and Tyrer, 1978; Bacon and Möhl, 1983). Although not a command neuron, it monosynaptically connects to flight motor neurons (Bacon and Tyrer, 1979) and is sufficient to elicit flight (Bicker and Pearson, 1983). It is quite intuitive that "wing group" DUM neurons, which are known to be inhibited due to input from the tegula, due to flight muscle contractions Morris et al. (1999) and in parallel to the central flight motor (Duch and Pflüger, 1999), which can be activated by either wind or TCG stimulation, are inhibited via this pathway. Although the connections are polysynaptic, the comparably short latency and the quite weak habituation (fig. 1.3E and table 1.2) imply a stable connection especially to DUM 3 neurons, which were most reliably inhibited by TCC stimulation. However, in spite of the relatively high response rate of DUM 3 neurons, "wing group" neurons still showed habituation, thus it is not known, if the inhibition via TCG may become less relevant during patterned activation at high frequency as realistic during flight (Bacon and Möhl, 1979). However, apart from being rhythmically active during flight in approximate synchrony with depressor muscle activity (Bacon and Möhl, 1983), TCG also mediates yaw-correcting behaviour (Möhl and Bacon, 1983). Thus, the realistic discharge of TCG in a turbulent airstream might result, due to yaw-angle coding of TCG, in a less regular spiking pattern. The neuron possesses extensive arborisations in the dorsal neuropils of each pterothoracic ganglion (Bacon and Tyrer, 1978), even in immediate proximity to DUM neuron branches (fig. 1.5C), and could convey the signal via local or intersegmental interneurons, populations of which have been shown to be GABAergic (Watson and Burrows, 1987; Watson and Laurent, 1990; Wildman et al., 2002).

In contrast to "wing group" neurons, DUM 1b neurons were clearly activated in response to TCC stimulation (fig. 1.2A/B). Although only two neurons were recorded, this is intriguing, since there is only a small data record of DUM 1b neuron activation in literature. They have previously been reported to show labile responses during hind leg kicks (Burrows and Pflüger, 1995) and to sensory stimulation (Baudoux and Burrows, 1998), where the weak (excitatory) response depended on

whether the locust performed active movements. Most effective in activating DUM 1b neurons were wind stimuli directed to the head (Baudoux and Burrows, 1998). The pathway via TCG could thus mediate this sensory information. Again, although DUM 1b action potentials during maintained stimulation soon failed to be elicited (fig. 1.2A), the stability and relevance of the connection during realistic TCG discharge may be different from the observed situation.

DUM 1b neurons innervate ventral longitudinal muscles, spiracle muscles and salivary glands and form extensive neurohaemal release sites on peripheral nerves, among which are the well described neurohaemal organs associated with the transversal nerves (Bräunig and Evans, 1994; Bräunig, 1997). Activation of DUM 1b due to sensory input and/or TCG activation could thus lead to enhanced release of octopamine into the circulation, in a possibly more pronounced manner than assumed for DUM 3,4,5 neurons. As mentioned before, octopamine haemolymph levels are increased at the onset of flight (Goosey and Candy, 1980) and may influence metabolism or release of hormones, as well as muscle performance. A targetted release of octopamine to spiracle muscles, which are active during flight (Miller, 1960) and have been shown to be modulated by octopamine similar to skeletal muscles (Bräunig and Evans, 1994), could enhance muscle force and relaxation rate during the initial flight phase to meet the enhanced energy demands via optimized oxygene supply. Although the function of other target muscles such as the ventral longitudinal muscles are elusive so far, they seem suited for adjusting body posture and might, if tuned by octopamine, more effectively contribute to flight stability. The octopaminergic influence on salivary glands remains undetermined so far, but suggests a less prominent and more indirect role on salivation (Baines et al., 1989; Ali, 1997).

Taken together, this study corroborates and supplements previous data reporting that DUM neurons are differentially activated in response to sensory stimulation (Field et al., 2008; Morris et al., 1999) and in parallel to motor behaviour (Duch and Pflüger, 1999; Burrows and Pflüger, 1995) and objects to the notion that this population is concomitantly active during arousal and flight (Hoyle and Dagan, 1978; Ramirez and Orchard, 1990). It provides evidence of flight-relevant pathways which seem suited to highly specifically activate DUM neurons to meet physiological demands and fine-tune behaviour by systemic and targetted release of octopamine. To gain further insight into DUM neuron central control, the identification of immediate presynaptic neurons remains a major aim of the future.

Putative GABAergic input sites to DUM neuron subtypes

In a high resolution confocal microscopy study, "b" branches of DUM 3,4 neurons were shown to be in contact with a greater number of putative presynapses than "b" branches of DUM 3,4,5 neurons, however, the putative GABAergic input area did not remarkably differ among both subgroups. These data indicate that the subset specific differential activation (see 3.1 and Duch and Pflüger, 1999; Duch et al., 1999; Burrows, 1996), revealed in electrophysiological recordings, is presumably not simply correlated with the amount of surface in touch with putative GABAergic presynaptic profiles.

In the past decades, there have been several approaches to reveal connections between labelled neuronal structures with the help of light and high resolution confocal microscopy (Peters et al., 1985; Distler and Boeck, 1997; Cabirol-Pol et al., 2000; Hiesinger et al., 2001; Nakagawa and Mulloney, 2001; Zhang et al., 2003; Meseke et al., 2009a; Börner, 2009). To enable identification of putative contacts in the present study, three dimensional geometric reconstructions of intracellularly stained DUM neurons served as a means to spatially relate immunopositive staining to the neuronal surface (see 3.2 and Schmitt et al., 2004; Evers et al., 2005. Although the scale of the synaptic structures investigated is at the border of confocal microscopy resolution (200-300 nm) and anatomical synapses can only be reliably determined by electron microscopy, a recent correlative confocal and electron microscopy study confirmed that mapping of one synaptic marker (anti-synapsin I) onto the reconstructed neuronal surface in principle reflected the actual synapse distribution, with about 83 % of the determined synapses being legitimately assigned (Hohensee et al., 2008). The number of false-positives were proposed to be further reduced by addition of a second marker (Meseke et al., 2009a).

For identification and visualisation of synaptic loci within the insect neuropil served an antibody raised against synapsin I from *Drosophila* (Klagges et al., 1996), which has been successfully used to label mainly type I terminals in insects (Godenschwege et al., 2004; Watson and Schürmann, 2002; Hohensee et al., 2008; Meseke et al., 2009a). This is owed to the fact that synapsins are abundant synaptic vesicle phosphoproteins; they are suggested to play an important role in the regulation of neurotransmission and synaptic strength, probably by controlling the balance between SVs of the reserve and the readily releasable pool (Greengard et al., 1993; Südhof, 2004; Evergren et al., 2007; Akbergenova and Bykhovskaia, 2010). Supporting this, synapsin I has been shown to be present in central terminals with round (type I synapses) and pleiomorphic (type II synapses) electron-lucent vesicles, presumably representing glutamatergic and GABAergic terminals (Watson, 1988; Killmann et al., 1999), and even to be associated with dense core vesicles (for review

see Fdez and Hilfiker, 2006).

The restriction to inhibitory input sites was enabled by simultaneous application of an antibody to glutamate decarboxylase (GAD), the enzyme catalysing the conversion from glutamate into γ-aminobutyric acid (GABA). GAD occurs in two isoforms with different function and subcellular localisation, either soluble (GAD 67) or membrane bound (GAD 65) (Kaufman et al., 1991); in presynaptic nerve endings GAD 65 is associated with synaptic vesicles (Salganicoff and DeRobertis, 1965), where it forms a functional complex with vesicular GABA transporters and may contribute to effective vesicle filling (Jin et al., 2003; Wu et al., 2007; Buddhala et al., 2009). An antiserum raised against rat GAD (Oertel et al., 1981) has been successfully applied in the insect nervous system, providing evidence for a protein with evolutionarily conserved domains (Breer and Heilgenberg, 1985; Breer et al., 1989). Subsequent studies verified that similar neurons displayed GAD- and GABA-ir in invertebrates (Homberg et al., 1993). GAD-ir was even suggested to be advantageous over the latter in its power to specifically label GABAergic neurons (Breer et al., 1989). The anti-GAD antibody used in the present study was shown to reliably stain neurons which were assumed to be GABAergic (see fig. 2.2 and Watson, 1986). Double-staining with anti-GAD and anti-synapsin resulted thus in labelled puncta which may correspond to those terminals containing pleiomorphic electron-lucent vesicles (Killmann et al., 1999). However, in *Drosophila*, it has been shown that GAD is also required in glutamatergic neurons at the neuromuscular junction to induce a postsynaptic receptor field (Featherstone et al., 2000).

The "b" branches of DUM neurons cover a neuropil region in anterior median and dorsal position of the mesothoracic ganglion. These dorsal neuropils house projections of different sets of interneurons, among which the GABAergic populations of spiking, non-spiking and intersegmental interneurons make output synapses to motor neurons and other interneurons (Laurent and Sivaramakrishnan, 1992; Watson and Laurent, 1990; Wildman et al., 2002) and are also possible candidates to maintain direct inhibitory synaptic contacts to DUM neurons. Some populations have been shown to receive and process input from mechanosensory organs such as exteroceptors on the hindleg (Siegler and Burrows, 1983; Burrows, 1987; Newland and Emptage, 1996). The fact that their projections are not restricted to specific motor neuropils and the quite uniform distribution of GABA/GAD-immunopositive labels in the entire neuropil (own data, Meseke et al., 2009a), led to the assumption that the investigation of only a subset of branches in the present study might yield representative data. Extrapolation of synaptic counts from restricted dendritic regions have been done in other approaches using electron microscopy (Killmann et al., 1999; Littlewood and Simmons, 1992; Meinertzhagen, 1996).

Although "b" branches of DUM 3,4 neurons were found to be targeted by a greater number of putative input synapses (14 % of the surface area in contrast to less than 9 % for DUM 3,4,5 neuron branches (fig. 2.6), the portion of putative inhibitory input sites did not differ significantly, with around 3-4 % for both groups. These data thus indicate a higher share of non-GABAergic input sites for DUM 3,4 neurons, with around 10 % of the surface being in contact with non-GABAergic input sites and only about 5 % of DUM 3,4,5 neurons. These non-GABAergic input sites could be argued to essentially represent excitatory synapses, however, it is known that also glutamate and other neuroactive substances can serve as inhibitory transmitters in the central nervous system (Wafford and Sattelle, 1986; Dubas, 1990). Supporting this, DUM neuron somata were shown to possess glutamate sensitive chloride channels (Janssen et al., 2007, 2010). The actual number of inhibitory input sites may therefore be higher than determined in this study. Since synapsin staining can also occur associated with exocytotic sites of large granular vesicles, it is possible that some of the putative input sites belong to neurosecretory cells. Such profiles have been detected adjacent to locust abdominal DUM neurons by electron microscopy (Pflüger and Watson, 1995).

These and further drawbacks render it very difficult to relate anatomical data to physiological activity. Undetermined properties such as dendritic computation parameters, synaptic scaling and individual synapse strength may characterise the input properties to an unpredictable degree (see Koch and Segev, 2000; London and Häusser, 2005; Turrigiano, 2008). In DUM neurons, spiking properties and excitability were shown to be distinctive for DUM neuron subgroups due to differing current densities (Heidel and Pflüger, 2006). The observed neuronal responses may thus depend on neuron intrinsic properties as well. Still, it has been shown at monosynaptic connections between sensory and motor neurons in invertebrates that the number of presynaptic contacts can be positively correlated with the size of (excitatory) postsynaptic potentials (Nakagawa and Mulloney, 2001; Zhang et al., 2003; Duch and Mentel, 2004).

The larger contact area for DUM 3,4 neurons in this study could either correspond to a greater number of presynaptic neurons or to an in general more extensive targeting. All data collected so far from electrophysiology hint to differential control of DUM 3,4 and DUM 3,4,5 neurons; in double intracellular recordings they had few synaptic potentials in common (Duch et al., 1999; Baudoux and Burrows, 1998). In addition, refering to personal observations, recordings of DUM 3,4 neurons in quiescent animals in general show a higher frequency of fast membrane oscillations and postsynaptic potentials than DUM 3,4,5 neurons, which may point to stronger synaptic drive of possibly more divergent provenance. These findings would suggest a

distinct set and probably a higher number of presynaptic neurons providing input to DUM 3,4 neurons. Interestingly in this context, the DUM 3,4 sample with the least high percentage of putative input sites (A3 in fig. 2.6B) belonged to the subgroup of DUM 3AC,4 neurons, which are possibly under differential control compared to DUM 3A,4 neurons (see 3.1 and Mentel et al., 2003). However, more data will be necessary to allow for further speculations.

DUM neuron branches of smaller diameter were more densely covered by putative input sites (fig. 2.8). This has also been reported for other neurons in electron microscopy studies, e.g. for locust spiking interneurons and the descending contralateral movement detector (DCMD) (Watson et al., 1985; Killmann et al., 1999). In the latter study, synapse density and branch diameter were in addition found to be negatively correlated with glial ensheathment of the neurites.

Both for DUM 3,4 and DUM 3,4,5 neurons, about 30-35 % of the putative input sites were GABAergic. This relation was essentially confirmed, if the data were categorised according to diameter classes of dendrites (fig. 2.8C/D). Nevertheless, due to the differing amounts in putative non-GABAergic input sites, DUM 3,4,5 neuron branches tended to a higher GABAergic share with more than 40 % in some radius classes. In principle these relations were similar to immunogold staining analyses perforemd for the ventral dendritic field of spiking local interneurons, where 43 % of the synapses investigated were GABAergic (Leitch and Laurent, 1993) and in abdominal DUM neurons, where the GABAergic share of all presynaptic profiles amounted to 39 % (Pflüger and Watson, 1995).

Direct application of GABA to abdominal DUM neurons led to hyperpolarisation, providing evidence of the existence of GABA-receptors on DUM neuron dendrites (Dubreil et al., 1994). However, their distribution pre- and postsynaptic to DUM neurons and the identity of receptor subtypes may strongly influence GABA induced inhibition. Indeed, different receptor subtypes (for review see Hosie et al., 1997) were at least assumed for the somatic and dendritic location, which showed divergent sensitivity to the GABA-receptor antagonist picrotoxin (Dubreil et al., 1994).

In summary, this approach provides a means to estimate the amount of putative GABAergic input sites for large dendrite regions or even whole neurons in a reliable manner. In principle it may further serve to model dendrite computational properties (Meseke et al., 2009a). Still, supplementary data from physiological, ultrastructural and molecular studies will be mandatory to precisely identify DUM neuron presynaptic profiles and fully understand pre- and postsynaptic activation or inhibition by GABA.

Octopamine- and tyramine-immunoreactivity in neuromodulatory varicosities

With the help of reliable antibodies to octopamine and tyramine the innervation pattern of neuromodulatory varicosities was visualized on locust skeletal muscle. For this purpose the previously examined flight steering muscle M85/M115 (Pflüger et al., 1986; Stevenson and Meuser, 1997; Biserova and Pflüger, 2004) provided an excellent means. In accordance to previous data, octopaminergic fibers were shown to evenly cover its parts a and b (fig. 3.1A). Stevenson and Meuser (1997) elucidated the innervation of this muscle by an individual DUM 3,4,5 (DUM 3,4,5a) neuron, providing evidence that the observed octopaminergic varicosities belong to this DUM neuron.

The appearance of individual boutons in many aspects resembled that of type II terminals described for other insect species. In *Manduca sexta*, larval abdominal body wall muscles receive innervation by unpaired median (UM) neurons (Pflüger et al., 1993) which can be easily distinguished from motor neuron terminals in that they are less densly packed and have diameters from 1-3 μm versus 3-7 μm (Consoulas et al., 1999). This is within the range of the average diameter of 1.7 $\pm$ 0.6 μm determined for octopaminergic boutons and the motor terminal size of 3-8 μm for locust muscle in the present study. With respect to the size, type II terminals of *Drosophila* are in the same scale with 1.4 μm $\pm$ 0.6 μm (Johansen et al., 1989; Jia et al., 1993), however, there are conspicuous differences regarding the innervation pattern and overall appearance. Monastirioti et al. (1995) have shown that two octopaminergic neurons supply almost all body wall muscles in *Drosophila* larvae and that its varicosities correspond to the earlier described type II endings (Johansen et al., 1989). In contrast to locust neuromodulatory fibers, which follow those of motor neurons in immediate vicinity (fig. 3.3A) and were rarely found to run solitarily, Drosophila type II varicosities cover the muscles more irregularly and are not restricted to the relatively small area supplied by motor terminals, which they often exceed in length (Johansen et al., 1989). This difference may be correlated with the fact that *Drosophila* type II endings are less enveloped in glial sheaths and come in direct contact with muscle fibers, whereas DUM neuron terminals in locusts are in close association with motor neurons, but do not directly contact muscle fibers (Rheuben, 1995). This was confirmed by ultrastructural analyses of the DUMETi and DUMDL axons (Hoyle et al., 1980). An electron microscopy study of the locust flight steering muscle furthermore indicated that possible neuromodulatory profiles lie next to putative motor terminals (Biserova and Pflüger, 2004). It is not known whether this difference is correlated with targetted octopamine release to either pre- or postsynaptic receptors, since octopamine as a neuromodulator and -hormone is known to cover larger distances by diffusion.

In contrast to motor terminals, neuromodulatory boutons were shown to con-

tain only small amounts of synapsin I (fig. 3.3Fii). This corresponds to results from *Drosophila*, where the authors considered the amount of synapsin I insignificant (Godenschwege et al., 2004). Proteins of the synapsin family are abundant in presynaptic boutons of both vertebrates and invertebrates and thought to regulate the release of synaptic vesicles clustered into ready releasable, recycling and reserve pools (see Greengard et al., 1993; Rizzoli and Betz, 2005). Although neuromodulatory neurons normally do not form conventional synaptic structures and clustering of dense core vesicles is rarely encountered, as shown for DUM neurons (Hoyle et al., 1980), synapsins have been recently reported to be associated with dense core vesicles as well (for review see Fdez and Hilfiker, 2006). Indeed, recent studies on vertebrate neurons stress that synapsins may regulate catecholamine release negatively and thus differently to that of small synaptic vesicles of conventional transmitters (Venton et al., 2006; Villanueva et al., 2007). However, many aspects of synaptic release regulation by synapsins remain enigmatic so far. A second synaptic marker, the protein bruchpilot (NC82), which is a crucial component of the presynaptic density in *Drosophila* (Wagh et al., 2006), was equally found to be present in locust motor terminals (fig. 3.2C). Preliminary data from *Drosophila* muscle, however, revealed no localisation of NC82 in type II varicosities (Pflüger, unpublished data), again supporting structural differences between motor terminals and neuromodulatory endings.

Interestingly, it could be shown that tyramine-like-immunoreactivity (TA-ir) was prominent on locust muscle in boutons and partially in fibers (fig. 3.1C) and exclusively restricted to those which also exhibited octopamine-immunoreactivity (fig. 3.1B). Unpublished results (Pflüger) confirm this co-localisation for *Drosophila* type II terminals. This implies that tyramine may be concentrated in vesicles like suggested for octopamine. Since tyramine is the precursor of octopamine in biosynthesis, the presence of tyramine is highly expected, and this co-localisation has been detected for locust central octopaminergic neurons as well (Kononenko et al., 2009). Tyramine conversion into octopamine via the enzyme tyramine-ß-hydroxylase (Tßh) would thus be assumed to take place within vesicles or in its immediate surroundings. Supporting this, Tßh in *C. elegans* was predominantly found in synaptic regions of identified neurons (RIC neurons), whereas mutants, which lacked a neuron-specific kinesin crucial for vesicle transport, accumulated Tßh in cell bodies Alkema et al. (2005). In addition, the highly related vertebrate dopamine-ß-hydroxylase was shown to be associated with synaptic vesicle membranes (Nelson and Molinoff, 1976; Potter and Axelrod, 1963). For more precise results, however, it is envisaged to specifically elucidate Tßh localisation in locust octopaminergic neurons and to determine subcellular tyramine and octopamine compartmentalisation via electron microscopy and immunogold staining techniques.

However, the exclusive co-localisation of tyramine and octopamine does not reflect the situation in the CNS, were purely tyraminergic varicosities have been identified (Kononenko et al., 2009); this is also true for the locust visceral nervous system, where tyraminergic innervation has been shown as well (Donini and Lange, 2004; da Silva and Lange, 2008).

Octopamine- and tyramine-immunoreactivity in dependence on behavioural experience

Recently, the ratio of octopamine and tyramine within octopaminergic neurons in the locust CNS was shown to depend considerably on the previous handling of the animals (Kononenko et al., 2009): Somata of neurons which under control conditions showed approximately equal intensity of both OA- and TA-ir, displayed stronger anti-OA and weaker anti-TA labelling following stress treatment. At the same time, TA-ir appeared predominantly in fibers of DUM neurons, as if due to active transport. Since it is assumed that general arousal is accompanied by DUM neuron activation (Hoyle, 1978; Ramirez and Orchard, 1990; Field et al., 2008; Burrows, 1996), these changes in OA- and TA-ir thus possibly reflected the behavioural state of the animal, where tyramine is rapidly converted into octopamine. Indeed, the turnover rates of these monoamines are high in vivo (Durden and Philips, 1980). As revealed in the present study, varicosities in peripheral tissue seem to be subject to behaviourally induced dynamics as well. After a flight period of at least 40 minutes and in response to stress exposure, i.e. treatments which are both thought to elicit DUM 3,4,5a activation and hence probably release of octopamine in the periphery (Stevenson and Meuser, 1997), the size distribution of octopaminergic boutons was biased towards larger boutons, as determined by quantitative evaluation of the antibody staining (fig. 3.4B). The effect was stronger for the stress-exposed animals both for bouton distributions evaluated for OA- and TA-ir. It is, however, impossible to tell whether these observations may reflect structural changes of the terminal surface size or of vesicle number, distribution or content. It has been shown before in vertebrate preparations that synapses following stimulation display structural plasticity (Boyne et al., 1975; Clark et al., 1972). In the locust, synaptic terminals of the locust retractor unguis muscle contained a reduced number and smaller sized synaptic vesicles immediately after nerve stimulation, obviously due to vesicle depletion (Reinecke and Walther, 1978, 1981). In these experiments, the terminal circumference and cross-section were increased and cell organelles like mitochondria and the SER were as well affected. Interestingly, these changes were reversed after only 2 minutes of rest. In a more recent study in *Drosophila*, stimulation of motor nerves led to changes in vesicle density, formation of new vesicle pools and shrinking of synaptic boutons, possibly due to enhanced endocytosis (Akbergenova and Bykhovskaia, 2009). Although these findings relate

to motor terminals and the exocytosis kinetics and release machinery of neuromodulatory boutons are different (Speese et al., 2007; Rettig and Neher, 2002; Martin, 2003), exocytosis of small clear synaptic and dense core vesicles, which are usually assumed to contain neuropeptides or biogenic amines, share many common principles (Rettig and Neher, 2002; Jahn et al., 2003; Sorensen, 2004).

Not only the bouton size, but also the intensity ratios (staining versus background) were examined for both octopamine and tyramine. These values in both groups did not show significant changes between control and pre-treated animals, however, the ratio of octopamine and tyramine relative staining intensity was altered for the stress-exposed group (fig. 3.4Dii), possibly indicating a more concentrated octopamine and more dispersed tyramine distribution in response to stress exposure. This could, similar to the central observations described by Kononenko et al. (2009), reflect a conversion of tyramine to octopamine due to DUM neuron activity. The fact that the effect was more pronounced for stress-exposed animals than for those which had experienced flight, may be owed to the recruitment of the DUM 3,4,5 neuron, which is probably not continuously active during long-term flight, but reacts differently in response to inpredictable stressing stimuli. Supportively, DUM 3,4,5 neurons tended to habituate quickly during sensory stimuli which are relevant during flight (see 3.1 and Field et al., 2008).

Since these results imply a dynamic change of transmitter content on the synaptic bouton level, but do not enable exact quantitation, more sensitive detection techniques are required. In a recent publication, Cooper and Venton (2009) introduced a method for the detection of fast changing amounts of released octopamine and tyramine in the nanomolar range by fast-scan cyclic voltammetry, which should be suited for invertebrate preparations.

Tyramine effects on muscle performance

Muscle force measurements showed that bath application of tyramine qualitatively evoked the same effect as octopamine on muscle contractions, namely increases in twitch amplitude, contraction and relaxation rate (see also Stevenson and Meuser, 1997), but was obviously less efficient than octopamine (fig. 3.5): At a concentration of 10 μM tyramine had approximately the same potency as octopamine at a 10fold lower concentration. A clear dose-dependency was observed; 1 μM to 0.1 μM tyramine was the lowest dose to elicit modulation of muscle twitches. These results fit in with previous data on octopaminergic modulation of locust leg and flight muscles, where the potency of different related substances was determined as well (Evans, 1981; Whim and Evans, 1988). For the dorsolongitudinal flight power muscle M112 Whim and Evans (1988) found a relaxation rate increase of about 52 % for

octopamine versus an increase of 21 % for tyramine, if both were applied at 10 μM. Using the same concentrations and equal conditions, Evans (1981) showed that the relaxation rate of slow extensor tibiae (SETi) twitches (see also Evans and O'Shea, 1977) was enhanced by about 110 % for octopamine in contrast to about 50 % for tyramine. Although obviously both biogenic amines enhanced leg muscle performance more thoroughly than flight muscle performance, the tyramine/octopamine ratio of potency was similar with 0.4 and 0.54. For the flight steering muscle in this study this ratio lay slightly higher, at about 0.66.

As reported by Evans (1981), additivity experiments, where octopamine and tyramine were applied together at concentrations yielding maximal responses if given alone, did not result in an accumulative effect. This is in accordance with the preliminary data provided in this study for the flight steering muscle (figs. 3.5E). These results, together with the parallel dose-response curves and similar maximal responses (Evans, 1981) indicate that octopamine and tyramine may affect the same receptor sites. Supporting this, application of tyramine together with the OAR antagonist epinastine, completely abolished the tyramine effect and sometimes even led to a reduction in muscle performance (figs. 3.5A,B,C).

Epinastine has been first used as histamine receptor antagonist in vertebrates (Adamus et al., 1987) and was recently shown to selectively and highly specifically block central neuronal OAR receptors in the locust and other insect species (Roeder et al., 1998) with low affinity for other biogenic amine receptors in central neuronal tissue like the histamine H_1 receptor and tyramine-receptors (TARs). The concentrations for epinastine applied in this study were in the micromolar range and thus comparable to concentrations used in other similar preparations (Unoki et al., 2006; Vehovszky et al., 2000; Packham et al., 2010). Apart from the inhibition of the tyramine effect, the observed reduction in performance due to epinastine could be owed to the inhibition of preparation intrinsic octopamine. This would be in accordance with previous observations, where the exogenously applied octopamine elicited variable increases of muscle force, probably depending on the internal arousal state of the animal (Evans, 1981).

Similar agonistic results for octopamine and tyramine were discribed for *C. elegans*, where both octopamine and tyramine inhibited pharyngeal pumping, with tyramine being less potent than octopamine (Packham et al., 2010). Epinastine in this study more effectively antagonised the octopamine effect than the tyramine effect, indicating either distinct receptor pathways or, in consideration of the weaker tyramine effect, a lower affinity of tyramine for OARs, as also assumed in the present study. Since most of the TARs characterised so far, function via attenuation of adenylyl cyclase, leading to decreased cAMP levels, whereas most OARs enhance

cAMP or intracellular calcium levels (see (Roeder, 2002)), a specific tyramine effect could be expected to be antagonistic to the one mediated by octopamine, as shown in *Drosophila* and on locust visceral muscle (Nagaya et al., 2002; Donini and Lange, 2004). In addition, yohimbine, which has been reported to be a specific TAR blocker (Saudou et al., 1990; Robb et al., 1994) but a weak neural OAR antagonist, was only effective in inhibiting the octopamine modulation of the myogenic rhythm in the locust extensor tibiae muscle, but not twitch amplitude or relaxation rate (Evans, 1981). In summary, these data render it unlikely that tyramine is also a specific modulator of locust skeletal muscle.

5 Abstract

The unique group of insect specific dorsal/ventral unpaired median (DUM/VUM) neurons is the principal source of peripherally released octopamine (OA), which as a neuromodulator/-hormone acts on essentially all system levels by modifying e.g. muscle properties, metabolism and complex behaviours. In the locust *Schistocerca gregaria*, pterothoracic DUM neurons form functional subpopulations which are differentially recruited during specific motor tasks. This study investigates subgroup specific DUM neuron activation and elucidates the peripheral distribution of OA and its precursor tyramine (TA) with respect to its role as independent neuroactive substance.

Following nerve stimulation of the tegula, a sensory organ at the wing base, intracellularly recorded "wing group" neurons, i.e. DUMDL, DUM 3 and DUM 3,4 neurons, in general were inhibited, whereas DUM 3,4,5 neurons were activated via a segmental polysynaptic pathway. Stimulation of the tritocerebral giant interneuron elicited likewise inhibitory responses in DUM 3 and DUM 3,4 neurons via polysynaptic connections, while DUM 1b neurons received excitatory input. These findings provide evidence of so far undescribed pathways and imply their functional relevance at the onset of and/or during flight. Since electrophysiological data imply pronounced inhibitory synaptic input to "wing group", but hardly to "leg group" neurons, the amount of putative inhibitory input sites to selected branches of DUM 3,4 and DUM 3,4,5 neurons was determined using immunocytochemistry and available neuron reconstruction tools. A greater surface area of DUM 3,4 neurons was covered by putative synaptic input sites, however, the inhibitory share of these contacts did not markedly differ from that of DUM 3,4,5 neurons. These data thus do not indicate a simple quantitative correlation.

The flight steering muscle M85/114 was examined to elucidate the distribution pattern of OA and TA in the periphery. With the help of reliable antibodies, TA was shown to be exclusively co-localised with OA in all neuromodulatory varicosities examined. The comparison of individual boutons from control and differentially treated animals, which had experienced flight or were exposed to stress immediately before examination, indicated dynamic activity-dependent changes of OA and TA contents. In muscle mechanograms, TA increased twitch amplitude as well as contraction and relaxation rate of individual muscle twitches, but less effectively than OA. Since the TA effect was suppressed by the OA-receptor antagonist epinastine, specific TA release and the existence of specific TA-receptors at this peripheral location seems unlikely.

6 Zusammenfassung

Im Nervensystem von Insekten ist die Gruppe der dorsal unpaired median (DUM / VUM) Neurone hauptverantwortlich für die periphere Ausschüttung von Octopamin (OA), das als Neuromodulator und -hormon nahezu alle Ebenen des Organismus beeinflusst, wie z.B. die Kontraktionseigenschaften von Muskeln, den Stoffwechsel oder komplexes Verhalten. In der Wüstenheuschrecke *Schistocerca gregaria* kann man die thorakalen DUM Neurone funktionellen Unterpopulationen zuordnen, die während spezifischer Bewegungsmuster differentiell rekrutiert werden. Die vorliegende Arbeit untersucht sowohl Wege der differentiellen Aktivierung von DUM Neuronen als auch die periphere Verteilung von Octopamin und seiner Vorstufe Tyramin (TA) im Hinblick auf dessen Rolle als unabhängige neuroaktive Substanz.

Nervreizung der Tegula, eines sensorischen Organs an der Flügelbasis, hatte in intrazellulär abgeleiteten "wing group", d.h. DUMDL, DUM 3 und DUM 3,4 Neruonen, inhibitorische, in "leg group", d.h. DUM 3,4,5 Neuronen exzitatorische Eingänge über jeweils segmentale und polysynaptische Verbindungen zur Folge. Ebenso löste die Stimulation des tritocerebral giant (TCG) Interneurons Inhibition von DUM 3 und DUM 3,4 Neuronen aus, während DUM 1b Neurone aktiviert wurden. Die Daten implizieren eine funktionelle Relevanz dieser Konnektivitäten während oder zu Beginn des Flugs. Da elektrophysiologische Daten darauf hindeuten, dass "wing group" Neurone generell in höherem Maße inhibitorische Eingänge erhalten als "leg group" Neurone, wurde der prozentuale Anteil an mutmaßlichen inhibitorischen synaptischen Kontakten auf ausgewählten Dendriten von DUM 3,4 und DUM 3,4,5 Neuronen mithilfe von Immunocytochemie (anti-Synapsin und anti-GAD) und der Rekonstruktion von Neuronen bestimmt. Bei DUM 3,4 Neuronen war zwar eine insgesamt größere Oberfläche in Kontakt mit präsynaptischen Profilen, der Anteil an mutmaßlichen inhibitorischen Kontakten unterschied sich jedoch nicht signifikant.

Mithilfe von Antikörpern konnte gezeigt werden, dass TA auf dem Flugsteuermuskel M85/M114 in neuromodulatorischen Terminalen ausschließlich ko-lokalisiert mit OA vorliegt. Der Vergleich einzelner Boutons von Kontroll-Tieren und solchen, die unmittelbar vor der Untersuchung geflogen oder Stress ausgesetzt waren, deutete auf aktivitätsbedingte dynamische Schwankungen von OA und TA hin. Wie Muskelmechanogramme zeigten, erhöhte TA die Amplitude einzelner Zuckungen sowie deren Kontraktions- und Relaxationsrate, allerdings in geringerem Maße als OA. Da dieser Effekt durch gleichzeitige Applikation des OA-Rezeptor Antagonisten Epinastin unterdrückt wurde, scheint die Existenz spezifischer TA-Rezeptoren auf dem Skelettmuskel unwahrscheinlich.

References

Adamo, S. A., Linn, C. E., and Hoy, R. R. (1995). The role of neurohormonal octopamine during "fight or flight" behavior in the field cricket, *Gryllus bimaculatus*. *J Exp Biol*, 198:1691–1700.

Adamus, W., Oldigs-Kerber, J., and Lohmann, H. (1987). Pharmacodynamics of the new H_1-antagonist 2-amino-9, 13*b*-dihydro-1 *H*-1dibenz(*c*,*f*)imidazo(1,5-*a*)azepine hydrochloride in volunteers. *Drug Res*, 37:569–572.

Akbergenova, Y. and Bykhovskaia, M. (2009). Stimulation-induced formation of the reserve pool of vesicles in *Drosophila* motor boutons. *J Neurophysiol*, 101:2423–2433.

Akbergenova, Y. and Bykhovskaia, M. (2010). Synapsin regulates vesicle organization and activity-dependent recycling at *Drosophila* motor boutons. *Neuroscience*, 170:441–452.

Ali, D. W. (1997). The aminergic and peptidergic innervation of insect salivary glands. *J Exp Biol*, 200:1941–1949.

Alkema, M. J., Hunter-Ensor, M., Ringstad, N., and Horvitz, H. R. (2005). Tyramine functions independently of octopamine in the *Caenorhabditis elegans* nervous system. *Neuron*, 46:247–260.

Altman, J. S., Anselment, E., and Kutsch, W. (1978). Postembryonic development of an insect sensory system: ingrowth of axons from hindwing sense organs in *Locusta migratoria*. *Proc Royal Soc Lond B*, 202:497–516.

Anthony, N. M., Harrison, J. B., and Sattelle, D. B. (1993). GABA receptor molecules of insects. *EXS*, 63:172–209.

Bacon, J. and Möhl, B. (1979). Activity of an identified wind interneurone in a flying locust. *Nature*, 278:638–640.

Bacon, J. and Möhl, B. (1983). The tritocerebral commissure giant (TCG) wind-sensitive interneurone in the locust. *J Comp Physiol A*, 150:439–452.

Bacon, J. and Tyrer, M. (1978). The tritocerebral commissure giant (TCG): A bimodal interneurone in the locust, *Schistocerca gregaria*. *J Comp Physiol A*, 126:317–325.

Bacon, J. and Tyrer, M. (1979). Wind interneurone input to flight motor neurones in the locust, *Schistocerca gregaria*. *Naturwissenschaften*, 66:116–117.

Baines, R. A., Tyrer, N. M., and Mason, J. C. (1989). The innervation of locust salivary glands. i. innervation and analysis of transmitters. *J Comp Physiol A*, 165:395–405.

Baudoux, S. and Burrows, M. (1998). Synaptic activation of efferent neuromodulatory neurones in the locust *Schistocerca gregaria*. *J Exp Biol*, 201:3339–3354.

Baudoux, S., Duch, C., and Morris, O. T. (1998). Coupling of efferent neuromodulatory neurons to rhythmical leg motor activity in the locust. *J Neurophysiol*, 79:361–370.

Bentley, D. R. (1970). A topological map of the locust flight system motor neurons. *J Insect Physiol*, 16:905–918.

Bicker, G. and Pearson, K. G. (1983). Initiation of flight by an identified wind sensitive neurone (TCG) in the locust. *J Exp Biol*, 104:289–293.

Biserova, N. M. and Pflüger, H.-J. (2004). The ultrastructure of locust pleuroaxillary "steering" muscles in comparison to other skeletal muscles. *Zoology (Jena)*, 107:229–242.

Blau, C. and Wegener, G. (1994). Metabolic integration in locust flight: the effect of octopamine on fructose 2,6-bisphosphate content of flight muscle in vivo. *J Comp Physiol B*, 164:11–15.

Blenau, W., Balfanz, S., and Baumann, A. (2000). Amtyr1: characterization of a gene from honeybee (*Apis mellifera*) brain encoding a functional tyramine receptor. *J Neurochem*, 7:900–908.

Blenau, W. and Baumann, A. (2001). Molecular and pharmacological properties of insect biogenic amine receptors: lessons from *Drosophila melanogaster* and *Apis mellifera*. *Arch Insect Biochem Physiol*, 48:13–38.

Borowsky, B., Adham, N., Jones, K., Raddatz, R., Artymyshyn, R., Ogozalek, K., Durkin, M., Lakhlani, P., Bonini, J., Pathirana, S., Boyle, N., Piu, X., Kouranova, E., Lichtblau, H., Ochoa, F., Branchek, T., and Gerald, C. (2001). Trace amines: identi?cation of a family of mammalian g protein-coupled receptors. *PNAS*, 98:8966–8971.

Boyan, G. S. and Ball, E. E. (1989). The wind-sensitive cercal receptor/giant interneurone system of the locust,*Locusta migratoria*. *J Comp Physiol A*, 165:511–521.

Boyne, A. F., Bohan, T. P., and Williams, T. H. (1975). Changes in cholinergic synaptic vesicle populations and the ultrastructure of the nerve terminal membranes of *Narcine brasiliensis* electron organ stimulated to fatigue in vivo. *J Cell Biol*, 67:814–825.

Breer, H. and Heilgenberg, H. (1985). Neurochemistry of gabaergic activities in the central nervous system of *Locusta migratoria*. *J Comp Physiol A*, 157:343–354.

Breer, H., Mädler, U., and Heilgenberg, H. (1989). Immunocytochemical localization of glutamate decarboxylase in the mesothoracic ganglion of *Locusta migratoria*. *Tissue Cell*, 21:581–587.

Brembs, B., Christiansen, F., Pflüger, H.-J., and Duch, C. (2007). Flight initiation and maintenance deficits in flies with genetically altered biogenic amine levels. *J Neurosci*, 27:11122–11131.

Börner, J. (2009). *Standardized Drosophila ventral nerve cord morphology: Atlas generation and atlas applications.* PhD thesis, Freie Universität Berlin.

Bräunig, P. (1990). The morphology of suboesophageal ganglion cells innervating the nervus corporis cardiaci iii of the locust. *Cell Tissue Res*, 260:95–108.

Bräunig, P. (1997). The peripheral branching pattern of identified dorsal unpaired median (DUM) neurones of the locust. *Cell Tissue Res*, 290:641–654.

Bräunig, P. and Eder, M. (1998). Locust dorsal unpaired median (DUM) neurones directly innervate and modulate hindleg proprioceptors. *J Exp Biol*, 201 (Pt 24):3333–3338.

Bräunig, P. and Evans, P. (1994). A locust octopamine-immunoreactive dorsal unpaired median neurone forming terminal networks on sympathetic nerves. *J Exp Biol*, 192:225–238.

Bräunig, P., Hustert, R., and Pflüger, H.-J. (1981). Distribution and specific central projections of mechanoreceptors in the thorax and proximal leg joints of locusts. I. morphology, location and innervation of internal proprioceptors of pro- and metathorax and their central projections. *Cell Tissue Res*, 216:57–77.

Bräunig, P. and Pflüger, H.-J. (2001). The unpaired median neurons of insects. *Adv Insect Physiol*, 28:185–266.

Büschges, A., Schmitz, J., and Bässler, U. (1995). Rhythmic patterns in the thoracic nerve cord of the stick insect induced by pilocarpine. *J Exp Biol*, 198:435–456.

Bässler, U. (1993). The walking (and searching) pattern generator of stick insects, a modular system composed of reflex chains and endogenous oscillators. *Biol Cybern*, 69:305–317.

Buddhala, C., Hsu, C.-C., and Wu, J.-Y. (2009). A novel mechanism for GABA synthesis and packaging into synaptic vesicles. *Neurochem Int*, 55:9–12.

Burrows, M. (1987). Parallel processing of proprioceptive signals by spiking local interneurons and motor neurons in the locust. *J Neurosci*, 7:1064–1080.

Burrows, M. (1996). *The neurobiology of an insect brain.* Oxford University Press Inc. , New York.

Burrows, M. and Fraser Rowell, C. (1973). Connections between descending visual interneurons and metathoracic motoneurons in the locust. *J Comp Physiol A*, 85:221–234.

Burrows, M. and Pflüger, H. J. (1995). Action of locust neuromodulatory neurons is coupled to specific motor patterns. *J Neurophysiol*, 74:347–357.

Cabirol-Pol, M. J., Mizrahi, A., Simmers, J., and Meyrand, P. (2000). Combining laser scanning confocal microscopy and electron microscopy to determine sites of synaptic contact between two identified neurons. *J Neurosci*, 97:175–181.

Campbell, H. R., Thompson, K. J., and Siegler, M. V. (1995). Neurons of the median neuroblast lineage of the grasshopper: a population study of the efferent DUM neurons. *J Comp Neurol*, 358:541–551.

Campbell, J. I. (1961). The anatomy of the nervous system of the mesothorax of *Locusta migratoria migratoides* (R. & F.). *Proc R Zool Soc Lond*, 137:403–432.

Candy, D. J. (1978). Regulation of locust flight-muscle metabolism by octopamine and other compounds. *Insect Biochem*, 8:177–181.

Cazzamali, G., Klaerke, D. A., and Grimmelikhuijzen, C. J. P. (2005). A new family of insect tyramine receptors. *Biochem Biophys Res Commun*, 338:1189–1196.

Clark, A. W., Hurlbut, W. P., and Mauro, A. (1972). Changes in the fine structure of the neuromuscular junction of the frog caused by black widow spider venom. *J Cell Biol*, 52(1):1–14.

Cole, S. H., Carney, G. E., McClung, C. A., Willard, S. S., Taylor, B. J., and Hirsh, J. (2005). Two functional but noncomplementing *Drosophila* tyrosine decarboxylase genes: distinct roles for neural tyramine and octopamine in female fertility. *J Biol Chem*, 280:14948–14955.

Consoulas, C., Johnston, R. M., Pflüger, H. J., and Levine, R. B. (1999). Peripheral distribution of presynaptic sites of abdominal motor and modulatory neurons in *Manduca sexta* larvae. *J Comp Neurol*, 410:4–19.

Cooper, S. E. and Venton, B. J. (2009). Fast-scan cyclic voltammetry for the detection of tyramine and octopamine. *Anal Bioanal Chem*, 394:329–336.

da Silva, R. and Lange, A. B. (2008). Tyramine as a possible neurotransmitter/neuromodulator at the spermatheca of the african migratory locust, *Locusta migratoria*. *J Insect Physiol*, 54:1306–1313.

Dacks, A. M., Christensen, T. A., Agricola, H.-J., Wollweber, L., and Hildebrand, J. G. (2005). Octopamine-immunoreactive neurons in the brain and subesophageal ganglion of the hawkmoth *Manduca sexta*. *J Comp Neurol*, 488:255–268.

De Cesare, D., Fimia, G. M., and Sassone-Corsi, P. (1999). Signaling routes to CREM and CREB: plasticity in transcriptional activation. *Trends Biochem Sci*, 24:281–285.

Delcomyn, F. (1980). Neural basis of rhythmic behavior in animals. *Science*, 210:492–498.

Distler, P. G. and Boeck, J. (1997). Synaptic connections between identified neuron types in the antennal lobe glomeruli of the cockroach, *Periplaneta americana*: I. uniglomerular projection neurons. *J Comp Neurol*, 378:307–319.

Dobzhansky, T. (1973). "Nothing in biology makes any sense except in the light of evolution.". *American Biology Teacher*, 35:125–129.

Donini, A. and Lange, A. B. (2004). Evidence for a possible neurotransmitter/neuromodulator role of tyramine on the locust oviducts. *J Insect Physiol*, 50:351–361.

Downer, R. G., Hiripi, L., and Juhos, S. (1993). Characterization of the tyraminergic system in the central nervous system of the locust, *Locusta migratoria migratoides*. *Neurochem Res*, 18:1245–1248.

Dubas, F. (1990). Inhibitory effect of l-glutamate on the neuropile arborizations of flight motoneurones in locusts. *J Exp Biol*, 148:501–508.

Dubreil, V., Sinakevitch, I. G., Hue, B., and Geffard, M. (1994). Neuritic GABAergic synapses in insect neurosecretory cells. *Neurosci Res*, 19:235–240.

Duch, C. and Mentel, T. (2004). Activity affects dendritic shape and synapse elimination during steroid controlled dendritic retraction in *Manduca sexta*. *J Neurosci*, 24:9826–9837.

Duch, C., Mentel, T., and Pflüger, H. J. (1999). Distribution and activation of different types of octopaminergic DUM neurons in the locust. *J Comp Neurol*, 403:119–134.

Duch, C. and Pflüger, H.-J. (1999). DUM neurons in locust flight: a model system for amine-mediated peripheral adjustments to the requirements of a central motor program. *J Comp Physiol A*, 184:489–499.

Durden, D. A. and Philips, S. R. (1980). Kinetic measurements of the turnover rates of phenylethylamine and tryptamine in vivo in the rat brain. *J Neurochem*, 34:1725–1732.

Eckert, M., Rapus, J., Nürnberger, A., and Penzlin, H. (1992). The octopaminergic system within the ventral nerve cord of the american cockroach. *Acta Biol Hung*, 43:201–211.

Elson, R. and Pflüger, H.-J. (1986). The activity of a steering muscle in flying locusts. *J Exp Biol*, 120:421–441.

Erspamer, V. and Boretti, G. (1951). Identification and characterization, by paper chromatography, of enteramine, octopamine, tyramine, histamine and allied substances in extracts of posterior salivary glands of octopoda and in other tissue extracts of vertebrates and invertebrates. *Arch Int Pharmacodyn Ther*, 88:296–332.

Evans, P. D. (1981). Multiple receptor types for octopamine in the locust. *J Physiol*, 318:99–122.

Evans, P. D. and Maqueira, B. (2005). Insect octopamine receptors: a new classification scheme based on studies of cloned *Drosophila* G-protein coupled receptors. *Invert Neurosci*, 5:111–118.

Evans, P. D. and O'Shea, M. (1977). An octopaminergic neurone modulates neuromuscular transmission in the locust. *Nature*, 270:257–259.

Evans, P. D. and O'Shea, M. (1978). The identification of an octopaminergic neurone and the modulation of a myogenic rhythm in the locust. *J Exp Biol*, 73:235–260.

Evans, P. D. and Siegler, M. V. (1982). Octopamine mediated relaxation of maintained and catch tension in locust skeletal muscle. *J Physiol*, 324:93–112.

Evergren, E., Benfenati, F., and Shupliakov, O. (2007). The synapsin cycle: a view from the synaptic endocytic zone. *J Neurosci Res*, 85:2648–2656.

Evers, J. F., Schmitt, S., Sibila, M., and Duch, C. (2005). Progress in functional neuroanatomy: precise automatic geometric reconstruction of neuronal morphology from confocal image stacks. *J Neurophysiol*, 93:2331–2342.

Farooqui, T. (2007). Octopamine-mediated neuromodulation of insect senses. *Neurochem Res*, 32:1511–1529.

Fdez, E. and Hilfiker, S. (2006). Vesicle pools and synapsins: new insights into old enigmas. *Brain Cell Biol*, 35:107–115.

Featherstone, D. E., Rushton, E. M., Hilderbrand-Chae, M., Phillips, A. M., Jackson, F. R., and Broadie, K. (2000). Presynaptic glutamic acid decarboxylase is required for induction of the postsynaptic receptor field at a glutamatergic synapse. *Neuron*, 27:71–84.

Ferber, M. and Pflüger, H.-J. (1990). Bilaterally projecting neurones in pregenital abdominal ganglia of the locust: anatomy and peripheral targets. *J Comp Neurol*, 302:447–460.

Field, L. H., Duch, C., and Pflüger, H.-J. (2008). Responses of efferent octopaminergic thoracic unpaired median neurons in the locust to visual and mechanosensory signals. *J Insect Physiol*, 54:240–254.

Flamm, R. E. and Harris-Warrick, R. M. (1986a). Aminergic modulation in lobster stomatogastric ganglion. I. effects on motor pattern and activity of neurons within the pyloric circuit. *J Neurophysiol*, 55:847–865.

Flamm, R. E. and Harris-Warrick, R. M. (1986b). Aminergic modulation in lobster stomatogastric ganglion. II. target neurons of dopamine, octopamine, and serotonin within the pyloric circuit. *J Neurophysiol 55:*, 55:866–881.

Fox, L. E., Soll, D. R., and Wu, C. F. (2006). Coordination and modulation of locomotion pattern generators in *Drosophila* larvae: effects of altered biogenic amine levels by the tyramine beta hydroxylase mutation. *J Neurosci*, 26:1486–1498.

Fussnecker, B. L., Smith, B. H., and Mustard, J. A. (2006). Octopamine and tyramine influence the behavioral profile of locomotor activity in the honey bee (*Apis mellifera*). *J Insect Physiol*, 52:1083–1092.

Gerhardt, C., Bakker, R., Piek, G., Planta, R., Vreug-Denhil, E., Leysen, J., and Van Heerikhuizen, H. (1997). Molecular cloning and pharmacological characterization of a molluscan octopamine receptor. *Mol Pharmacol*, 51:293–300.

Godenschwege, T. A., Reisch, D., Diegelmann, S., Eberle, K., Funk, N., Heisenberg, M., Hoppe, V., Hoppe, J., Klagges, B. R. E., Martin, J.-R., Nikitina, E. A., Putz, G., Reifegerste, R., Reisch, N., Rister, J., Schaupp, M., Scholz, H., Schwärzel, M., Werner, U., Zars, T. D., Buchner, S., and Buchner, E. (2004). Flies lacking all synapsins are unexpectedly healthy but are impaired in complex behaviour. *Eur J Neurosci*, 20:611–622.

Goosey, M. W. and Candy, B. J. (1980). The d-octopamine content of the hemolymph of the locust, *Schistocerca americana gregaria*, and its elevation during flight. *Insect Biochem*, 10:393–397.

Greengard, P., Valtorta, F., Czernik, A. J., and Benfenati, F. (1993). Synaptic vesicle phosphoproteins and regulation of synaptic function. *Science*, 259:780–785.

Grillner, S. (1985). Neurobiological bases of rhythmic motor acts in vertebrates. *Science*, 228:143–149.

Grolleau, F. and Lapied, B. (2000). Dorsal unpaired median neurones in the insect central nervous system: towards a better understanding of the ionic mechanisms underlying spontaneous electrical activity. *J Exp Biol*, 203:1633–1648.

Gudermann, T., Kalkbrenner, F., and Schultz, G. (1996). Diversity and selectivity of receptor-g protein interaction. *Annu Rev Pharmacol Toxicol*, 36:429–459.

Hammer, M. (1993). An identified neuron mediates the unconditioned stimulus in associative olfactory learning in honeybees. *Nature*, 366:59–63.

Hammer, M. and Menzel, R. (1998). Multiple sites of associative odor learning as revealed by local brain microinjections of octopamine in honeybees. *Learning Memory*, 5:146–156.

Han, K.-A., Millar, N. S., and Davis, R. L. (1998). A novel octopamine receptor with preferential expression in *Drosophila* mushroom bodies. *J Neurosci*, 18:3650–3658.

Heidel, E. and Pflüger, H.-J. (2006). Ion currents and spiking properties of identified subtypes of locust octopaminergic dorsal unpaired median neurons. *Eur J Neurosci*, 23:1189–1206.

Hiesinger, P. R., Scholz, M., Meinertzhagen, I. A., Fischbach, K.-F., and Obermayer, K. (2001). Visualization of synaptic markers in the optic neuropils of *Drosophila* using a new constrained deconvolution method. *J Comp Neurol*, 429:277–288.

Hiripi, L., Juhos, S., and Downer, R. G. (1994). Characterization of tyramine and octopamine receptors in the insect (*Locusta migratoria migratorioides*) brain. *Brain Res*, 633:119–126.

Hohensee, S., Bleiss, W., and Duch, C. (2008). Correlative electron and confocal microscopy assessment of synapse localization in the central nervous system of an insect. *J Neurosci Methods*, 168:64–70.

Homberg, U., Bleick, A., and Rathmayer, W. (1993). Immunocytochemistry of GABA and glutamic acid decarboxylase in the thoracic ganglion of the crab *Eriphia spinifrons*. *Cell and Tissue Research*, 271:279–288.

Hosie, A. M., Aronstein, K., Sattelle, D. B., and ffrench Constant, R. H. (1997). Molecular biology of insect neuronal GABA receptors. *Trends Neurosci*, 20:578–583.

Hoyle, G. (1975). Evidence that insect dorsal unpaired median (DUM) neurons are octopaminergic. *J Exp Zool*, 193:425–431.

Hoyle, G. (1978). The dorsal, unpaired, median neurons of the locust metathoracic ganglion. *J Neurobiol*, 9:43–57.

Hoyle, G. (1985). *Comparative Insect Physiology, Biochemistry and Pharmacology, vol. 5*, chapter Generation of motor activity and control of behaviour: the role of the neuromodulator octopamine and the orchestration hypothesis., page 521–607. Pergamon Press, Toronto.

Hoyle, G., Colquhoun, W., and Williams, M. (1980). Fine structure of an octopaminergic neuron and its terminals. *J Neurobiol*, 11:103–126.

Hoyle, G. and Dagan, D. (1978). Physiological characteristics and reflex activation of DUM (octopaminergic) neurons of locust metathoracic ganglion. *J Neurobiol*, 9:59–79.

Jahn, R., Lang, T., and Südhof, T. C. (2003). Membrane fusion. *Cell*, 112:519–533.

Janssen, D., Derst, C., Buckinx, R., den Eynden, J. V., Rigo, J.-M., and Kerkhove, E. V. (2007). Dorsal unpaired median neurons of *Locusta migratoria* express ivermectin- and fipronil-sensitive glutamate-gated chloride channels. *J Neurophysiol*, 97:2642–2650.

Janssen, D., Derst, C., Rigo, J.-M., and Kerkhove, E. V. (2010). Cys-loop ligand-gated chloride channels in dorsal unpaired median neurons of *Locusta migratoria*. *J Neurophysiol*, 103:2587–2598.

Jia, X. X., Gorczyca, M., and Budnik, V. (1993). Ultrastructure of neuromuscular junctions in drosophila: comparison of wild type and mutants with increased excitability. *J Neurobiol*, 24:1025–1044.

Jin, H., Wu, H., Osterhaus, G., Wei, J., Davis, K., Sha, D., Floor, E., Hsu, C.-C., Kopke, R. D., and Wu, J.-Y. (2003). Demonstration of functional coupling between gamma -aminobutyric acid (GABA) synthesis and vesicular GABA transport into synaptic vesicles. *Proc Natl Acad Sci U S A*, 100:4293–4298.

Johansen, J., Halpern, M. E., Johansen, K. M., and Keshishian, H. (1989). Stereotypic morphology of glutamatergic synapses on identified muscle cells of *Drosophila* larvae. *J Neurosci*, 9:710–725.

Johnston, R. M., Consoulas, C., Pflüger, H.-J., and Levine, R. B. (1999). Patterned activation of unpaired median neurons during fictive crawling in *Manduca sexta* larvae. *J Exp Biol*, 202:103–113.

Katz, P. S. (1998). Comparison of extrinsic and intrinsic neuromodulation in two central pattern generator circuits in invertebrates. *Exp Physiol*, 83:281–292.

Kaufman, D. L., Houser, C. R., and Tobin, A. J. (1991). Two forms of the gamma-aminobutyric acid synthetic enzyme glutamate decarboxylase have distinct intraneuronal distributions and cofactor interactions. *J Neurochem*, 56:720–723.

Kien, J. and Altman, J. S. (1979). Connections of the locust wing tegulae with metathoracic flight motoneurons. *J Comp Physiol A*, 133:299–310.

Killmann, F., Gras, H., and Schürmann, F. (1999). Types, numbers and distribution of synapses on the dendritic tree of an identified visual interneuron in the brain of the locust. *Cell Tissue Res*, 296:645–665.

Klagges, B. R., Heimbeck, G., Godenschwege, T. A., Hofbauer, A., Pflugfelder, G. O., Reifegerste, R., Reisch, D., Schaupp, M., Buchner, S., and Buchner, E. (1996). Invertebrate synapsins: a single gene codes for several isoforms in *Drosophila*. *J Neurosci*, 16:3154–3165.

Kobayashi, E. A. (2001). Role of catecholamine signaling in brain and nervous system functions: new insights from mouse molecular genetic study. *J Investig Dermatol Symp Proc*, 6:115–121.

Koch, C. and Segev, I. (2000). The role of single neurons in information processing. *Nat Neurosci*, 3 Suppl:1171–1177.

Kononenko, N. L. and Pflüger, H.-J. (2007). Dendritic projections of different types of octopaminergic unpaired median neurons in the locust metathoracic ganglion. *Cell Tissue Res*, 330:179–195.

Kononenko, N. L., Wolfenberg, H., and Pflüger, H.-J. (2009). Tyramine as an independent transmitter and a precursor of octopamine in the locust central nervous system: an immunocytochemical study. *J Comp Neurol*, 512:433–452.

Kreissl, S., Eichmüller, S., Bicker, G., Rapus, J., and Eckert, M. (1994). Octopamine-like immunoreactivity in the brain and subesophageal ganglion of the honeybee. *J Comp Neurol*, 348:583–595.

Kutsch, W., Hanloser, H., and Reinecke, M. (1980). Light- and electron-microscopic analysis of a complex sensory organ: the tegula of *Locusta migratoria*. *Cell Tissue Res*, 210:461–478.

Kutsch, W. and Schneider, H. (1987). Histological characterization of neurones innervating functionally different muscles of *Locusta*. *J Comp Neurol*, 261:515–528.

Kutsukake, M., Komatsu, A., Yamamoto, D., and Ishiwa-Chigusa, S. (2000). A tyramine receptor gene mutation causes a defective olfactory behavior in *Drosophila melanogaster*. *Gene*, 245:31–42.

Kyriakides, M. and Mccrohan, C. (1989). Effect of putative rhythmic buccal motor output in *Lymnea stagnalis*. *J Neurobiol*, 20:635–650.

Lange, A. B. (2009). Tyramine: from octopamine precursor to neuroactive chemical in insects. *Gen Comp Endocrinol*, 162:18–26.

Lange, A. B. and Orchard, I. (1986). Identified octopaminergic neurons modulate contractions of locust visceral muscle via adenosine 3',5'-monophosphate (cyclic AMP). *Brain Res*, 363:340–349.

Laurent, G. and Sivaramakrishnan, A. (1992). Single local interneurons in the locust make central synapses with different properties of transmitter release on distinct postsynaptic neurons. *J Neurosci*, 12:2370–2380.

Leitch, B. and Laurent, G. (1993). Distribution of gabaergic synaptic terminals on the dendrites of locust spiking local interneurones. *J Comp Neurol*, 337:461–470.

Littlewood, P. M. and Simmons, P. J. (1992). Distribution and structure of identified tonic and phasic synapses between l-neurones in the locust ocellar tract. *J Comp Neurol*, 325:493–513.

London, M. and Häusser, M. (2005). Dendritic computation. *Annu Rev Neurosci*, 28:503–532.

Madison, D. V. and Nicoll, R. A. (1986). Actions of noradrenaline recorded intracellularly in rat hippocampal CA1 pyramidal neurones, in vitro. *J Physiol*, 372:221–244.

Martin, T. F. (2003). Tuning exocytosis for speed: fast and slow modes. *Biochim Biophys Acta*, 1641:157–165.

Meinertzhagen, I. A. (1996). Ultrastruture and quantification of synapses in the insect nervous system. *J Neurosci Methods*, 69:59–73.

Mentel, T., Duch, C., Stypa, H., Wegener, G., Müller, U., and Pflüger, H.-J. (2003). Central modulatory neurons control fuel selection in flight muscle of migratory locust. *J Neurosci*, 23:1109–1113.

Mentel, T., Weiler, V., Büschges, A., and Pflüger, H.-J. (2008). Activity of neuromodulatory neurones during stepping of a single insect leg. *J Insect Physiol*, 54:51–61.

Mesce, K. A. (2002). Metamodulation of the biogenic amines: second-order modulation by steroid hormones and amine cocktails. *Brain Behav Evol*, 60:339–349.

Meseke, M., Evers, J. F., and Duch, C. (2009a). Developmental changes in dendritic shape and synapse location tune single-neuron computations to changing behavioral functions. *J Neurophysiol*, 102:41–58.

Meseke, M., Evers, J. F., and Duch, C. (2009b). PTX-induced hyperexcitability affects dendritic shape and GABAergic synapse density but not synapse distribution during *Manduca* postembryonic motoneuron development. *J Comp Physiol A*, 195:473–489.

Meuser, S. and Pflüger, H.-J. (1998). Programmed cell death specifically eliminates one part of a locust pleuroaxillary muscle after the imaginal moult. *J of Exp Biol*, 201:2367–2382.

Möhl, B. and Bacon, J. (1983). The tritocerebral commissure giant (TCG) wind-sensitive interneurone in the locust. *J Comp Physiol A*, 150:453–465.

Miller, P. L. (1960). Respiration in the desert locust. i. the control of ventilation. *J Exp Biol*, 37:224–236.

Monastirioti, M. (1999). Biogenic amine systems in the fruit fly *Drosophila melanogaster*. *Microsc Res Tech*, 45:106–121.

Monastirioti, M., Gorczyca, M., Rapus, J., Eckert, M., White, K., and Budnik, V. (1995). Octopamine immunoreactivity in the fruit fly *Drosophila melanogaster*. *J Comp Neurol*, 356:275–287.

Morris, O. T., Duch, C., and Stevenson, P. A. (1999). Differential activation of octopaminergic (DUM) neurones via proprioceptors responding to flight muscle contractions in the locust. *J Exp Biol*, 202 Pt 24:3555–3564.

Morton, D. B. and Evans, P. D. (1984). Octopamine release from an identified neurone in the locust. *J Exp Biol*, 113:269–287.

Nagaya, Y., Kutsukake, M., Chigusa, S. I., and Komatsu, A. (2002). A trace amine, tyramine, functions as a neuromodulator in *Drosophila melanogaster*. *Neurosci Lett*, 329:324–328.

Nakagawa, H. and Mulloney, B. (2001). Local specification of relative strengths of synapses between different abdominal stretch-receptor axons and their common target neurons. *J Neurosci*, 21:1645–1655.

Nelson, D. L. and Molinoff, P. B. (1976). Distribution and properties of adrenergic storage vesicles in nerve terminals. *J Pharmacol Exp Ther*, 196:346—-359.

Neumann, L., Möhl, B., and Nachtigall, W. (1982). Quick phase-specific influence of the tegula on the locust flight motor. *Naturwissenschaften*, 69:393–394.

Neville, A. C. (1963). Motor unit distribution of the dorsal longitudinal flight muscles in locusts. *J Exp Biol*, 40:123–136.

Newland, P. L. and Emptage, N. J. (1996). The central connections and actions during walking of tibial campaniform sensilla in the locust. *J Comp Physiol A*, 178:749–762.

Oertel, W. H., Schmechel, D. E., Tappaz, M. L., and Kopin, I. J. (1981). Production of a specific antiserum to rat brain glutamic acid decarboxylase by injection of an antigen-antibody complex. *Neuroscience*, 6:2689–2700.

Ohta, H., Utsumi, T., and Ozoe, Y. (2003). B96bom encodes a *Bombyx mori* tyramine receptor negatively coupled to adenylate cyclase. *Insect Mol Biol*, 12:217–223.

Orbeli, L. A. (1923). Die sympathetische Innervation der Skelettmuskeln. *Bull Inst Sci Leshaft*, 6:194–197.

Orchard, I. and Lange, A. B. (1986). Neuromuscular transmission in an insect visceral muscle. *J Neurobiol*, 17:359–372.

Orchard, I., Ramirez, J., and Lange, A. B. (1993). A multifunctional role for octopamine in locust flight. *Ann Rev Entomol*, 38:227–249.

Packham, R., Walker, R. J., and Holden-Dye, L. (2010). The effect of a selective octopamine antagonist, epinastine, on pharyngeal pumping in *Caenorhabditis elegans*. *Invert Neurosci*, 10:47–52.

Pearson, K. G. (1993). Common principles of motor control in vertebrates and invertebrates. *Annu Rev Neurosci*, 10:1811–1815.

Pearson, K. G. and Wolf, H. (1988). Connections of hindwing tegulae with flight neurones in the locust, *Locusta migratoria*. *J Exp Biol*, 135:381–409.

Peters, B. H., Altman, J. S., and Tyrer, N. M. (1985). Synaptic connections between the hindwing stretch receptor and flight motor neurones in the locust revealed by double cobalt labelling for electron microscopy. *J Comp Neurol*, 233:269–284.

Pflüger, H.-J., Bräunig, P., and Hustert, R. (1981). Distribution and specific central projections of mechanoreceptors in the thorax and proximal leg joints of locust. ii. the external mechanoreceptors: hair plates and tactile hairs. *Cell Tissue Res*, 216:79–96.

Pflüger, H.-J. and Büschges, A. (2006). *Microcircuits: The interface between neurons and global brain function.*, chapter Neuromodulation of microcurcuits in motor systems with special reference to invertebrates., pages 57–74. MIT PRESS.

Pflüger, H.-J., Elson, R., Binkle, U., and Schneider, H. (1986). The central nervous organization of the motor neurones to a steering muscle in locusts. *J Exp Biol*, 120:403–420.

Pflüger, H. J. and Watson, A. H. (1988). Structure and distribution of dorsal unpaired median (DUM) neurones in the abdominal nerve cord of male and female locusts. *J Comp Neurol*, 268:329–345.

Pflüger, H. J. and Watson, A. H. (1995). GABA and glutamate-like immunoreactivity at synapses received by dorsal unpaired median neurones in the abdominal nerve cord of the locust. *Cell Tissue Res*, 280:325–333.

Pflüger, H. J., Witten, J. L., and Levine, R. B. (1993). Fate of abdominal ventral unpaired median cells during metamorphosis of the hawkmoth, *Manduca sexta*. *J Comp Neurol*, 335:508–522.

Pirri, J., McPherson, A., Donnelly, J., Francis, M., and Alkema, M. (2009). A tyramine-gated chloride channel coordinates distinct motor programs of a *Caenorhabditis elegans* escape response. *Neuron*, 62:526–538.

Pitman, R. M. (1971). Transmitter substances in insects: a review. *Comp Gen Pharmacol*, 2:347–371.

Potter, C. J. and Luo, L. (2008). Octopamine fuels fighting flies. *Nat Neurosci*, 11:989–990.

Potter, L. T. and Axelrod, J. (1963). Subcellular localization of catecholamines in tissues of the rat. *J Pharmacol Exp Ther*, 142:291–298.

Ramirez, J.-M. and Orchard, I. (1990). Octopaminergic modulation of the forewing stretch receptor in the locust *Locusta migratoria*. *J Exp Biol*, 149:255–279.

Ramirez, J. M. and Pearson, K. G. (1991). Octopamine induces bursting and plateau potentials in insect neurones. *Brain Res*, 549:332–337.

Reinecke, M. and Walther, C. (1978). Aspects of turnover and biogenesis of synaptic vesicles at locust neuromuscular junctions as revealed by zinc iodide-osmium tetroxide (ZIO) reacting with intravesicular SH-groups. *J Cell Biol*, 78:839–855.

Reinecke, M. and Walther, C. (1981). Ultrastructural changes with high activity and subsequent recovery at locust motor nerve terminals. a stereological analysis. *Neuroscience*, 6:489–503.

Rettig, J. and Neher, E. (2002). Emerging roles of presynaptic proteins in ca_{2+}-triggered exocytosis. *Science*, 298:781–785.

Rex, E. and Komuniecki, R. (2002). Characterization of a tyramine receptor from *Caenorhabditis elegans*. *J Neurochem*, 82:1352–1359.

Rheuben, M. B. (1995). Specific associations of neurosecretory or neuromodulatory axons with insect skeletal muscles. *Amer. Zool.*, 35:566–577.

Rillich, J., Schildberger, K., and Stevenson, P. A. (2010). Octopamine and occupancy: an aminergic mechanism for intruder-resident aggression in crickets. *Proc Biol Sci*.

Rizzoli, S. O. and Betz, W. J. (2005). Synaptic vesicle pools. *Nat Rev Neurosci*, 6:57–69.

Robb, S., Cheek, T., Hannan, F., Hall, L., Midgley, J., and Evans, P. (1994). Agonist-specific coupling of a cloned *Drosophila* octopamine/tyramine receptor to multiple second messenger systems. *EMBO J*, 13:1325–1330.

Robinson, G., Heuser, L., Leconte, Y., Lenquette, F., and Hollingworth, R. (1999). Neurochemicals aid bee nestmate recognition. *Nature*, 399:534–535.

Roeder, T. (1999). Octopamine in invertebrates. *Prog Neurobiol*, 59:533–561.

Roeder, T. (2002). Biochemistry and molecular biology of receptors for biogenic amines in locusts. *Microsc Res Tech*, 56:237–247.

Roeder, T. (2005). Tyramine and octopamine: ruling behavior and metabolism. *Annu Rev Entomol*, 50:447–477.

Roeder, T., Degen, J., and Gewecke, M. (1998). Epinastine, a highly specific antagonist of insect neuronal octopamine receptors. *Eur J Pharmacol*, 349:171–177.

Rollenhagen, A. and Lübke, J. H. R. (2006). The morphology of excitatory central synapses: from structure to function. *Cell Tissue Res*, 326:221–237.

Rotte, C., Krach, C., Balfanz, S., Baumann, A., Walz, B., and Blenau, W. (2009). Molecular characterization and localization of the first tyramine receptor of the american cockroach (*Periplaneta americana*). *Neuroscience*, 162:1120–1133.

Ryckebusch, S. and Laurent, G. (1993). Rhythmic patterns evoked in locust leg motor neurons by the muscarinic agonist pilocarpine. *J Neurophysiol*, 69:1583–1595.

Salganicoff, L. and DeRobertis, E. (1965). Subcellular distribution of the enzymes of the glutamic acid, glutamine and gamma-aminobutyric acid cycles in rat brain. *J Neurochem*, 12:287–309.

Saraswati, S., Fox, L. E., Soll, D. R., and Wu, C.-F. (2004). Tyramine and octopamine have opposite effects on the locomotion of *Drosophila* larvae. *J Neurobiol*, 58:425–441.

Saudou, F., Amlaiky, N., Plassat, J.-L., Borrelli, E., and Hen, R. (1990). Cloning and characterization of a *Drosophila* tyramine receptor. *EMBO J*, 9:3611—-3617.

Schmitt, S., Evers, J. F., Duch, C., Scholz, M., and Obermayer, K. (2004). New methods for the computer-assisted 3-D reconstruction of neurons from confocal image stacks. *Neuroimage*, 23:1283–1298.

Schwaerzel, M., Monastirioti, M., Scholz, H., Friggi-Grelin, F., Birman, S., and Heisenberg, M. (2003). Dopamine and octopamine differentiate between aversive and appetitive olfactory memories in *Drosophila*. *J Neurosci*, 23:10495–10502.

Südhof, T. C. (2004). The synaptic vesicle cycle. *Annu Rev Neurosci*, 27:509–547.

Siegler, M. V. and Burrows, M. (1983). Spiking local interneurons as primary integrators of mechanosensory information in the locust. *J Neurophysiol*, 50:1281–1295.

Snodgrass, R. (1929). The thoracic mechanism of a grasshopper and its antecedents. *Smithson misc Collns*, 82:1–111.

Sombati, S. and Hoyle, G. (1984). Generation of specific behaviors in a locust by local release into neuropil of the natural neuromodulator octopamine. *J Neurobiol*, 15:481–506.

Sorensen, J. B. (2004). Formation, stabilisation and fusion of the readily releasable pool of secretory vesicles. *Pflügers Arch*, 448:347–362.

Speese, S., Petrie, M., Schuske, K., Ailion, M., Ann, K., Iwasaki, K., Jorgensen, E. M., and Martin, T. F. J. (2007). UNC-31 (CAPS) is required for dense-core vesicle but not synaptic vesicle exocytosis in *Caenorhabditis elegans*. *J Neurosci*, 27(23):6150–6162.

Stern, M. (1999). Octopamine in the locust brain: cellular distribution and functional significance in an arousal mechanism. *Microsc Res Tech*, 45:135–141.

Stern, M. (2009). The pm1 neurons, movement sensitive centrifugal visual brain neurons in the locust: anatomy, physiology, and modulation by identified octopaminergic neurons. *J Comp Physiol A*, 195:123–137.

Stevenson, P. and Kutsch, W. (1986). Basic circuitry of an adult-specific motor program completed with embryogenesis. *Naturwissenschaften*, 73:741–743.

Stevenson, P. A., Dyakonova, V., Rillich, J., and Schildberger, K. (2005). Octopamine and experience-dependent modulation of aggression in crickets. *J Neurosci*, 25:1431–1441.

Stevenson, P. A. and Meuser, S. (1997). Octopaminergic innervation and modulation of a locust flight steering muscle. *J Exp Biol*, 200:633–642.

Stevenson, P. A., Pflüger, H. J., Eckert, M., and Rapus, J. (1992). Octopamine immunoreactive cell populations in the locust thoracic-abdominal nervous system. *J Comp Neurol*, 315:382–397.

Stevenson, P. A. and Spörhase-Eichmann, U. (1995). Localization of octopaminergic neurones in insects. *Comp Biochem Physiol A Physiol*, 110:203–215.

Taylor, C., Fricker, A. D., Devi, L. A., and Gomes, I. (2005). Mechanisms of action of antidepressants: from neurotransmitter systems to signaling pathways. *Cell Signal*, 17:549–557.

Trautwein, W. and Hescheler, J. (1990). Regulation of cardiac l-type calcium current by phosphorylation and g proteins. *Annu Rev Physiol*, 52:257–274.

Turrigiano, G. G. (2008). The self-tuning neuron: synaptic scaling of excitatory synapses. *Cell*, 135:422–435.

Tyrer, N. M. and Altman, J. S. (1974). Motor and sensory flight neurones in a locust demonstrated using cobalt chloride. *J Comp Neurol*, 157:117–138.

Tyrer, N. M. and Gregory, G. E. (1982). A guide to the neuroanatomy of locust suboesophageal and thoracic ganglia. *Phil Trans R Soc Lond B*, 297:pp. 91–123.

Tyrer, N. M., Pozza, M. F., Humbel, U., Peters, B. H., and Bacon, J. P. (1988). The tritocerebral commissure 'dwarf' (TCD): a major GABA-immunoreactive descending interneuron in the locust. *J Comp Physiol A*, 164:141–150.

Unoki, S., Matsumoto, Y., and Mizunami, M. (2006). Roles of octopaminergic and dopaminergic neurons in mediating reward and punishment signals in insect visual learning. *J Neurosci*, 24:2031–2038.

Usherwood, P. N. and Grundfest, H. (1965). Peripheral inhibition in skeletal muscle of insects. *J Neurophysiol*, 28:497–518.

Usherwood, P. N., Machili, P., and Leaf, G. (1968). L-glutamate at insect excitatory nerve-muscle synapses. *Nature*, 219:1169–1172.

Vanden Broeck, J., Vulsteke, V., Huybrechts, R., and De Loof, A. (1995). Characterization of a cloned locust tyramine receptor cDNA by functional expression in permanently transformed *Drosophila* S2 cells. *J Neurochem*, 64:2387–2395.

Vehovszky, A., Hiripi, L., and Elliott, C. J. H. . (2000). Octopamine is the synaptic transmitter between identified neurons in the buccal feeding network of the pond snail *Lymnaea stagnalis*. *Brain Res*, 867:188–199.

Venton, B. J., Seipel, A. T., Phillips, P. E. M., Wetsel, W. C., Gitler, D., Greengard, P., Augustine, G. J., and Wightman, R. M. (2006). Cocaine increases dopamine release by mobilization of a synapsin-dependent reserve pool. *J Neurosci*, 26:3206–3209.

Vierk, R., Pflueger, H. J., and Duch, C. (2009). Differential effects of octopamine and tyramine on the central pattern generator for *Manduca* flight. *J Comp Physiol A*, 195:265–277.

Villanueva, M., Augustine, G. J., and Wightman, R. M. (2007). Synapsin ii negatively regulates catecholamine release. *Brain Cell Biol*, 35:125–136.

Wafford, K. A. and Sattelle, D. B. (1986). Effects of amino acid neurotransmitter candidates on an identified insect motoneurone. *Neurosci Letts*, 63:135–140.

Wagh, D. A., Rasse, T. M., Asan, E., Hofbauer, A., Schwenkert, I., Dürrbeck, H., Buchner, S., Dabauvalle, M.-C., Schmidt, M., Qin, G., Wichmann, C., Kittel, R., Sigrist, S. J., and Buchner, E. (2006). Bruchpilot, a protein with homology to ELKS/CAST, is required for structural integrity and function of synaptic active zones in *Drosophila*. *Neuron*, 49:833–844.

Watson, A. H. (1984). The dorsal unpaired median neurons of the locust metathoracic ganglion: neuronal structure and diversity, and synapse distribution. *J Neurocytol*, 13:303–327.

Watson, A. H. (1988). Antibodies against GABA and glutamate label neurons with morphologically distinct synaptic vesicles in the locust central nervous system. *Neurosci*, 26:33–44.

Watson, A. H. and Burrows, M. (1987). Immunocytochemical and pharmacological evidence for GABAergic spiking local interneurons in the locust. *J Neurosci*, 7:1741–1751.

Watson, A. H., Burrows, M., and Hale, J. P. (1985). The morphology and ultrastructure of common inhibitory motor neurones in the thorax of the locust. *J Comp Neurol*, 239:341–359.

Watson, A. H. and Laurent, G. (1990). GABA-like immunoreactivity in a population of locust intersegmental interneurones and their inputs. *J Comp Neurol*, 302:761–767.

Watson, A. H. D. (1986). The distribution of GABA-like immunoreactivity in the thoracic nervous system of the locust *Schistocerca gregaria*. *Cell Tissue Res*, 246:331–341.

Watson, A. H. D. and Schürmann, F.-W. (2002). Synaptic structure, distribution, and circuitry in the central nervous system of the locust and related insects. *Microsc Res Tech*, 56:210–226.

Watson, A. H. D. and Seymour-Laurent, K. J. (1993). The distribution of glutamate-like immunoreactivity in the thoracic and abdominal ganglia of the locust (*Schistocerca gregaria*). *Cell Tissue Res*, 273:557–570.

Wegener, G., Michel, R., and Newsholme, E. A. (1986). Fructose 2,6-bisphosphate as a signal for changing from sugar to lipid oxidation during flight in locusts. *FEBS Lett*, 201:129–132.

Whim, M. D. and Evans, P. D. (1988). Octopaminergic modulation of flight muscle in the locust. *J Exp Biol*, 134:247–266.

Wildman, M., Ott, S. R., and Burrows, M. (2002). GABA-like immunoreactivity in nonspiking interneurons of the locust metathoracic ganglion. *J Exp Biol*, 205:3651–3659.

Wolf, H. and Pearson, K. G. (1988). Proprioceptive input patterns elevator activity in the locust flight system. *J Neurophysiol*, 59:1831–1853.

Wu, H., Jin, Y., Buddhala, C., Osterhaus, G., Cohen, E., Jin, H., Wei, J., Davis, K., Obata, K., and Wu, J.-Y. (2007). Role of glutamate decarboxylase (GAD) isoform, GAD65, in GABA synthesis and transport into synaptic vesicles-evidence from GAD65-knockout mice studies. *Brain Res*, 1154:80–83.

Zhang, H., Wainwright, M., Byrne, J., and Cleary, L. (2003). Quantitation of contacts among sensory, motor, and serotonergic neurons in the pedal ganglion of *Aplysia*. *Learn Mem*, 10:387–393.

Zhou, C., Rao, Y., and Rao, Y. (2008). A subset of octopaminergic neurons are important for *Drosophila* aggression. *Nat Neurosci*, 11:1059–1067.

Zucchi, R., Chiellini, G., Scanlan, T. S., and Grandy, D. K. (2006). Trace amine-associated receptors and their ligands. *Br J Pharmacol*, 149:967–978.

Danksagung

Sehr herzlich danke ich Prof. Dr. Hans-Joachim Pflüger, der mir die Anfertigung der vorliegenden Arbeit unter seiner Betreuung im Rahmen des Graduiertenkollegs 837 ermöglicht hat. Er hat Material, Wissen und Zeit großzügig zur Verfügung gestellt und mich mit den internationalen Foren der Neurowissenschaften vertraut gemacht.
Für die Aufnahme ins Graduiertenkolleg danke ich außerdem Prof. Dr. Bernd Walz von der Universität Potsdam als Sprecher des Graduiertenkollegs und Organisator diverser Rahmen- und Förderveranstaltungen.
Prof. Dr. Dorothea Eisenhardt gebührt Dank für die Begutachtung meiner Arbeit.
Ganz besonders fühle ich mich Jan Rillich für seine fachliche und kameradschaftliche Unterstützung verbunden. Er hat Konzept und Ausführung meiner Arbeit positiv beeinflusst und es verstanden, den Blick auf das Wesentliche zu lenken.
Freundliche, kompetente und tatkräftige Hilfe im Labor fand ich stets bei Heike Wolfenberg.
Natalia Kononenko bin ich für die Einführung in die Immunocytochemie und Konfokalmikroskopie sowie Jürgen Rybak für Anregungen und Hilfe bezüglich der Software Amira, histologischer Techniken und der Arbeit am konfokalen Mikroskop Dank schuldig.
Für die Weitergabe wertvoller Erfahrungen herzlichen Dank an meine ehemaligen Mitdoktorandinnen und -doktoranden Jana Börner, Maurice Meseke, Ricardo Vierk, Stevie Ryglewski und Anja Fröse.
Eine besondere Arbeitserleichterung war Doreen Johannes' Sorgfalt bei der Zucht und Bereitstellung der Tiere.
Das freundschaftliche und konkurrenzarme Klima in der Arbeitsgruppe sowie unter den Mitarbeitern im Institut wusste ich sehr zu schätzen.
Die Arbeit wurde finanziell unterstützt von der Deutschen Forschungsgemeinschaft (Graduiertenkolleg 837 "Functional Insect Science").